Propulsion Systems Utilizing Planetary Magnetic Fields

(Brian Faircloth)

Note: Apologies for the lack of fancy and beautiful formatting throughout this document. It was meant to be a working document. It is an intermediate draft on the way to filing patents on the technology described herein. It was never meant for public eyes. There are a few typos and errata here and there, but for the most part it is complete and has all the necessary information for understanding the ultra-magnet and magnetic propulsion technology and how it can be used. It contains more detail than the patents themselves and may provide a deeper understanding of the technology.

Background

A number of technologies have been developed over the centuries in order for humankind to realize the dream of flight. Hot air balloons , based on Archimedes' principle, a physics law from over 2000 years ago, is one of the first realized technologies for manned flight. Later propeller-based blimps, zeppelins were developed based on both Archimedes' and Bernoulli's principals. With Bernoulli's principals, the physics moved into the 16th century. Later in the 20th century jet airplanes and rockets were developed to help planes travel faster and to get humankind into Earth's orbit and ultimately the moon. However, the physics is still fundamentally that of Isaac Newton and resides in the 16th century. In fact, the well-known rocket equations can be directly derived from Newton's equations. Fundamentally, all of the modern technologies in use today to travel any useful distance from one point on the Earth to another point on the Earth or to achieve orbit around the Earth or escape Earth's gravitational field altogether involve the use of chemical reactions, be it combustion for airplanes or a controlled explosion for that of rockets.

The invention proposed herein dispenses with the chemical combustion paradigm and moves propulsion and aeronautics and space travel into the realm of electromagnetics. An all-electric system based primarily on Maxwellian and Lorentzian physics, and utilizing planetary magnetic fields is proposed in which chemical combustion is not required; nor outwardly visible tails, wings, fins, ailerons, flaps, or airfoils of any type are required in order to achieve flight. In fact, air as a medium is not a requirement to realize lift or thrust, therefore, craft built with the proposed propulsion systems presented herein may exit and enter the atmosphere without penalty. A craft with the proposed propulsion system would not require jets, propellers, or rockets or outwardly visible flight control features, and yet would be highly maneuverable, including being able to hover in place at a fixed altitude.

By far the most expensive and difficult part of realizing space travel is getting from the surface of the Earth into orbit. A technology that allows one to easily and repeatably achieve orbit and return to the point of origin, or any other point on Earth, would be an enabling technology of unimaginable value. Large, livable, workable structures could be constructed in orbit. Once a spaceport in orbit were constructed, launching to other bodies within the solar system would be much easier and cost efficient. Being able to launch from orbit would enable much easier inter-planetary and intra-solar system travel. Low cost, efficient space travel allows access to practically limitless resources within the solar system. To wit, an average sized asteroid holds resources in the trillions of U.S. dollars with some asteroids estimated to hold resources in the many quadrillions of U.S. dollars. In fact, one asteroid has been identified as having the value of 70,000 times the current global economy [1]. Besides the clear economic value, such a technology would be invaluable for allowing humans to explore and colonize the solar system; allowing humankind to achieve the long sought-after dream of becoming a spacefaring race.

On a related noted, while propulsion within the atmosphere and in space are mainly described as the exemplary embodiment herein, propulsion can similarly be achieved on the surface of the ocean or underneath the surface of the ocean; the Earth's magnetic field being nearly unperturbed by ocean waters. This allows the movement of surface and sub-surface craft (i.e., submarines) without propellers or visible means of propulsion or steering elements. Conceivably a craft built with the disclosed propulsion technology could travel from underwater, through the atmosphere, and into outer space (or vice versa) in a single contiguous trip.

Force pounds (lbs) and Newtons are both used throughout to signify lift and thrust force. The conversion used is 1 N = 0.2248 lbs. Units may occasionally be mixed such as using pounds and Pascals in the same chart.

The Technology

The technology is largely based on the use of dynamic super-capacitors (DSCs) as described in the patent “Methods and Apparatuses for Producing Ultra-strong Magnetic Fields”, serial no. 63/162,137, which is included herein in its entirety.

Three types of propulsion are described in the current invention. The first will be known as Type I, which is the familiar repulsion between two magnets, to which the layperson is likely familiar. The second type of electromagnetic propulsion will be known as Type II propulsion which involves the force a charged particle experiences when moving through a magnetic field. This force is known as the Lorentz force or sometimes the Maxwell force. Type III is similar to Type II, being Lorentzian, differing only in the orientation of the force on the electrodes of the DSC.

As was done in “Methods and Apparatuses for Producing Ultra-strong Magnetic Fields”, computer simulation will primarily be used to estimate the fields, charges, and forces produced by the proposed inventions. Finite element methods and analysis (FEM or FEA) is the primary tool of choice with QuickField™, Ansys Maxwell™, and MATLAB™ being the software tools primarily used.

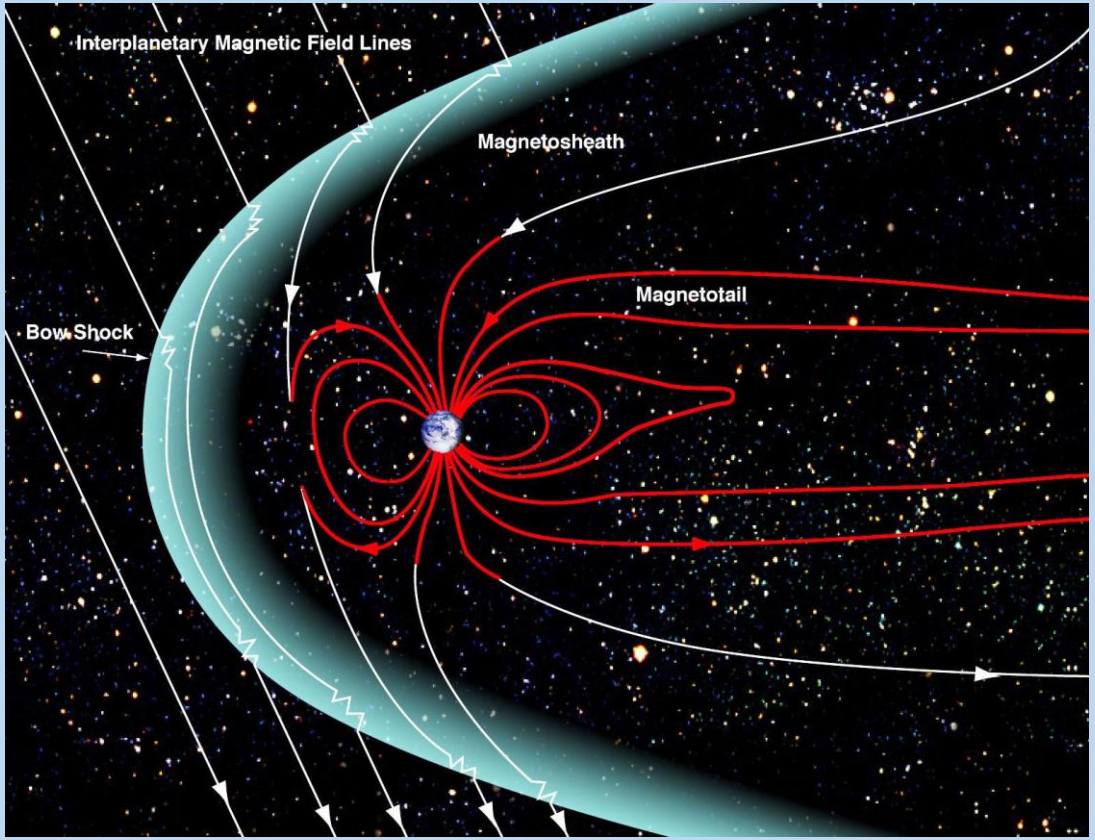

Figure 0. Earth’s magnetic field.
Credit: NASA/Goddard/Aaron Kaase

Dynamic Super Capacitors

At the heart of the present invention is the dynamic super-capacitor (DSC). These are capacitors that hold immense amounts of charge on their electrodes with the electrodes being put into motion. These dynamic super-capacitors were covered in detail in a previous patent "Methods and Apparatuses for Producing Ultra-strong Magnetic Fields". Some highlights will be covered here.

Figure 1, conducting, solid electrodes are coated with a super-dielectric layer with dielectric constants on the order of k = 1 x 10^9, with Cortes and Phillips [23, 24] being the exemplary example, though other super-dielectrics with different voltage profiles and dielectric properties are available. An optional, 'non-stick' film is applied on top of the super-dielectric, though the non-stick film is not recommended except under certain circumstances since the super-dielectric matrix material can usually serve this purpose since the super-dielectric matrix material can be made out of low adhesive materials such as metal oxides, metal fluorides, metal chlorides, metal sulfides, and other ceramics which naturally possess low adhesion properties and low coefficients of friction. The non-stick film will degrade the charge capacity of the electrodes and is mostly recommended for extending the life of the device if needed. The super-dielectric layer can be manufactured with sub-micron tolerances, thus making very large charge capacity possible. The capacitance of two circular plates, ignoring fringe fields, is given by

$$C = \frac{k\varepsilon_0 A}{d} \qquad (1)\,,$$

where C is the capacitance given in charge per unit voltage, k is the unitless dielectric constant, A is the area of the plates, and d is the separation of the plates, i.e., the thickness of the super-dielectric layer. Equation 1 assumes the space between the plates is filled with the dielectric material. The charge held on each plate is Q = C * V, where V is the voltage difference between the plates. In the current embodiment, a conductive fluid serves as one of the electrodes, in the exemplary case mercury. This is done such that the charged solid electrodes can move, putting the charges in motion. A second, oppositely charged electrode is likewise coated with a super-dielectric layer and put into contact with the same conductive slip-joint fluid. The conductive slip-slip joint fluid is held at an intermediate potential, here ground. This allows charge to build on both solid electrodes, in the preferred embodiment these charge polarities are opposite. Charge will also build on the surface of the conductive fluid in contact with the super-dielectric layer, however, as discussed in the previous disclosure, care has been taken to mitigate movement of the charge in the conductive fluid; an additional method of manipulating the mercury flow characteristics will also be discussed later. Mercury is an excellent choice of the conductive slip joint fluid as it has extremely strong cohesion and does not adhere, i.e., stick, to many materials. Mercury is also a non-magnetic conductor, meaning it is minimally affected by the powerful magnetic fields the DSCs produce. A point slip method was covered in the previously mentioned disclosure that forgoes the use of a conductive slip-joint fluid; this method will be revisited later. In the present invention, the conductive slip-joint fluid is the exemplary embodiment.

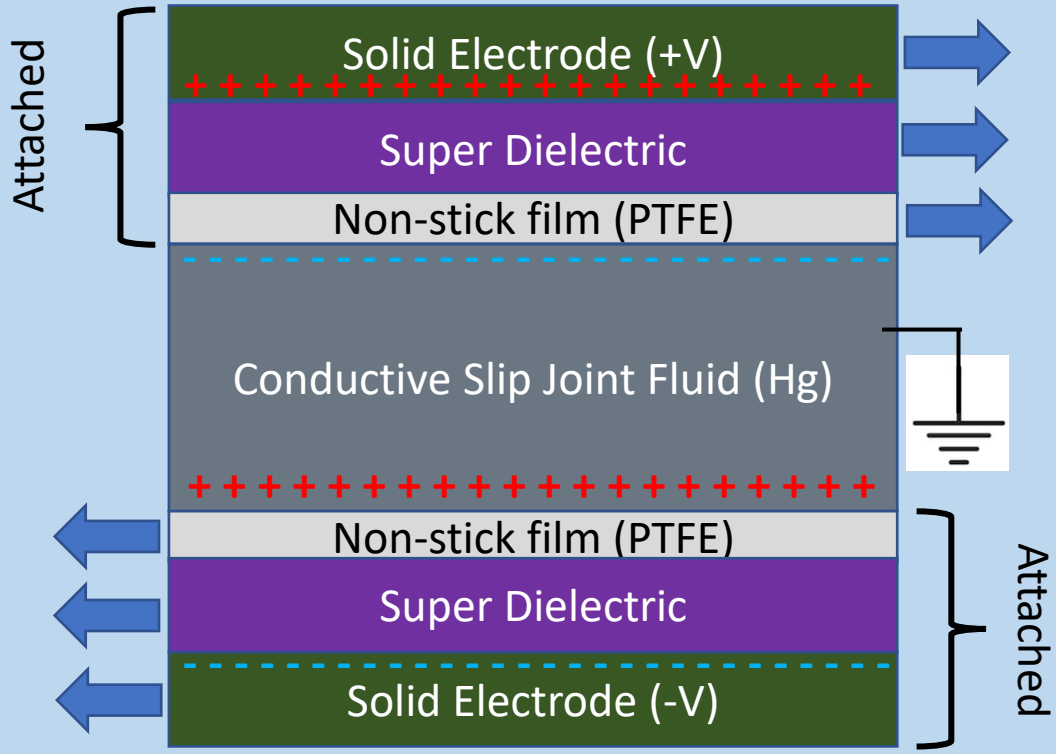

Figure 1. Schematic of interface geometry. Individual electrode super-dielectric layers. Both positive and negative electrodes possesses a super-dielectric coating.

Dynamic Super-Capacitors

Figure 2 shows a schematic diagram of the dual polarity counter-rotating super-capacitor design with N sets of rotating discs. A series of discs is attached to the inner drive shaft which also serves as the electrode to provide voltage potential and charge to those discs. The discs are coated with the super-dielectric layer as described previously. These discs are referred to as the inner discs.

The other polarity discs are attached to a cylindrical body, the outside casing, that also serves as the supply electrode for those discs; to deliver voltage potential and charge. These discs are referred to as the outer discs. These outer discs are also coated with super-dielectric layer as described previously. The cylindrical body is attached to an outer shaft driveshaft. The outer driveshaft is hollow to allow the inner driveshaft to pass through and rotationally drive the inner discs independently of the outer discs. The outer discs have a hole in their center to allow the inner drive shaft to pass through.

A conductive slip joint fluid, in the exemplary example mercury (Hg), encapsulates both inner and outer discs. One electrode is powered to +2 V and the other electrode is powered to -2 V, and the mercury is held at ground potential; two volts is used as two volts is the voltage at which the exemplary super-dielectric begins to experience a degradation in performance. This allows charge to build on the inner and outer discs, in figure 2 the outer discs are at positive potential and the inner discs are at negative potential, though this choice is arbitrary. The inner and outer discs are then rotated at high angular velocity in opposite rotational directions.

If rotatory bearings are required, the rotary bearing can be placed between the inner shaft and one or more of the outer discs and/or the outer drive shaft (as shown in figure 2). If outer discs are used, these support discs can be modified such as being thicker to provide structural support. Smaller diameter rotary bearings and rotary seals have the advantage of being more conducive to higher rotation speeds, and thus more powerful magnetic fields and/or Lorentz forces; as the strength of the generated magnetic field, or Lorentz force in an external magnetic field, is directly proportional to the rotation speed of the discs.

Additionally, it should be pointed out, the outside casing/electrode is insulated from the mercury slip-joint fluid as to not electrically short the casing to the slip-joint fluid. This can be done by either depositing a thin film insulator on the inner diameter of the outside casing, masked where the outer discs attach to the casing; or using a non-conductive, strong, lightweight material for the outside casing and selectively applying metal coatings to the areas that need conduction paths, masking those areas that are wetted by the mercury; or metal coating the inside of a non-conductive casing and etching the metal away in the areas that would be wetted by the mercury. It should be noted that, while not shown in the figure, the inner walls of the outside casing electrode can likewise be coated by the super-dielectric layer to act as the separation barrier between the electrode and the slip-joint fluid. This will build up a strong charge on the cylindrical inner diameter (ID) part of the outside casing which is a rotating member, further enhancing the magnetic field, or Lorentz force, when the apparatus is in rotational motion. Similar insulating processing could be taken with the inner electrode/shaft, although due to its small radius, very little additional advantage would be gained by coating the inner electrode with a super-dielectric layer. In the simulations that follow, it is assumed that the ID of the outer casing is not charged nor the OD of the inner shaft, only the disc surfaces themselves.

Locally, the mercury holds an equal and opposite charge to the electrodes near to the super-dielectric layer. However, due to the mercury having high surface tension (the highest of all known liquids), the super-dielectric matrix being constructed of a low adhesive material, combined with the two electrodes being counter-rotated which creates opposite, cancelling, shear stresses in the fluid, parasitic charge motions are mitigated. Parasitic charge motion is when the charges in the mercury move in the same directional as their corresponding DSC electrode. The mercury charges should remain stationary or ideally move oppositely to their corresponding electrode motion. The thinner the mercury fluid (i.e., the closer the inner and outer counter-rotating electrode plates are to one another) the greater the parasitic charge motion mitigation will be, see serial no. 63/162,137 for more details. In addition to mitigating parasitic charge motion, having high electrode densities also equates to higher volumetric charge density, which results in higher effective amps/unit area which result in stronger magnetic fields and stronger magnetic dipole moments and larger lift/thrust forces as described later.

Other dynamic super-capacitor configurations are also possible as outlined in the previous disclosure on ultra-strong magnetic field devices, such as concentric cylinders or spheres.

A rotation rate of 100,000 RPM is used throughout as a reference. Turbo-molecular vacuum pumps operate in the 20-100,000 RPM range [56], figure 2a. Jet engines operate up to 25,000 RPM and micro-turbines operate up to 500,000 RPM [57].

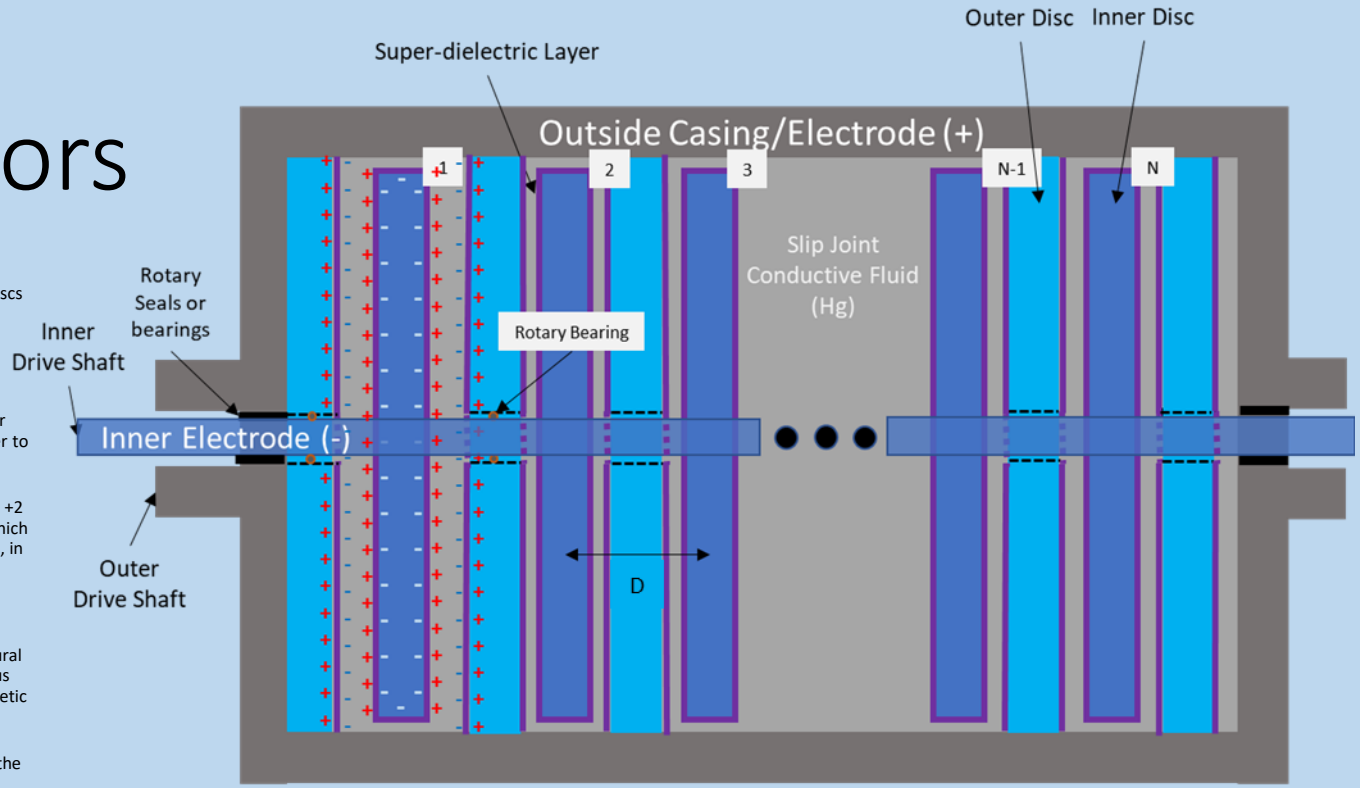

Figure 2. Multi-disc Ultra-magnet (MDU) inner and outer counter-rotating shafts, doubly charged rotation schematic design. Charge is only shown on first disc pair for simplicity. Choice of charge polarity is arbitrary (depends on direction of rotations and desired polarity of magnet).

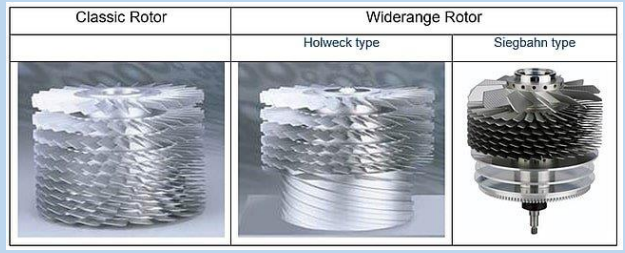

Figure 2a. Rotors of a typical turbo-molecular vacuum pump [56].

The Fundamental Physics

The propulsion methods herein are describable using classical electromagnetics. The foundational equations at the root of the calculations are:

$$\nabla \times \vec{E} = -\frac{\partial \vec{B}}{\partial t} \quad (2)$$

$$\nabla \times \vec{H} = \vec{J} + \frac{\partial \vec{D}}{\partial t} \quad (3)$$

$$\nabla \cdot \vec{D} = \rho_V \quad (4)$$

$$\nabla \cdot \vec{B} = 0 \quad (5)$$

$$\vec{F} = q\vec{E} + q\vec{v} \times \vec{B} \quad (6)$$

$$\vec{D} = [\epsilon]\vec{E} + [\alpha]\vec{H} \quad (7)$$

$$\vec{B} = [\mu]\vec{H} + [\alpha]\vec{E} \quad (8)$$

Equations 2-5 are the well-known Maxwell equations in differential form. $\vec{E}$ is the electric field, $\vec{B}$ is the magnetic flux density, $\vec{H}$ is the magnetic field strength, $\vec{D}$ is the electric displacement field, $\vec{J}$ is the current density, ρ_V is the volumetric charge density. It should be noted that while $\vec{H}$ is formally the magnetic field strength, it is common practice to informally refer to $\vec{B}$ as the magnetic field strength or simply the magnetic field since $\vec{B}$ is the field that produces the force on charged particles (equation 6).

Equation 6 is the Lorentz force equation for a charged particle travelling in an electric and magnetic field. $\vec{F}$ is the force on the particle, q is the charge of the particle, and $\vec{v}$ is the velocity of the particle relative to the magnetic field.

Equation 7 and 8 are the constitutive relationships for the fields in matter. $[\epsilon]$ is the electric permittivity tensor, $[\mu]$ is the magnetic permeability tensor, and $[\alpha]$ is the magnetoelectric tensor. In free space and linear, homogenous, isotropic (LHI) media, $[\epsilon]$ and $[\mu]$ reduce to scalars and $[\alpha]$ goes to zero; these will be the assumptions that follow.

Type I Propulsion

Type I propulsion is the force two magnets experience when in close proximity to one another, either attractive or repulsive.

The effective magnetic dipole moment of the Earth is 7.95 x 10^{22} Amp-m^2 [2]. The magnetic dipole moment, $\vec{m}$, of a charged spinning disc is given by

$$\vec{m} = \tfrac{1}{4} Q R^2 \vec{\omega} \qquad (9),$$

where Q is the charge on the disc, R is the radius of the disc and $\vec{\omega}$ is the angular velocity of the disc.

The force between two ideal magnetic dipoles with their moments aligned is given by [3,4]

$$F(r) = \frac{3\mu_0}{2\pi} m_1 m_2 \frac{1}{r^4} \qquad (10),$$

where μ_0 is the permeability of free space, m_1 is the magnetic dipole moment of body 1, m_2 is the magnetic dipole moment of body 2, and r is the co-axial distance between the two dipoles.

A single dynamic super-capacitor, i.e., two plates that counter-rotate, ten meters in diameter, with one-micron super dielectric layers, a dielectric constant k = 1 x 10^9, and a two-volt potential can hold a charge of 1.39 x 10^6 Coulombs on one electrode and -1.39 x 10^6 Coulombs on the other electrode. If spun at 100,000 RPM this configuration produces a magnetic moment of 1.83 x 10^{11} Amp-m^2. The radius of the Earth is 6.38 x 10^6 meters. When the axial separation and magnetic dipole moments are used in equation 3, the calculated force is 5.3 Newtons at the magnetic poles of the Earth; not an overly impressive amount of lift, but lift, nonetheless.

This result is the lift for a single disc pair. An assembly like that shown in figure 2 can be used to stack multiple discs and increase the net force. A 10-meter-tall assembly with 5 mm disc spacings would produce a lift of 21,200 N (or 4770 pounds), where the disc spacing, D, is that shown in figure 2. Twenty-one thousand Newtons is a more impressive lift number, but still unlikely to overcome the weight of the propulsion system itself.

It is worth noting, that since charge on the discs goes as R^2 and the magnetic moment goes as R^2 as well, the total magnetic dipole force goes as R^4; therefore, increasing the radius of the discs helps tremendously with the lift. To wit, a 100 m diameter disc pair produces a 53,000 N (11,900 lbs) lift. A much larger number, but still unlikely to overcome the weight of the propulsion assembly itself. A 10-meter stack of 100-meter discs spaced 5 mm apart produces a force of 211,000,000 N (47,000,000 lbs). These type of lift numbers are much more impressive, but such a large propulsion assembly rotating at such a high rate of speed would be impractical to impossible to build.

Given the numbers above and the impracticability of the construction of such extreme structures, Type I lift is unlikely to propel a vehicle into orbit given the current state of technology. However, as improvements are made to super-dielectrics and stronger and lighter materials are developed more charge can be stored more compactly and less lift is needed to overcome the weight of the craft; more lift can be generated by smaller, lighter propulsion systems; Type I propulsion may become practical in the future but appears impractical at this time.

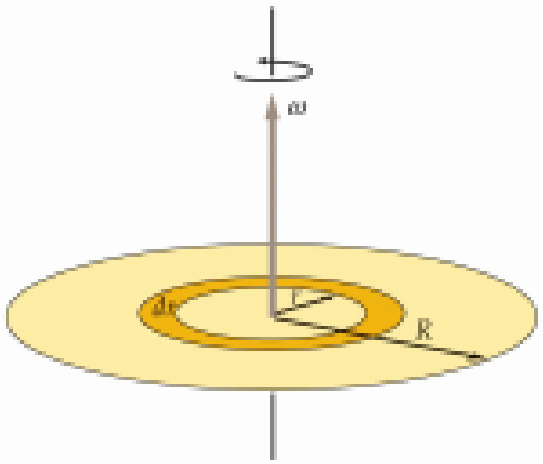

Figure 3. Spinning charged disc.

Type II Propulsion

A more practical thrust/lift can be produced by exploring the force exerted on the charged particles in motion on the spinning plates, Lorentz force. Equation (6) is for a single charged particle in motion. However, for charge distributions/currents this can be rewritten as, ignoring electric fields,

$$d\vec{F} = dQ\vec{v} \times \vec{B} \qquad (11)$$

in differential form, where $d\vec{F}$ is the differential force, dQ is a differential charge element, $\vec{v}$ is the velocity of that charge element, and $\vec{B}$ is the external magnetic field vector where dQ exists. The total Lorentz force can be written as

$$\vec{F} = \iiint_V \vec{J}dV \times \vec{B} \qquad (12)$$

in integral form, where V is the volume in which the effective current is contained, i.e., the rotating charged discs, $\vec{J}$ is the electric current density, and $\vec{B}$ is the applied external magnetic field, in the exemplary case, the magnetic field of the Earth. When the current is produced by the charges being on an electrode in motion, *J* is referred to as the effective current, $\vec{J}_{eff}$. Conventional current would be electrons flowing in a wire for example.

Equations 2-8 can be combined, assuming LHI conditions, and solved to produce the rank two Maxwell stress tensor [5,6];

$$T_{ij} \equiv \epsilon\left(E_iE_j - \tfrac{1}{2}\delta_{ij}E^2\right) + \tfrac{1}{\mu}\left(B_iB_j - \tfrac{1}{2}\delta_{ij}B^2\right) \qquad (13)$$

where T_{ij} are the *i-th* and *j-th* components of the Maxwell Stress Tensor, $\overleftrightarrow{T}$. Here *i* and *j* represent the basis vectors in three-dimensional space, for cartesian coordinates $\hat{x}$ = 1, $\hat{y}$ = 2, $\hat{z}$ = 3. E_i and E_j are the components of the electric field vector in the *i*th and *j*th direction, similarly, B_i and B_j are the components of the magnetic field vector in the *i*th and *j*th direction. δ_{ij} is the Kronecker delta function.

Type II Propulsion

The divergence of $\overleftrightarrow{T}$ yields the following equation [5,6];

$$\nabla \cdot \overleftrightarrow{T} = \vec{F} + \epsilon\mu \frac{\partial \vec{S}}{\partial t} \qquad (14)$$

where $\vec{F}$ is the total force on the system and $\vec{S}$ is the familiar Poynting vector, $\vec{S} = \vec{E} \times \vec{H}$. It is worth noting in the analyses that follow, it is assumed the system is running at steady-state to show the steady state propulsion force (lift/thrust) of the system, therefore, the time derivative of the Poynting vector term on the right will not contribute to the force calculation. This term would contribute on power up or power down of the system or if one wished to change the amount of thrust the system was producing, otherwise the time derivative is zero. Taking the divergence of a tensor lowers its order by one, therefore the long vector equation version of equation 14 can be written as, after solving for the force vector and writing purely in terms of *E* and *B*;

$$\vec{F} = \epsilon\left[(\nabla \cdot \vec{E})\vec{E} - (\vec{E} \cdot \nabla)\vec{E}\right] + \frac{1}{\mu}\left[(\nabla \cdot \vec{B})\vec{B} - (\vec{B} \cdot \nabla)\vec{B}\right] - \frac{1}{2}\nabla\left(\epsilon E^2 + \frac{1}{\mu}B^2\right) - \epsilon\frac{\partial(\vec{E}\times\vec{B})}{\partial t} \qquad (15)$$

The advantage to using the Maxwell Stress Tensor is the overall system force can be calculated. The fields, *E* and *B*, are the overall fields, inclusive of the external fields, such as the Earth's magnetic field, and the intrinsic fields, such as the fields generated by the dynamic super-capacitors (DSCs). Internal electromagnetic stresses on the components and structure can be calculated at any point resulting from the external and intrinsic fields combined. Very strong magnets, such as the DSCs, can produce strong electromagnetic stresses on themselves and their surroundings and these stresses should be accounted for in the structural design of the components and system.

As a point of note, the net force in equation 15 does possess electric field as a force generating component and the Earth does possess an electric field [7] that can be used to generate lift. However, electric fields start on charged particles and end on charged particles, therefore the span of the Earth's electric field is limited, not being able to propagate much past the Earth's atmosphere, specifically the ionosphere. The energy density of the Earth's magnetic field is about three to four orders of magnitude larger than the Earth's electric field energy density close to the surface. An additional challenge to electric field lift is the voltages and electric fields that would be needed by the propulsion system to produce appreciable lift would be difficult to maintain due to ionization, arcing, coronal discharge, and field emissions. Magnetic fields do not suffer from these drawbacks and the Earth's magnetic field extends tens of thousands of kilometers into space (40-65,000 km); for reference the international space station orbits at around 420 km and geosynchronous orbit is about 37,000 km. Therefore, the current invention will focus on magnetic propulsion only and forgo the electric field terms in equation 15. It is worth noting there is a lift mechanism employed using high voltage that ionizes the atmospheric gases and creates an ionic wind to lift small craft, known as high voltage ionic lifters [8]. These devices do not act on the fields themselves to generate the thrust but depend on using the atmospheric gases as an ionized propellant or have on-board gas storage in the case of ionic propulsion in space [9]. These are touted as all-electric lift/thrust devices; however, these operate on a propellant exhaust principle, i.e., mass ejection, and require a gas supply of some type; using ions as opposed to combusted or pressurized gas molecules.

Type II Propulsion Principles

In order to understand the mechanics of how lift and thrust can be realized utilizing the Earth's magnetic field, it is instructive to start with equation 11 which describes the differential force vector produced by a differential charge element travelling through an external magnetic field, e.g., the Earth's magnetic field.

Figure 4 shows a disc with surface charge, σ, spinning about a central axis at an angular velocity of ω. The x and y axis lie in the plane of the disc. A differential surface area, dS, is shown which contains a differential charge $dQ = \sigma\, dS$. The magnitude of the tangential velocity for dQ is simply $v = r\omega$. With a magnetic field in the negative x direction and a tangential velocity in the y direction, it is a simple matter of cross product multiplication to show that a force is exerted on the charge, dQ, in the positive z direction. A magnetic field in the x direction would be similar to the tangential magnetic field one would encounter at the equator of the Earth if $\hat{x}$ was pointing towards one of the magnetic poles, i.e., running parallel (north-south) to the surface of the Earth locally. Locally the field would appear uniform.

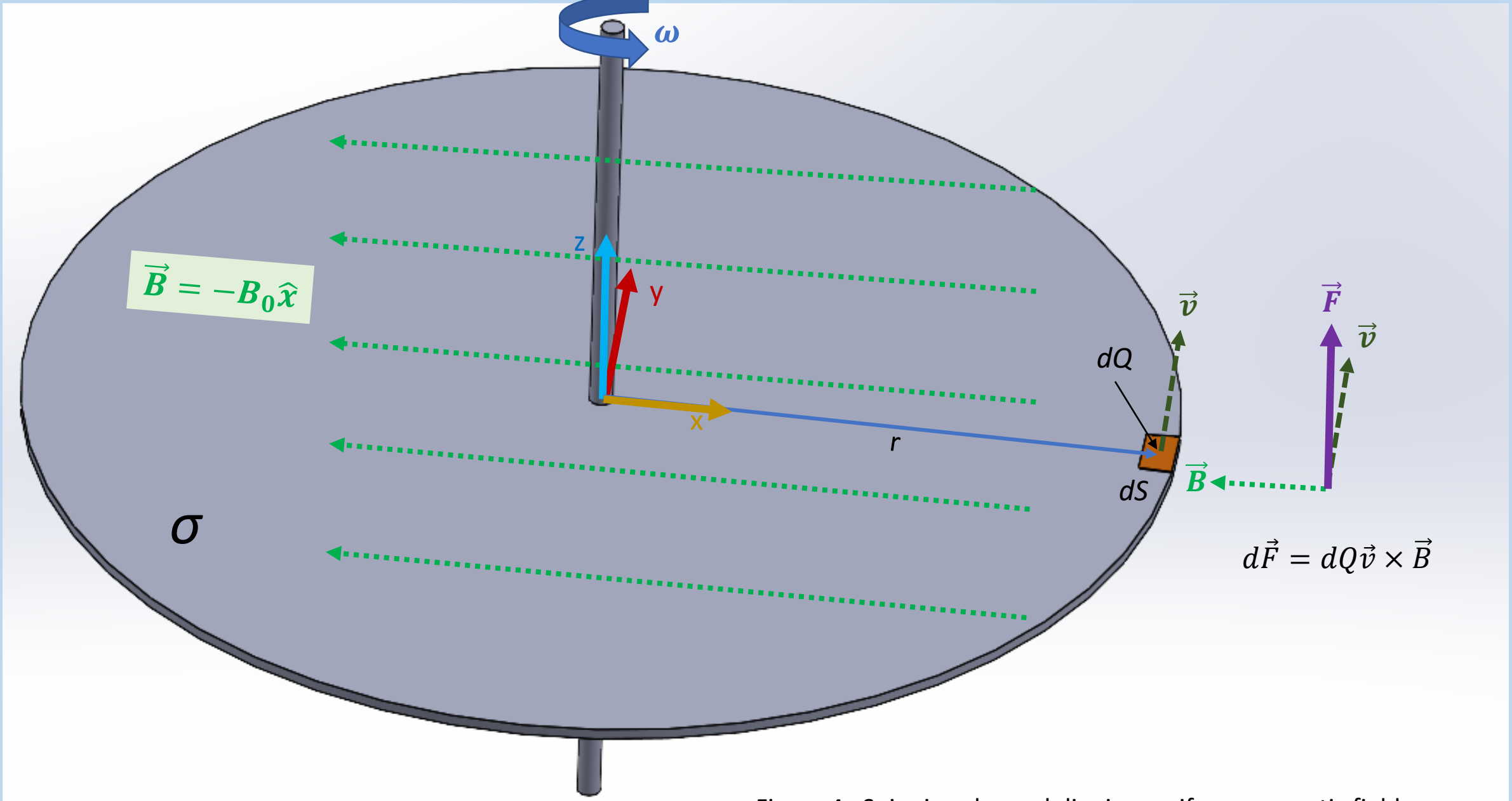

Figure 4. Spinning charged disc in a uniform magnetic field.

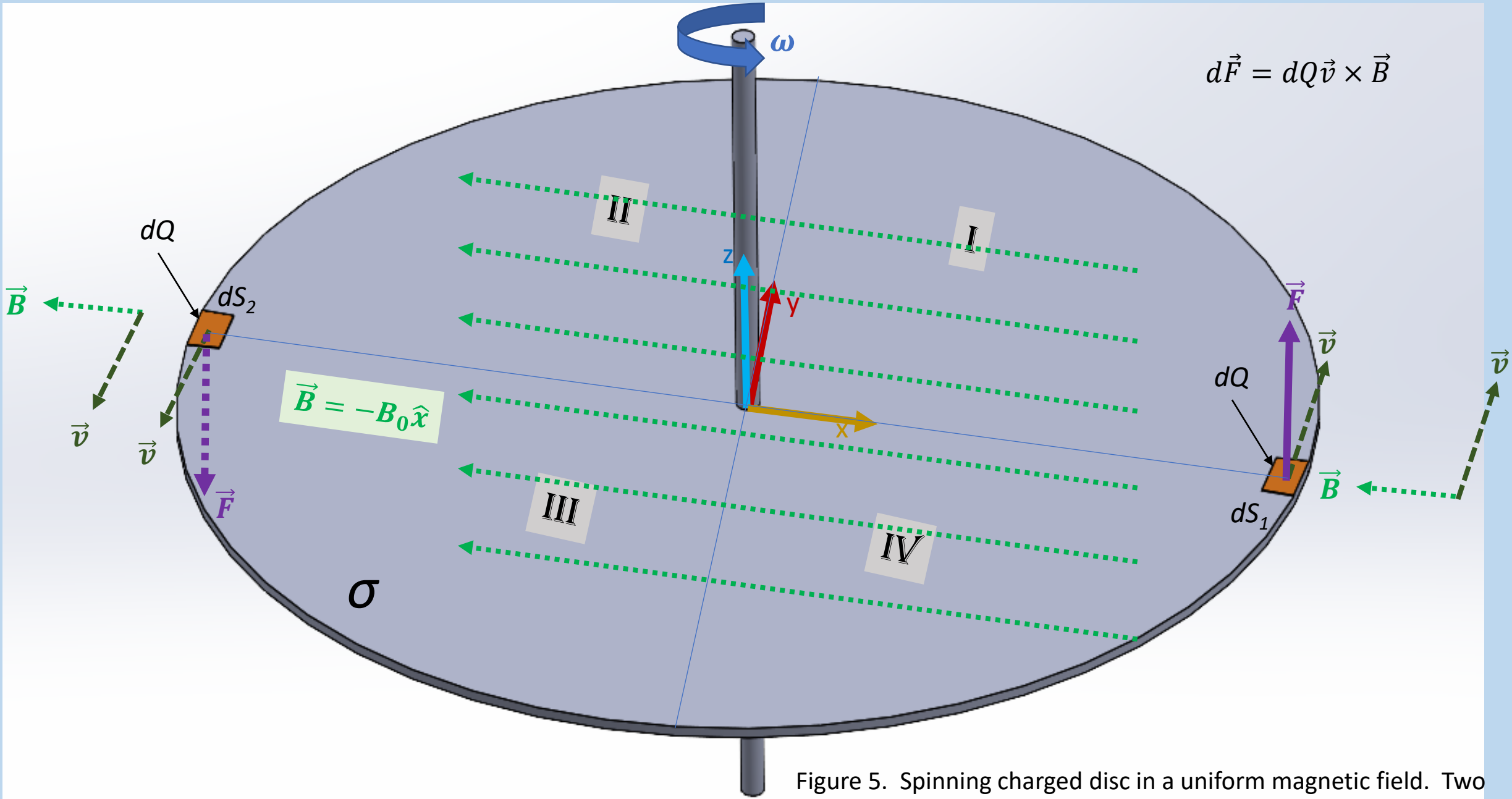

Figure 5. Spinning charged disc in a uniform magnetic field. Two differential areas with corresponding charges, *dQ*, are shown on opposite sides of the disc.

Force on a Spinning Charged Disc

Calculating the force on a spinning charged disc in a uniform magnetic field parallel to the disc; the differential area, *dS*, in cylindrical coordinates is

$dS = rd\varphi dr$.

The differential charge is given by

$dQ = \sigma dS = \sigma r d\varphi dr$.

Plugging *dQ* and *v* in terms of the rotational velocity, $v = r\omega$, into equation 11 yields

$d\vec{F} = dQ\vec{v} \times \vec{B} = (\sigma r d\varphi dr)(r\omega)(\hat{v} \times \vec{B})$.

Since $\vec{v}$ lies in the x-y plane and $\vec{B}$ only has an -x component, $\hat{v} \times \vec{B} = B_0 \sin(\varphi + \frac{\pi}{2})\hat{z}$, therefore,

$d\vec{F} = dQ\vec{v} \times \vec{B} = B_0\, \sigma\, \omega\, r^2\, cos\varphi d\varphi dr\, \hat{z}$ (16)

The force on a wedge of the disc, caused by the magnetic field, can be calculated as

$\vec{F} = B_0\, \sigma\omega \int_{\varphi_1}^{\varphi_2} \int_{R_1}^{R_2} r^2 cos\varphi d\varphi dr\, \hat{z}$ (17)

where φ_1 is the angular start of the wedge and φ_2 is the angular ending of the wedge and R_1 and R_2 are the starting and ending radius of the wedge, see figure 6. Evaluation of equation 17 leads to

$\vec{F} = \frac{1}{3} B_0\, \sigma\omega (R_2^3 - R_1^3)(sin\varphi_2 - sin\varphi_1)\, \hat{z}$ (18) or

$\vec{F} = \frac{1}{3} B_0\, \omega (\frac{Q}{\pi R^2})(R_2^3 - R_1^3)(sin\varphi_2 - sin\varphi_1)\, \hat{z}$ (19)

if written in terms of the total charge on the disc $Q = \sigma(\pi R^2)$.

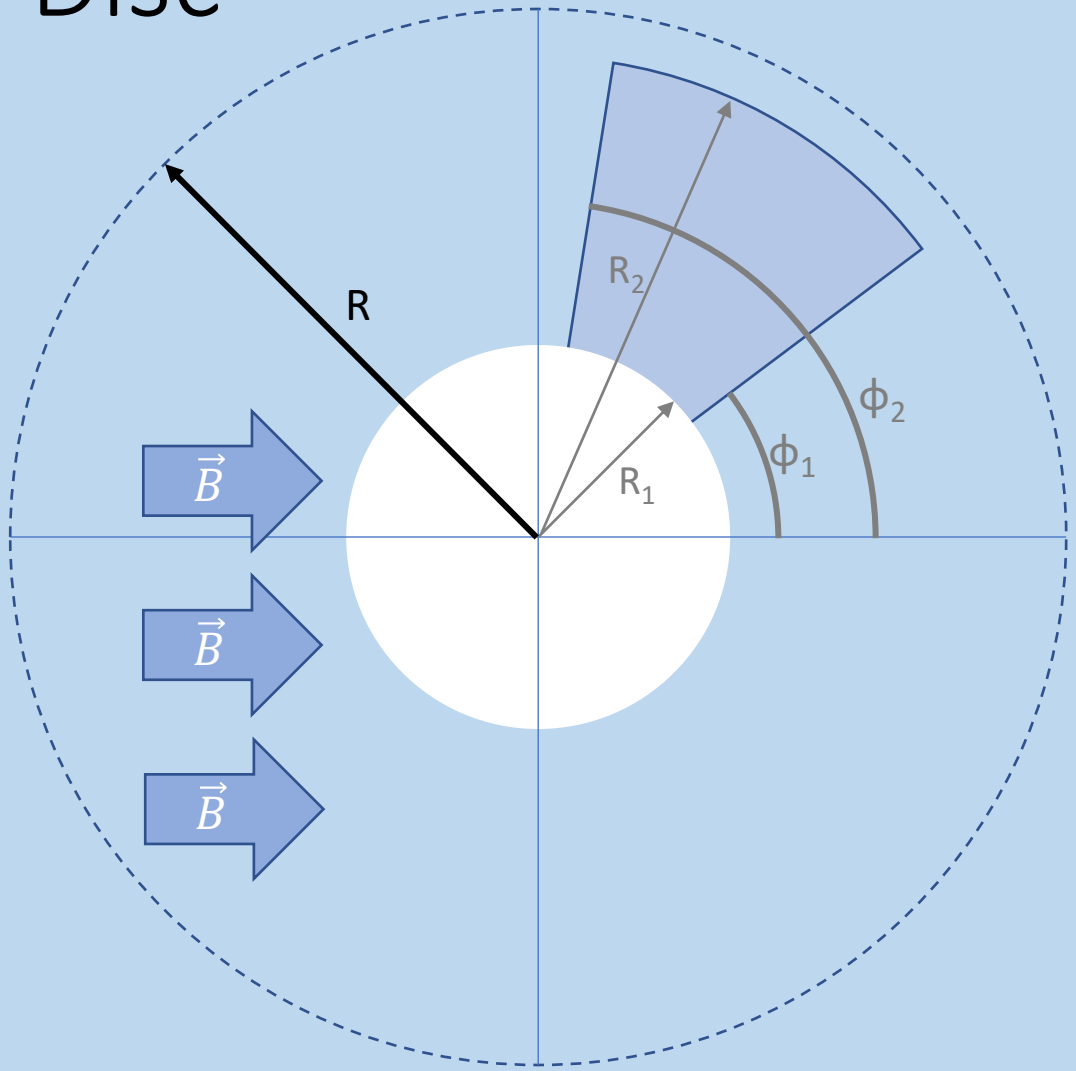

Figure 6. Geometric set up to derive force equations.

Force on a Spinning Charged Disc

If the discs in figure 4 and 5 were a dynamic super-capacitor with counter rotating electrodes, aka discs, the total charge on each electrode would be

$$Q = CV \tag{20}$$

where *C* is the capacitance of the super-capacitor, given by equation 1, and *V* is the voltage difference on the super-capacitor plates. If equation 1 is substituted into equation 20 and equation 20 is then substituted into equation 19, one obtains the total force on a single spinning charged disc. However, since there are two discs of opposite charge spinning in opposite directions, the overall force is doubled, thus the calculated force on a wedge area of the counter-rotating electrode super-capacitor is given as (adding a factor of 2)

$$\vec{F} = \tfrac{2}{3}B_0\,\omega\left(\frac{CV}{\pi R^2}\right)(R_2^3 - R_1^3)(sin\varphi_2 - sin\varphi_1)\,\hat{z}$$

$$\vec{F} = \tfrac{2}{3}B_0\,\omega\left(\frac{\frac{k\varepsilon_0 A}{d}V}{\pi R^2}\right)(R_2^3 - R_1^3)(sin\varphi_2 - sin\varphi_1)\,\hat{z}$$

$$\vec{F} = \tfrac{2}{3}B_0\,\omega\left(\frac{\frac{k\varepsilon_0 \pi R^2}{d}V}{\pi R^2}\right)(R_2^3 - R_1^3)(sin\varphi_2 - sin\varphi_1)\,\hat{z}$$

$$\vec{F} = \tfrac{2}{3}B_0\,\omega\left(\frac{k\varepsilon_0 V}{d}\right)(R_2^3 - R_1^3)(sin\varphi_2 - sin\varphi_1)\,\hat{z} \tag{21}$$

For simplicity, the previous calculations assumed we were at the Earths equator where we assume the magnetic field is tangential to the Earth and lies in the x-y plane, specifically with x pointing towards the poles and y pointing east-west. It should be clear from the mechanics of the cross product that when the charged disc spins in the plane of the magnetic field (i.e., the angular momentum vector of the disc is perpendicular to the external magnetic field), the force on the disc will point along the axis of the angular momentum vector, i.e., perpendicular to the plane of the disc. In other words, the maximum force experienced by the charged spinning disc is perpendicular to the local magnetic field. In spherical coordinates, as long as one is not at the magnetic poles there will always be a radial component to the force, $\hat{R}$, pointing either towards the magnetic center of the Earth or away from it. At the equator there will only be an $\hat{R}$ component pointing towards or away from the center of the Earth. Away from the equator there will also be a north-south, or $\hat{\theta}$ component; assuming the Earth is a semi-perfect magnetic dipole with no appreciable $\hat{\varphi}$ component to its magnetic field, which in general is a good approximation with some local deviations. This discussion is for the configuration shown in figures 4 and 5, other orientations of the DSC electrodes are possible. For the purpose of illustration of the technology, it will be assumed the propulsion system is operating at a point at the equator or directly above the equator for simplicity of understanding, however, operation at the equator is not required to produce forces in the positive R direction (i.e., lift away from the Earth's surface). More will be said on orientation and thrust vector later.

Torque on a Spinning Charged Disc

If equation 18 or 21 is evaluated over the entire disc, one gets a net force of zero. From figure 5 this should be somewhat apparent as regions I and IV provide a force in the positive z direction and regions II and III provide an equal and opposite force in the negative z direction; summing up to zero net force. As is commonly known, these equal and opposite forces produce a torque on current loops in magnetic fields, here the current loops being infinitesimal rings of effective current on the spinning charged discs. The torque on a magnetic dipole is given by

$$\vec{\tau} = \vec{m} \times \vec{B} \qquad (22),$$

where $\vec{m}$ was given earlier in equation 9. Substituting equation 9 into equation 22, yields a torque of

$$\vec{\tau} = \tfrac{1}{4}QR^2\vec{\omega} \times \vec{B} = \tfrac{1}{4}QR^2(\omega\hat{z}) \times (-B_0\hat{x}) = -\frac{1}{4}B_0\omega QR^2\hat{y} \qquad (23)$$

Further using Q = CV, and using equation 1 to calculate the capacitance of this parallel plate super-capacitor, equation 23 can be written as

$$\vec{\tau} = -\frac{1}{2}B_0\omega\frac{k\varepsilon_0\pi R^2 V}{d}R^2\hat{y}$$

$$\vec{\tau} = -\frac{\pi}{2}B_0\omega R^4\frac{k\varepsilon_0 V}{d}\hat{y} \qquad (24)$$

where a factor of two comes in assuming there are two oppositely charged discs that are counter-rotating and both contributing to the torque.

Torque on a Spinning Charged Disc

As an example, the Earth's magnetic field at the equator is approximately 30 x 10^{-6} Tesla running approximately north-south tangent to the Earth's surface. If we consider a parallel dual disc dynamic super-capacitor with the discs counter-spinning at 100,000 RPM (ω = 10,472 rad/s), with a super-dielectric constant of k = 1x10^{9}, a voltage potential of 2 volts, and a dielectric thickness of 5 microns, all on a one-meter radius disc, the calculated torque from equation 24 is about 1750 N-m (1290 ft-lbs) about the y-axis. This is the equivalent torque of an average sized semi-truck. This is an impressive amount of torque considering this dynamic super-capacitor 'motor' uses the Earth's magnetic field as its permanent magnet component.

While it is practical to do analytic calculations for simple geometries such as a single spinning disc or a pair of discs, it can become intractable for complex geometries. Moving forward, magnetic fields, torques, and forces can be closely approximated by the finite element method (FEM or FEA). An ANSYS Maxwell3D™ model predicts the torque on the aforementioned counter-rotating charged disc super-capacitor in the Earth's magnetic field at the equator to be approximately 1746 N-m (1288 ft-lbs), in excellent agreement with the earlier analytical calculation of 1750 N-m. Figure 7 shows the Maxwell3D disc model with mesh. Figure 8 shows the disc with a notional torque transfer shaft if one wished to convert the torque to work.

It is worth noting from equation 24 that the torque goes as the radius of the disc(s) to the 4th power. This means large diameter discs can generate extremely large torques. As an example, a 10-meter disc with all other parameters the same would generate a torque over 17,000,000 Newton-meters (12,800,000 ft-lbs) at the equator; this is more than twice the torque generated by the Wärtsilä-Sulzer RTA96-C engine [10], the largest container cargo ship engine in existence today. However, it would be difficult to build a disc this size that rotates at 100,000 RPM at this writing, but nonetheless shows the power and potential of the technology. From equation 24, it can be seen the torque goes linearly with the radial velocity, ω, while going to the fourth power of the radius of the discs; therefore, even a 10-m disc spinning at 1,000 RPM would generate a torque over 174,000 N-m (128,000 ft-lbs); about four times that of the GE AC6000CW locomotive engine [11], one of the most powerful commercial locomotive engines available today.

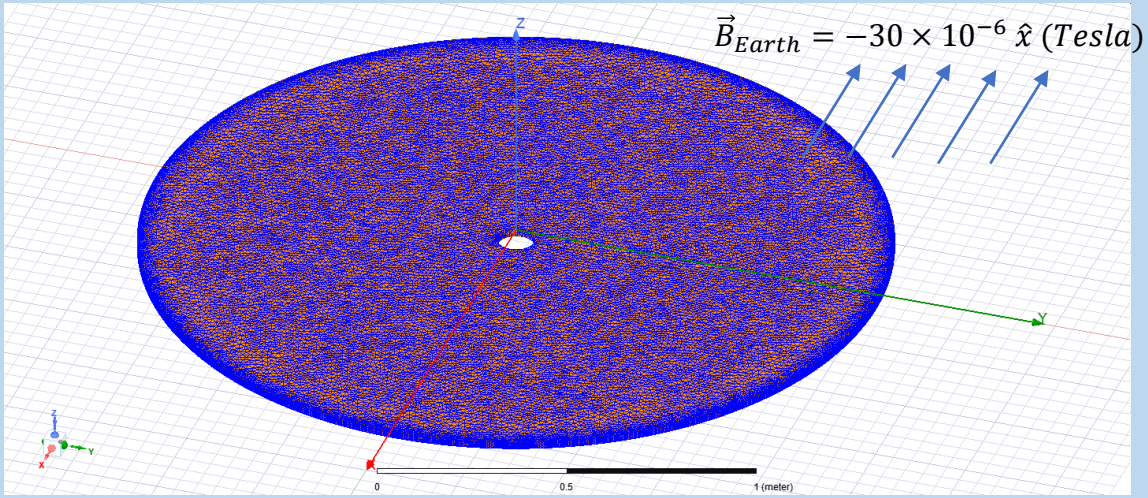

Figure 7. ANSYS Maxwell3D™ model of charged spinning disc from figure 5. Meshed for Finite Element Analysis (FEM or FEA).

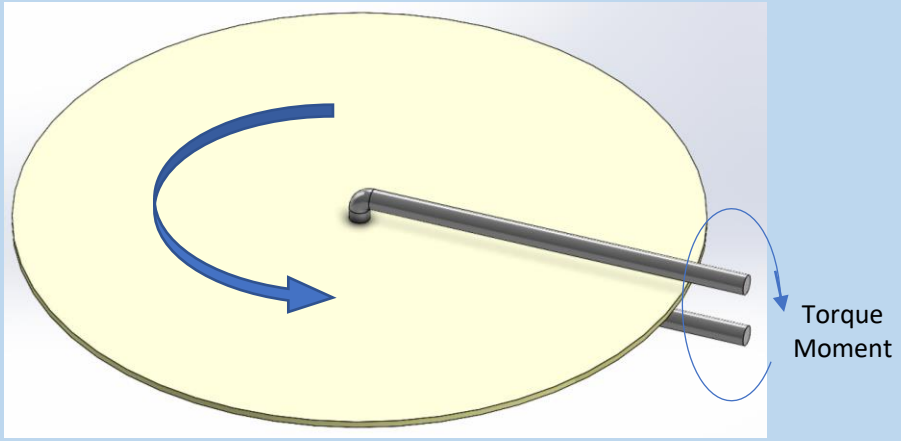

Figure 8. Spinning disc with notional torque transfer shaft.

Lift of a Charged Spinning Disc

Torque does not produce lift or thrust directly, however, the torque calculations and simulations are good benchmarks for modeling and also demonstrate the magnitude of the forces that can be generated by dynamic super-capacitors using the Earth's magnetic field. Net forces generated from the interaction of the electromagnetic fields, i.e., between the Earth and the dynamic super-capacitor(s), play the central role in the production of lift/thrust capable of propelling a craft.

It can be shown from equation 21 that the net force on a charged spinning disc in a uniform magnetic field is zero. The net zero force is simply due to the axisymmetric nature of the effective current and homogeneity of the external magnetic field. If the symmetry or homogeneity of the system is broken, then the system will experience a net force (i.e., thrust or lift). The first method of breaking this symmetry is to break the uniformity of the external magnetic field the propulsion system components experiences. If parts of the disc are shielded from the external magnetic field, then the charged particles within those shielded areas will not experience an externally induced force

$d\vec{F} = dQ\vec{v} \times \vec{B}_{ext}$ in non-shielded areas

$d\vec{F} = dQ\vec{v} \times \vec{0} = 0$ in shielded areas.

Looking at figure 5, if the external magnetic field is shielded in quadrants II and III, and unshielded in quadrants I and IV, then equation 21 reduces to

$$\vec{F} = \tfrac{4}{3} B_0\, \omega \left(\frac{k\varepsilon_0 V}{d}\right) R^3\, \hat{z} \qquad (25),$$

where R is the radius of the disc. A one-meter radius disc spinning at 100,000 RPM, with k = 1 x 10^9, V = 2 volts, and d = 2 microns at the Earth's equator yields a force of about 3709 Newtons (834 lbs) in the z-direction, i.e., away from the Earth - lift. Notice in equation 25 that the lift goes linearly as the rotational velocity and as the cube of the radius of the disc. A 10-meter disc spinning at a rotation rate of 1000 RPM produces the same lift of 3709 N (834 lbs) as the one-meter disc spinning at 100,000 RPM. Figure 9 shows the spinning disc(s) with a magnetic shielding element. A central shaft attaches to a top disc and a second shaft (not visible) attaches to the bottom disc. These shafts transfer rotational energy to the discs and subsequently transfer the force generated from the discs to the craft. It is assumed these shafts rotate in opposite directions for the two oppositely charged discs, however, if only one disc is rotated, only a single shaft is needed. However, it is desirable to have counter-rotation such that reactionary torques cancel out. If the discs are not counter rotated, a net-reactionary torque will be experienced and must be accommodated somewhere else in the craft, such as with a separate balanced flywheel, otherwise, the propulsion system and craft will experience a net reactionary torque which will build unwanted angular momentum in the system/craft. A simulation of the model shown in figure 9, with a perfect magnetic shield, gives a result of 3340 N (750 lbs) in the positive z-direction. The simulation result is in reasonable agreement with the analytically calculated value of 3709 N (834 lbs).

Figure 10 shows a plot of the relationship between Lift versus Radius of the Discs and Rotational Speed as calculated from equation 21. Table 1 shows selected values from this chart for reference. As can be seen, large radii disc spinning at high rotational rates are capable of producing tremendous lifts in the Earth's magnetic field. Of course, building large diameter discs that rotate at such high rates can be an engineering challenge, however, even smaller diameter discs at moderate rotational speeds can generate significant lift.

The magnitude of the electromagnetic stresses produced by the dynamic super-capacitor itself can also be a limiting factor. The intrinsic electromagnetic stresses induced in the dynamic super-capacitor can be calculated using equation 15 and can result in large electromagnetic stresses depending on the diameter and rotational speed of the discs. Ideally the assemblies described would be constructed of ultra-strong materials such as diamond, sapphire, silicon carbide, strong ceramics, or other ultra-strong materials.

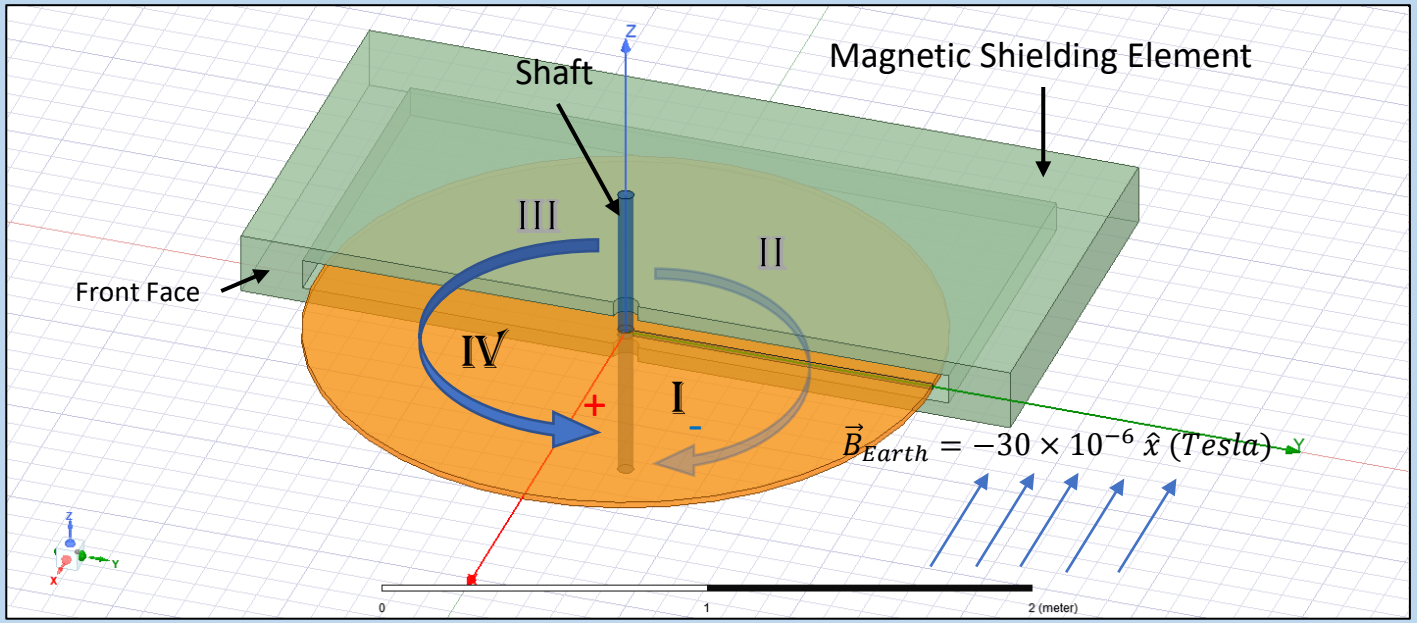

Figure 9. ANSYS Maxwell™ model of oppositely charged counter-rotating discs with magnetic shielding element. The shielding element blocks half of the disc from 'seeing' the external magnetic field (i.e., Earth's magnetic field at the equator ~30 x 10^{-6} Tesla). It is assumed positive charged disc is on top and rotates in the counterclockwise direction and the negatively charged disc is on the bottom and rotates in the clockwise direction, though the converse will work as well. The discs rotate, the shield remains stationary.

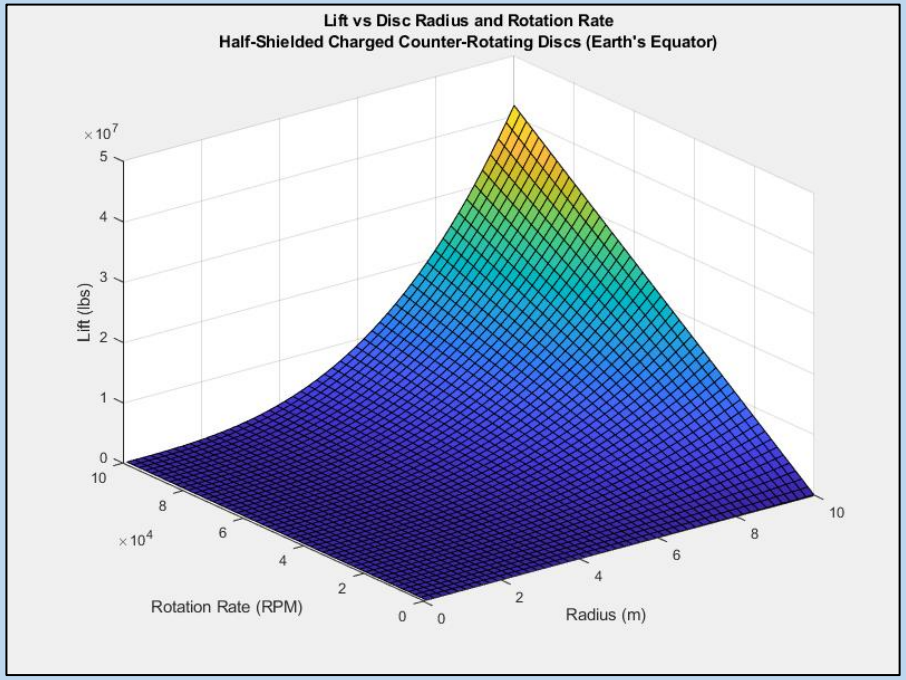

Figure 10. Relationship between Lift versus Disc Radius and Rotation Speed. Pair of counter-rotating oppositely charged discs. k = 1 x 10^9, V = 2 volts, d = 2 microns.

Disc Radius (m) / RPM	0.1	0.5125	0.925	1.3375	1.75	2.1625	2.575	2.9875	3.4	3.8125	4.225	4.6375	5.05	5.4625	5.875	6.2875	6.7	7.1125	7.525	7.9375	8.35	8.7625	9.175	9.5875	10
100	0	1	5	15	31	57	94	145	211	294	397	522	671	845	1047	1279	1543	1841	2175	2547	2960	3415	3914	4459	5053
4262.5	1	25	114	314	668	1220	2015	3096	4508	6295	8500	11169	14345	18072	22394	27356	33002	39375	46521	54482	63303	73029	83703	95370	108073
8425	2	48	223	613	1304	2383	3935	6047	8805	12295	16603	21815	28019	35299	43741	53434	64461	76910	90866	106417	123647	142644	163493	186280	211093
12587.5	3	71	332	912	1941	3546	5856	8998	13102	18295	24706	32462	41693	52525	65089	79511	95920	114444	135212	158351	183991	212258	243282	277191	314112
16750	3	95	441	1212	2578	4709	7776	11950	17399	24295	32808	43109	55367	69752	86436	105588	127379	151978	179557	210286	244334	281873	323072	368101	417132
20912.5	4	118	550	1511	3214	5872	9697	14901	21696	30296	40911	53755	69041	86979	107783	131665	158838	189513	223903	262221	304678	351487	402861	459012	520152
25075	5	142	659	1810	3851	7035	11617	17852	25993	36296	49014	64402	82714	104206	129130	157742	190297	227047	268249	314155	365022	421102	482651	549923	623172
29237.5	6	165	767	2109	4487	8198	13538	20803	30290	42296	57117	75049	96388	121433	150478	183820	221756	264582	312594	366090	425365	490717	562441	640833	726192
33400	7	189	876	2409	5124	9361	15458	23754	34587	48296	65219	85695	110062	138659	171825	209897	253214	302116	356940	418025	485709	560331	642230	731744	829211
37562.5	8	212	985	2708	5761	10524	17379	26705	38884	54297	73322	96342	123736	155886	193172	235974	284673	339650	401285	469959	546053	629946	722020	822655	932231
41725	9	235	1094	3007	6397	11687	19299	29657	43182	60297	81425	106989	137410	173113	214519	262051	316132	377185	445631	521894	606396	699560	801809	913565	1035251
45887.5	9	259	1203	3306	7034	12850	21220	32608	47479	66297	89528	117635	151084	190340	235866	288129	347591	414719	489977	573829	666740	769175	881599	1004476	1138271
50050	10	282	1312	3606	7670	14013	23140	35559	51776	72297	97630	128282	164758	207567	257214	314206	379050	452253	534322	625763	727084	838790	961388	1095386	1241290
54212.5	11	306	1421	3905	8307	15176	25061	38510	56073	78297	105733	138928	178432	224793	278561	340283	410509	489788	578668	677698	787427	908404	1041178	1186297	1344310
58375	12	329	1529	4204	8944	16339	26981	41461	60370	84298	113836	149575	192106	242020	299908	366360	441968	527322	623013	729633	847771	978019	1120967	1277208	1447330
62537.5	13	352	1638	4503	9580	17502	28902	44413	64667	90298	121939	160222	205780	259247	321255	392438	473427	564857	667359	781567	908115	1047633	1200757	1368118	1550350
66700	14	376	1747	4802	10217	18665	30822	47364	68964	96298	130041	170868	219454	276474	342602	418515	504886	602391	711705	833502	968458	1117248	1280547	1459029	1653370
70862.5	14	399	1856	5102	10853	19828	32743	50315	73261	102298	138144	181515	233128	293701	363950	444592	536345	639925	756050	885437	1028802	1186863	1360336	1549939	1756389
75025	15	423	1965	5401	11490	20991	34664	53266	77558	108299	146247	192162	246802	310927	385297	470669	567804	677460	800396	937371	1089145	1256477	1440126	1640850	1859409
79187.5	16	446	2074	5700	12127	22154	36584	56217	81855	114299	154350	202808	260476	328154	406644	496746	599263	714994	844741	989306	1149489	1326092	1519915	1731761	1962429
83350	17	470	2183	5999	12763	23317	38505	59169	86152	120299	162452	213455	274150	345381	427991	522824	630722	752528	889087	1041241	1209833	1395706	1599705	1822671	2065449
87512.5	18	493	2291	6299	13400	24480	40425	62120	90449	126299	170555	224101	287824	362608	449338	548901	662181	790063	933433	1093175	1270176	1465321	1679494	1913582	2168469
91675	19	516	2400	6598	14036	25643	42346	65071	94747	132300	178658	234748	301498	379835	470686	574978	693640	827597	977778	1145110	1330520	1534936	1759284	2004492	2271488
95837.5	20	540	2509	6897	14673	26806	44266	68022	99044	138300	186761	245395	315172	397062	492033	601055	725098	865131	1022124	1197045	1390864	1604550	1839073	2095403	2374508
100000	20	563	2618	7196	15310	27969	46187	70973	103341	144300	194863	256041	328846	414288	513380	627133	756557	902666	1066469	1248979	1451207	1674165	1918863	2186314	2477528

Table 1. Relationship between Lift (in lbs) versus Disc Radius and Rotation Speed (rotations per minute). Pair of counter-rotating oppositely charged discs. $k = 1 \times 10^9$, V = 2 volts, d = 2 microns.

Breaking Symmetry

To break the symmetry of the external uniform field, magnetic shielding is required. Common magnetic shielding is typically constructed of ferromagnetic materials. However, most ferromagnetic materials saturate on the order of about a tesla. Ferromagnetic materials are also typically thick and heavy. Additionally, ferromagnetic materials would be strongly attracted to the ultra-magnet created by the dynamic super-capacitor. As an alternative, the magnetic shielding element can be constructed of super-conducting material. Super-conductors are capable of repelling large magnetic fields, due to the Meissner effect; figure 11 shows a chart of a number of superconducting materials and their corresponding breakdown fields [12, 13, 14], i.e., the maximum magnetic field the superconductor can withstand. Superconductors can also be made thin and lightweight, though cryogenic cooling is required and is a notable drawback. It should be noted that it is important the superconductor shield be cooled in the absence of magnetic fields, i.e., the zero-field cooled (ZFC) condition.

The characteristics of the spinning discs,- spin rate, charge, radius, etc.; and the design and choice of material for the shielding element should be chosen such that the superconductor shield does not experience a magnetic field in excess of its breakdown field at any point, otherwise quenching will occur which causes the superconductor to lose its superconductivity. Avoidance of superconductor magnetic breakdown can be achieved by either limiting the magnetic field strength produced by the dynamic super-capacitor and/or ensuring that the surfaces of the superconductor shield are spaced far enough away from the dynamic super-capacitor such that the field strength from the dynamic super-capacitor has dropped to a safe level before encountering the superconductor shield. Figure 12 shows an edge on view of the magnetic field strength around the spinning discs described in the prior torque example, figure 7. It can be seen that the field strength drops rapidly as one moves away from the discs, reaching safe magnetic field strength levels for the superconducting materials in relatively short distances. It is also worth noting that the strongest magnetic fields are near the center of the disc. The strongest effective currents, which are responsible for the lift, are towards the outside of the disc (figure 13), where the magnetic field produced by the discs is least strong and extends the least distance, a favorable outcome. Figure 14, shows the magnetic shield being removed in the volume where superconductor magnetic quenching would occur; simulation predicts no significant penalty in lift is experienced. The resistance of the superconductor to magnetic quenching may also be enhanced. Research has shown that coating superconductors with nano-meter thick layers of gold can increase the superconductor's resistance to magnetic fields by up to an order of magnitude [15]. Recent research into atomically thin superconductors has also shown a greatly enhanced resistance to magnetic fields [16] which may be employed in the superconducting magnetic shielding component, multiple atomically thin superconductor stacked layers for instance.

The net center of force produced from the disc will not be collinear with the axis of rotation of the discs, it will be offset as shown in figure 14. This will produce a net torque around the y-axis. The simplest solution to keep the net torque at zero on the craft is to have a companion DSC unit that mirrors the base unit. Figure 15 shows a side-by-side configuration in which either the disc polarities are reversed or the discs spin in opposite directions on the companion unit. Shown is only one of many possible configurations, such as the units could be stacked or back-to-back. The selected unit(s)-companion unit(s) layout depends on the design requirements of the craft; figure 15 is only an illustrative example, it serves to highlight the need for a companion (or counter) propulsion unit to counteract potentially unwanted torques in the system. For simplicity this is the only time the counter unit will be mentioned, it will be assumed to be present as a mirror of the base unit under discussion from here on out. The counter-unit need not be in close proximity to the base unit to perform its function. The complementary unit also doubles the lift/thrust force experienced by the overall system.

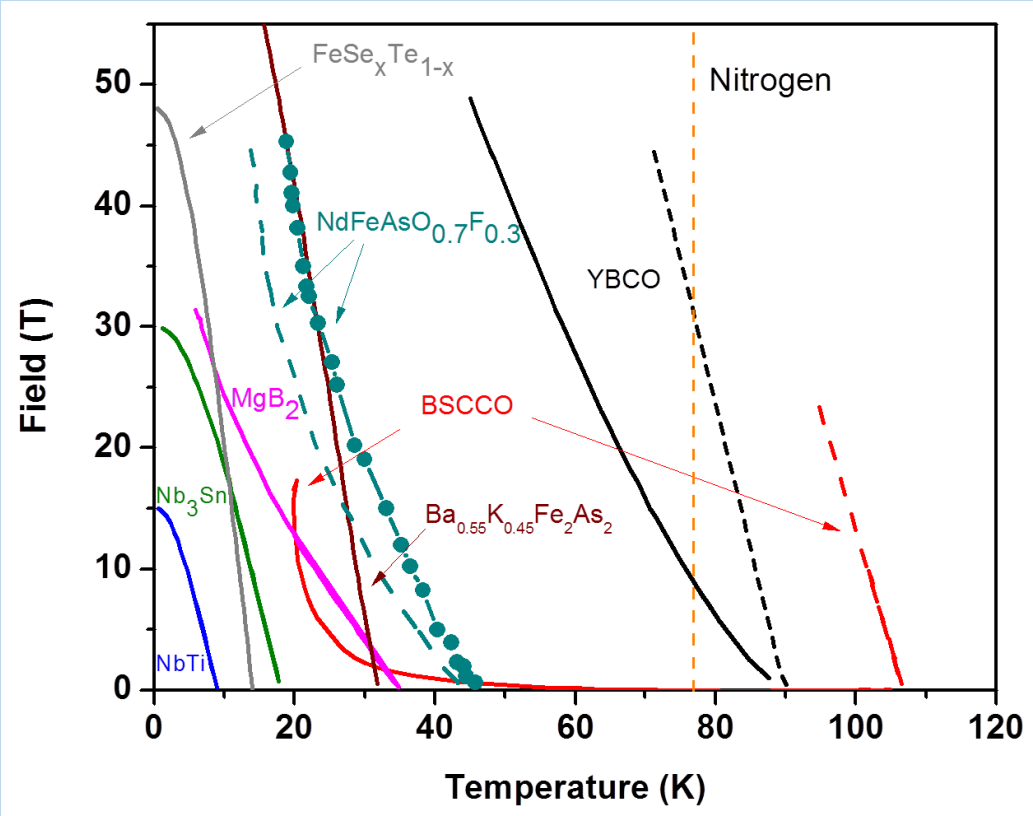

Figure 11. Superconductors and the maximum magnetic fields they can withstand, vs temperature, before losing their superconductivity [12, 13, 14].

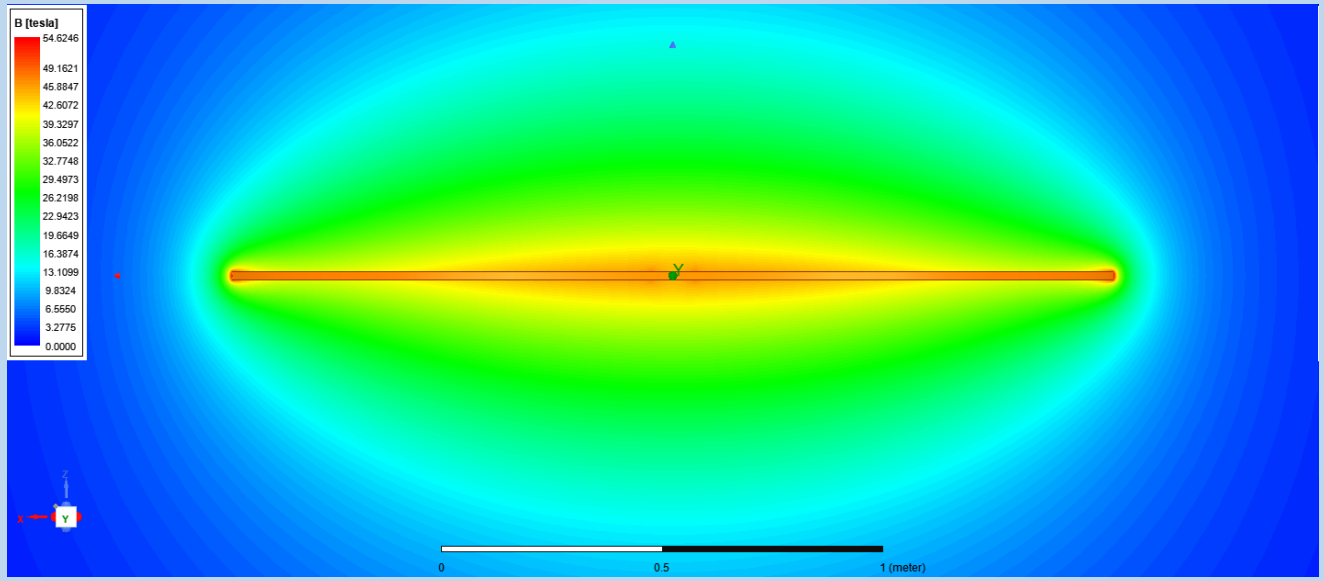

Figure 12. Magnetic field strength surrounding the spinning charged disc of figure 7.

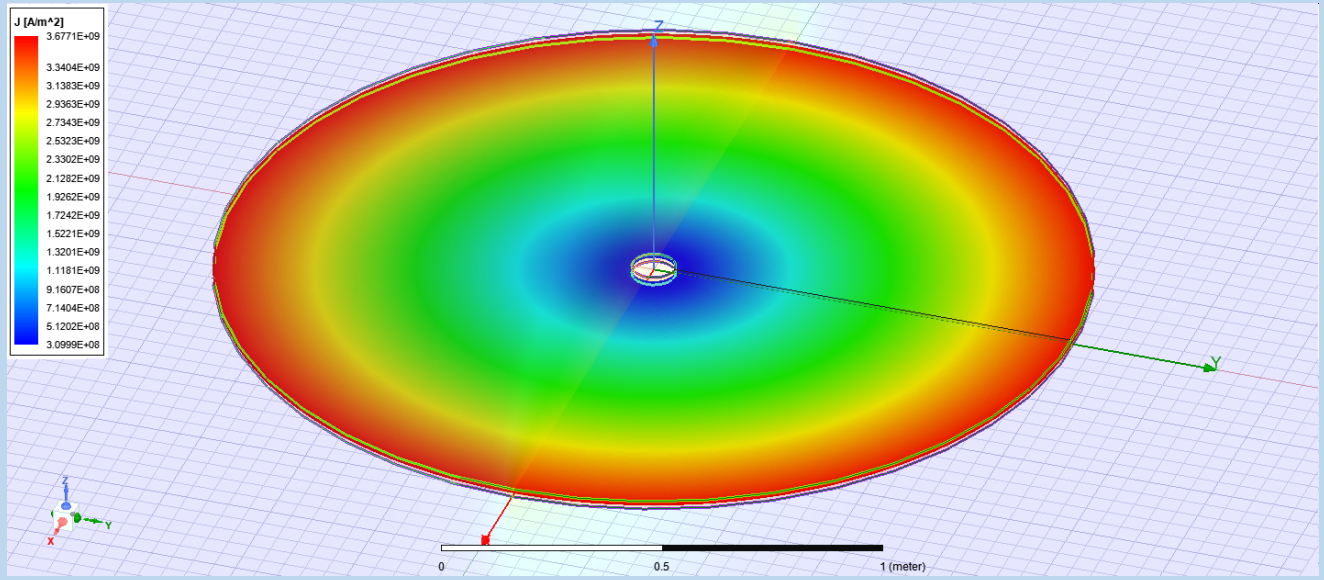

Figure 13. Effective current distribution of the spinning discs of figure 7. Thickness of assembly is 2 cm.

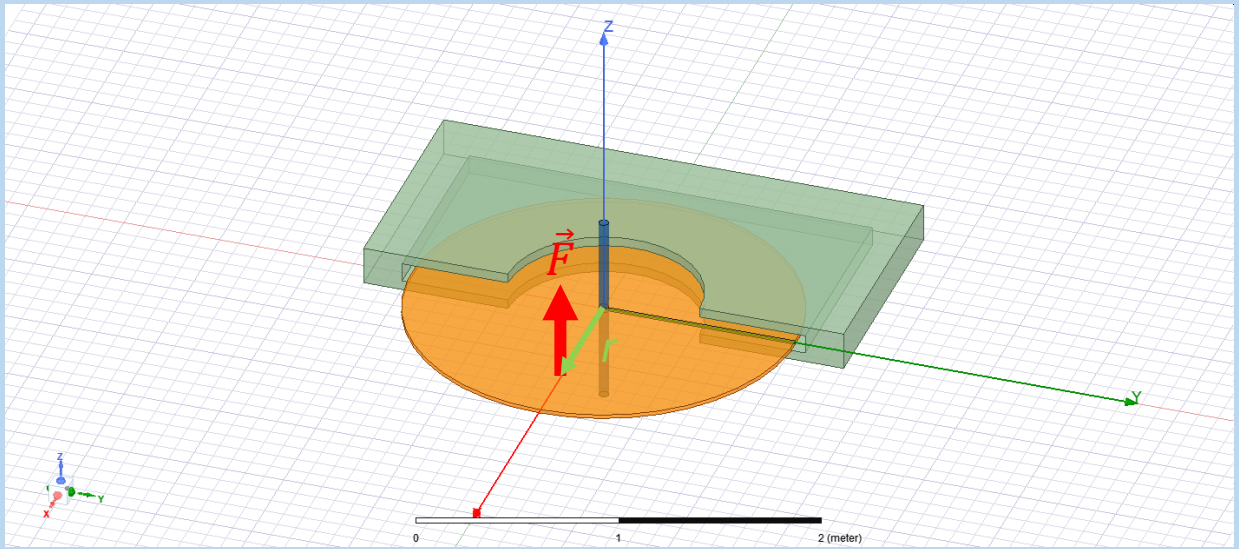

Figure 14. Superconductor magnetic shield removed in volume where the hazard of magnetic quenching could occur (assuming no magnetic hardening of the superconductor material), e.g., greater than 45 Tesla. One meter radius super-capacitor counter-rotating discs, k = 1 x 10^9, V = volts, d = 2 microns, RPM = 100,000. Also shown the off-axis net lift force creating a moment about the y-axis.

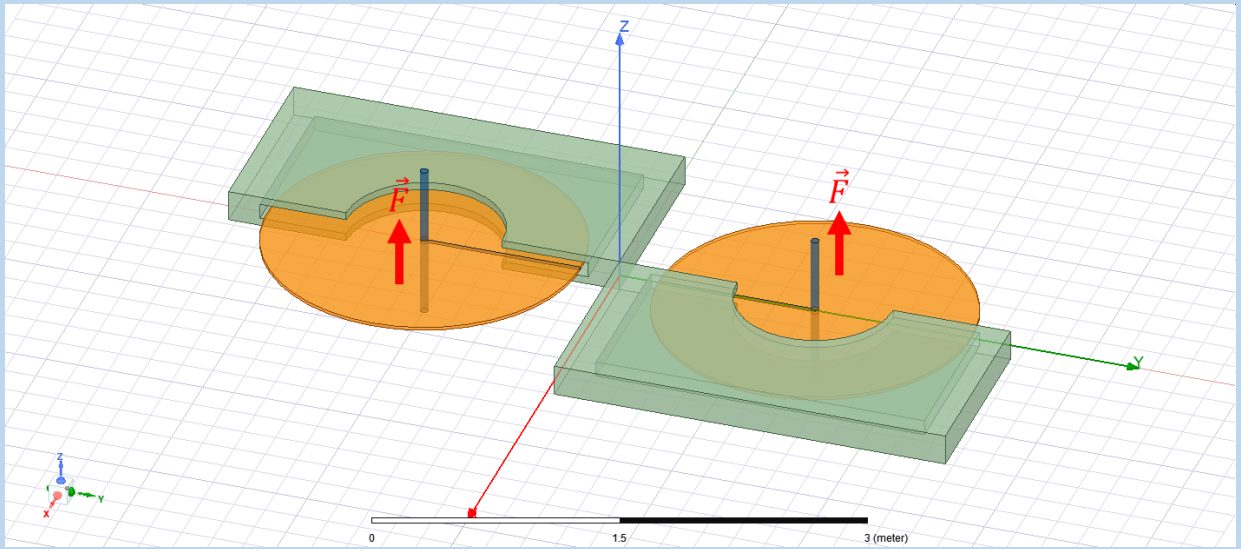

Figure 15. Complementary propulsion unit to negate the resulting torque moment about the y-axis. Either the polarity of the discs need to be reversed on the second unit or the direction of spin needs to be reversed.

Throttling the Lift

One of the advantages to the current invention is the ability to energize the propulsion system before the craft lifts off e.g., while still on the ground or launch pad. The dynamic super-capacitor can be charged and put into motion before the craft is released. This saves on the amount of energy needed to achieve orbit. Over time the system will lose energy due to non-conservative forces, but the bulk of energy can be supplied to the propulsion system before lift off. This means a smaller on-board power source can be used to compensate for non-conservative losses (e.g., frictional/drag elements) and the potential and kinetic energy required to lift the craft into orbit.

The magnitude of lift the propulsion system produces can be adjusted from zero up to the maximum amount achievable by adjusting the position of the magnetic shielding. Shown in figure 9 the external magnetic field intersects the front face of the magnetic shielding; in other words, the external magnetic field is perpendicular to the front face of the magnetic shield. This produces the maximum amount of lift; both regions I and IV produce positive z-axis lift, regions II and III produce near zero lift due to shadowing of the external magnetic field by the magnetic shield. If the magnetic shield front face runs parallel to the external magnetic field, rotating the magnetic shield 90 degrees, produces a net zero z-axis force; a positive z-axis force in region I and an equal and opposite, negative, force in region II. This will result in a net torque on the system. To avoid a net torque on the system a second disc pair should be implemented, figure 16, with the second magnetic shield 180 degrees to the first magnetic shield. This will balance the torques, resulting in a net zero torque. Any lift between zero and the maximum achievable can be obtained by rotating the shielding at intermediate angles relative to the external magnetic field. Also note, rotating the shielding in figure 9 by 180 degrees will produce the maximum force in the negative z-direction, so it is equally possible to provide a force towards the Earth as well as away from the Earth. The second unit can also be the complementary-unit as described previously, figure 15. Only how the shielding is rotated will change, the complementary unit being rotated 180 degrees to that shown in figure 16.

It should be apparent that while a single rotating disc pair DSC has been discussed for instructional purposes, any number of stacked super capacitors can be employed to amplify the total lift the system can produce. For instance, the configuration in figure 16(a) can produce approximately twice the lift of a single dynamic super-capacitor. A system with four dynamic super capacitors would produce approximately four times the lift of a single dynamic super-capacitor and so on. Multiple super-capacitors can be used with a single magnetic shield if the maximum magnetic flux density of the superconductor is not exceeded. Figure 17 shows five dynamic super-capacitors with a single shield with a 0.5-meter radius section removed from the center of the shield. This is based on the multi-electrode disc ultra-magnet (MDU) described in serial number 63/162,137. The simulated lift is 7358 Newtons (1654 lbs) for a 5-micron thick dielectric (d = 5 um) and 18,396 Newtons (4135 lbs) for a 2-micron thick dielectric (d = 2um). Because of the large magnetic fields involved, nanometer layer gold coated superconductors with enhanced magnetic resistance may be required as described by Wu, Adams, Yang, and McCarley [15] or atomically thick superconductor layers as described by Yoshizawa et al [16].

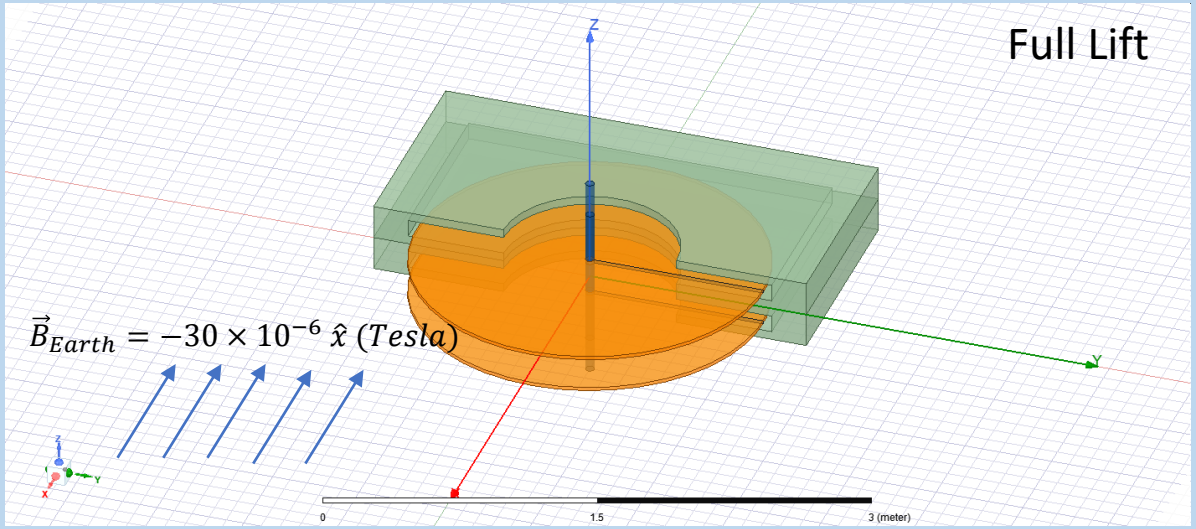

(a)

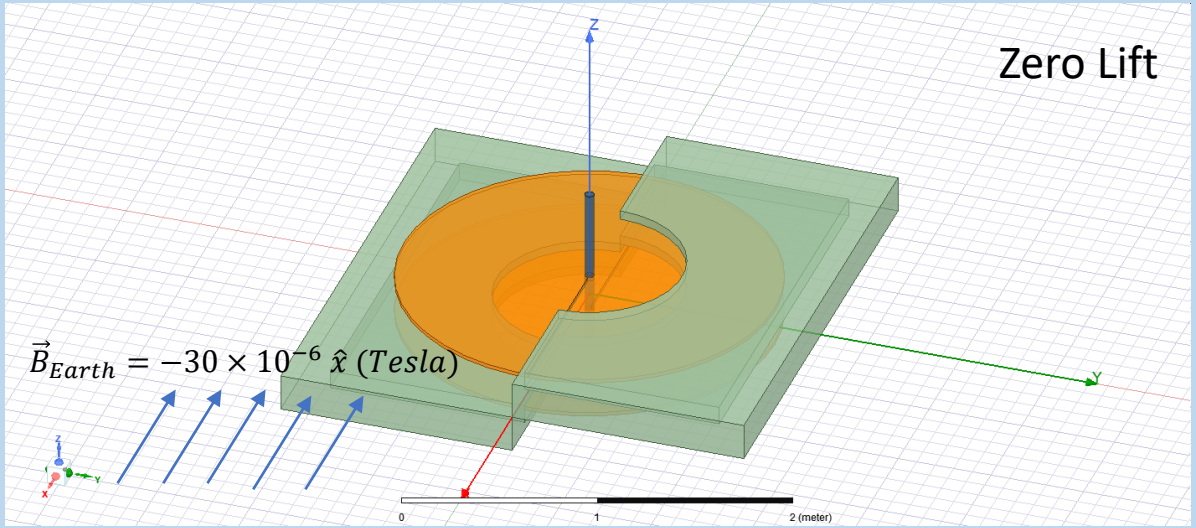

(b)

Figure 16. Dynamic super-capacitor pair with shielding configured to produce (a) maximum lift, (b) configured to produce zero lift.

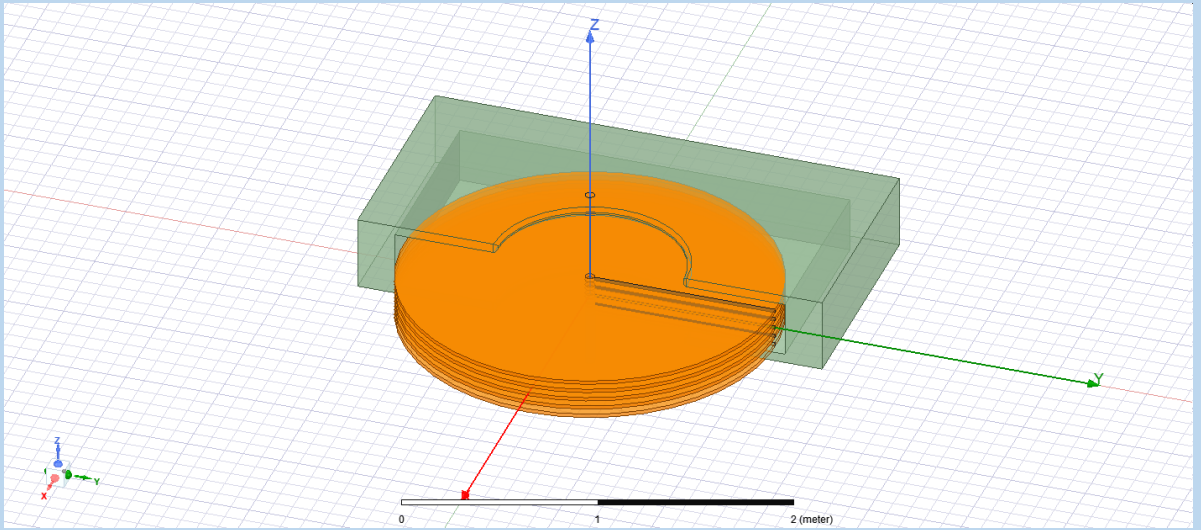

(a)

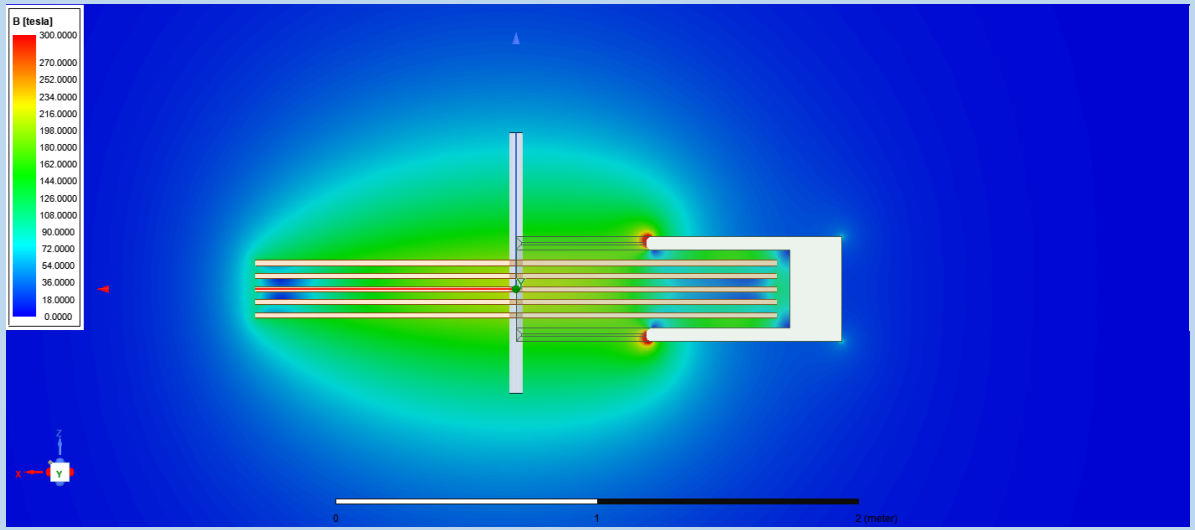

(b)

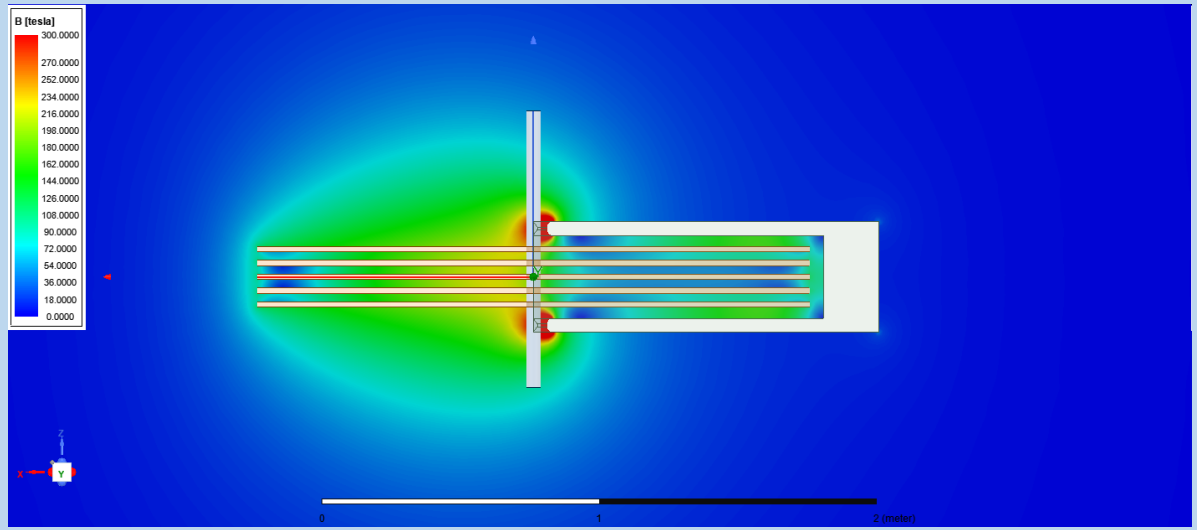

(c)

Figure 17. (a) Five dynamic disc super-capacitors with a single superconductor magnetic shield; based on the multi-electrode disc ultra-magnet (MDU). (b) Magnetic field distribution for five-micron thick super-dielectric (d = 5 um) case, center 0.5-meter radius removed from magnetic shield. (c) With center 0.05-meter radius removed from magnetic shield. R = 1 meter, center r = 0.5 meter removed from shield; RPM = 100,000; V = 2 volts; k = 1 x 10^9. ANSYS Maxwell™ simulations.

Breaking the Symmetry, Current $\vec{J}$

Breaking the symmetry of the external magnetic field, in the exemplary case the Earth's locally uniform magnetic field, is one method of breaking the symmetry and producing lift as discussed so far. Another way to break symmetry and produce lift is to break the symmetry of the effective current distribution, $\vec{J}$. This allows forgoing the use of magnetic shielding as previously shown.

Figure 13 shows the current density profile of a uniformly charged disc in axial rotational motion. As can be seen this current density profile is axisymmetric and as discussed produces a net zero force in a uniform magnetic field when unshielded. This effective current density profile can be modified to produce lift in regions I through IV of the disc. This can be achieved by segmenting the super-capacitor into individual regions, electrically isolated from one another, and reversing the polarity of the charge on the regional electrodes as they pass tangent to the external magnetic field, see figure 18. For conceptual purposes, the segments are shown as 45-degree wedges. In practice, these segments would likely be much smaller. The top plate electrode is shown. The bottom electrode would have the opposite polarity profile and spin in the opposite direction. It should be noted that, as always, it is not mandatory that both discs spin, spinning both discs simply doubles the effective current and balances the reactionary torque.

It is apparent from equations 11 and 12, and the nature of the right-hand rule for the cross product, that the configuration shown in figure 18a produces lift (force out of the page) throughout the entire rotation of the disc. Figure 19 shows the effective current distribution for the configuration shown in figure 18a at that instant in time. It should be apparent there will be a transient period in which the charge polarization of the segment is reversed at the plane of polarity change. In figure 18a, the charge has been fully transferred before the edge of the wedge (aka segment) falls on the plane of polarity change.

Figure 18b shows a side view schematic of the segmented two-disc electrode configuration with mercury as the conductive slip joint fluid between them. Due to strength and weight considerations and the strong internal electromagnetic stresses on the components very strong materials, such as ceramics, crystals, or composites can be used as the substrate material and can further be made conductive by metal coating/plating. The metal plating can be deposited by vapor deposition (e.g., thermal or e-beam evaporation) and electroplating if thicker layers are needed. Thicknesses from nanometers to many microns are achievable. The metal can be selectively removed by lithography and etching, not unlike the traces on a printed circuit board (PCB). Anyone familiar in the art of microchip fabrication will readily understand the patterning process. An insulator can be deposited in the etched areas to prevent shorting to the conductive slip-joint fluid. In figure 18b, the insulating points are shown offset as a reminder the discs are in relative motion to one another. The charges are also shown reversed on top and bottom as a reminder the bottom segments have the opposite polarity to the top segments.

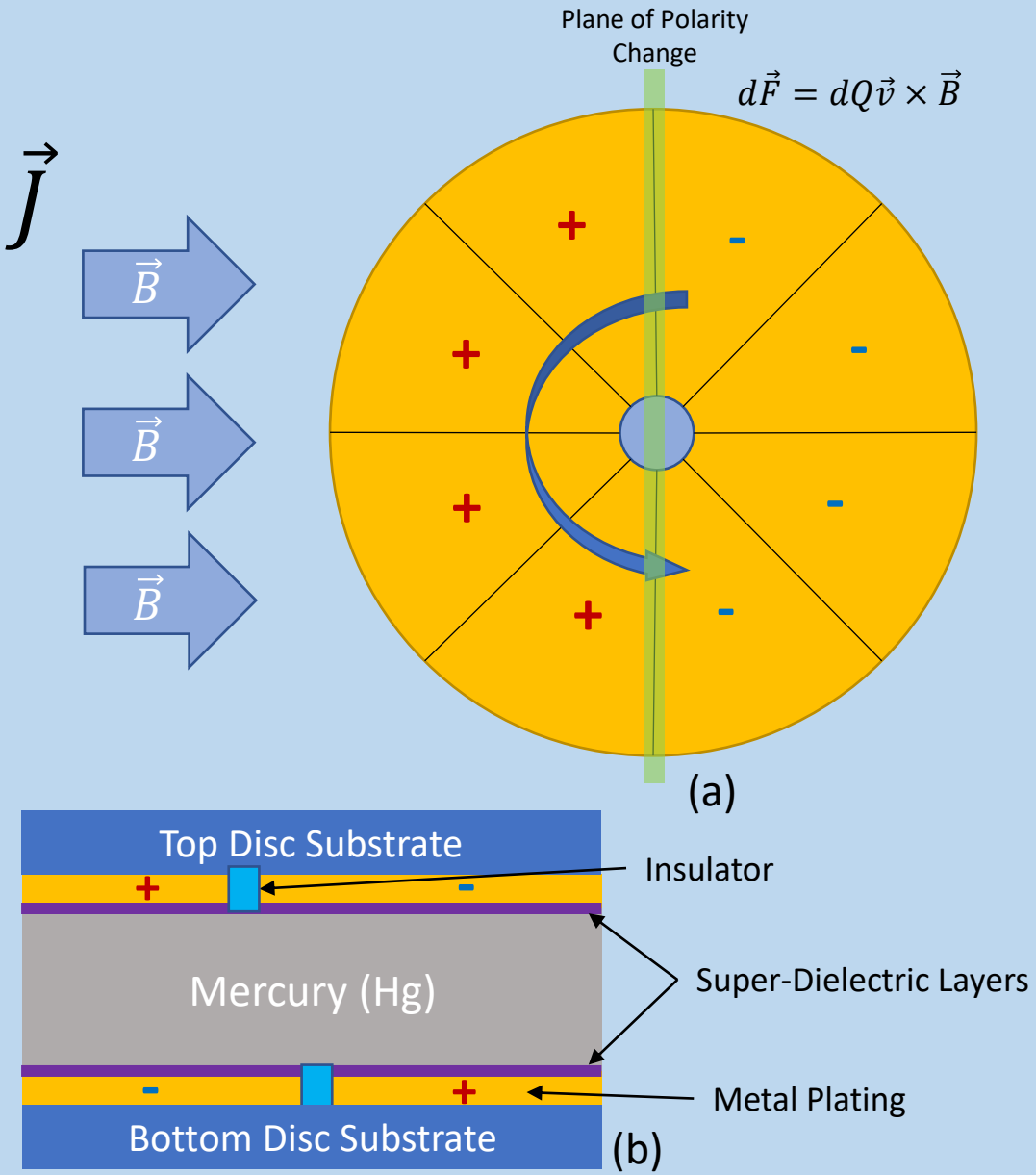

Figure 18. (a) Top view of segmented disc dynamic super-capacitor electrode. The bottom disc would have the opposite polarity distribution, and spin in the opposite direction (can also be stationary if desired). (b) schematic of interface side view.

Breaking $\vec{J}$ the Symmetry

There are two ways to change the polarity as the disc segments pass through the plane of polarity change. The first is to have a power supply, or power supplies, which reverse the segment voltage potentials and provide the current drive to reverse the charge polarity, figure 20. The voltage and current can be supplied through the shaft, with the shaft being electrically segmented similar to the disc electrode. Figure 20 also shows the equivalent circuit. R[An] is the combined resistance of the conductive path and internal resistance of the power supply, V[An], for the n^{th} segment of the top disc. R[Hg] is the resistance of the mercury fluid since it is the common conductive ground path. L[An] is the intrinsic inductance of the system. C[An] is the electrical capacitance of the n^{th} segment of the top disc super-capacitor. In the shown figure n = 1, 2, …, 10, although ten is illustrative and can be more or less than ten. A 'B' subscript denotes the bottom disc super-capacitor with m representing the segment number of the electrically segmented bottom super-capacitor disc. Again m = 1, 2, …, 10, with ten being only an illustrative example.

The second method of switching polarities at the plane of polarity change is to oscillate the energy stored in the capacitive segments with an inductive element to create an oscillatory LC circuit. The LC_n circuit inductive element can be tuned to have the same oscillation frequency as the rotational frequency of the Dynamic Super-Capacitor (DSC). This configuration allows the charge to oscillate between the lower and bottom electrode segments as needed at the frequency required. There will be ohmic losses in the conductive paths so energy will need to be put back into the system as power is dissipated by any ohmic resistances encountered in the conductive paths. Only the first method will be discussed in detail. LCR (inductor-capacitor-resistor) circuits are well studied in control systems theory.

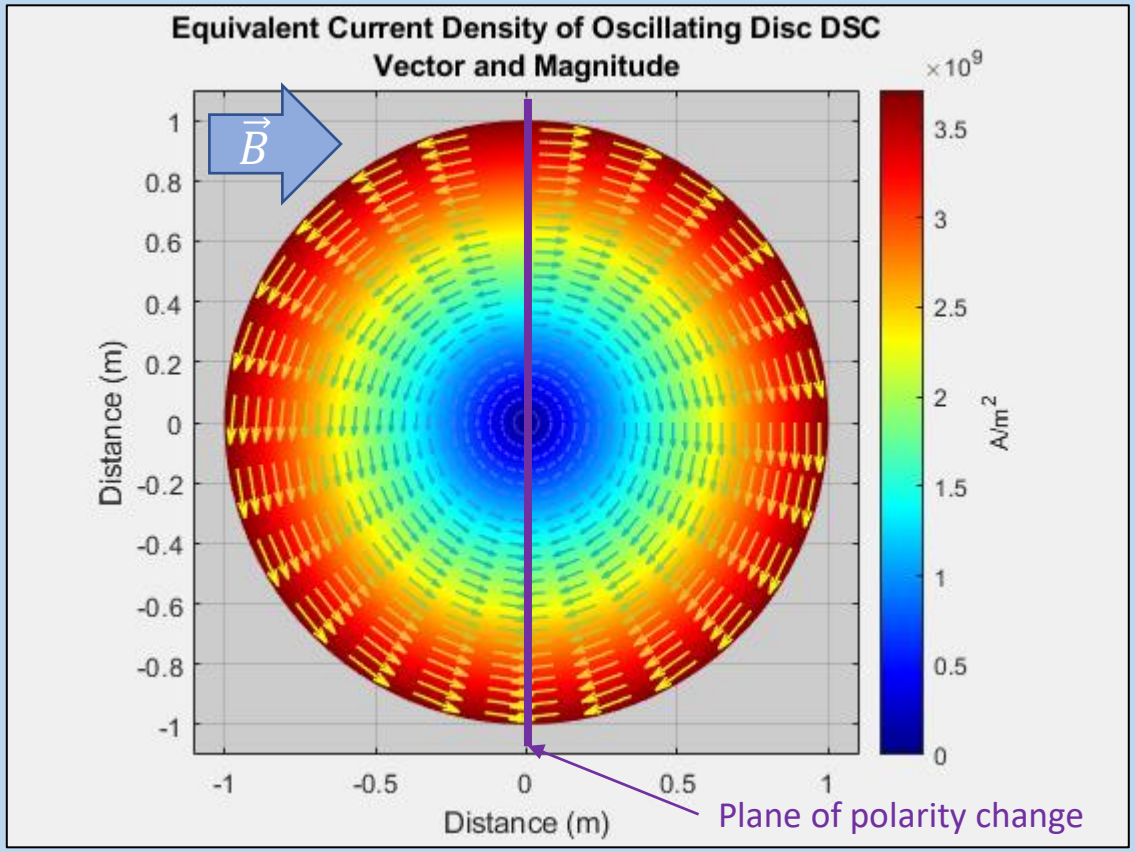

Figure 19. Effective current density distribution of the disc Dynamic Super-Capacitor (DSC) shown in figure 18. R = 1 meter; RPM = 100,000; V = 2 volts; k = 1 x 10^9, d = 5 um.

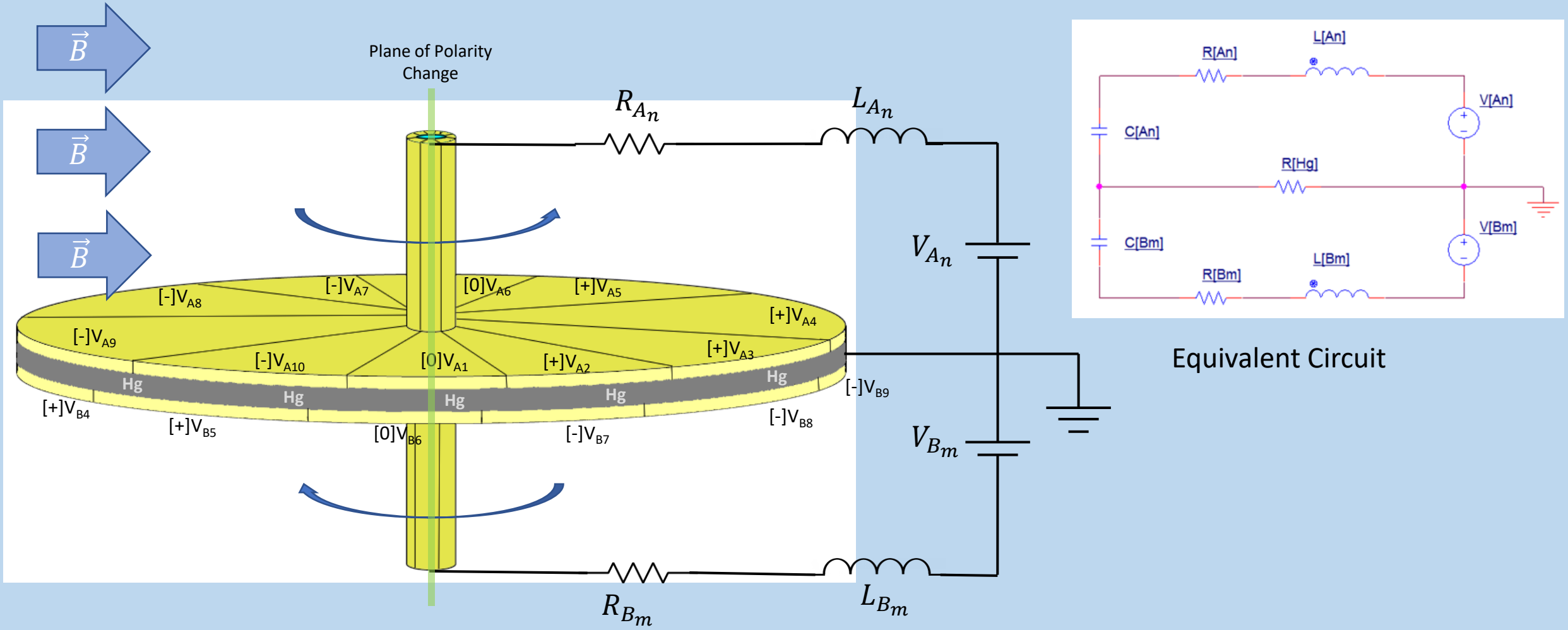

Figure 20. Top and bottom electrodes of DSC divided into ten segments and equivalent circuit when power supplies are used to reverse the polarity on electrode segments. The plane of polarity change is orthogonal to the plane of the page and coincides with the axis of rotation at the center of the shaft. Electrodes are counter-rotating with grounded mercury between. [+] – electrode segment is positively charged, [-] – electrode segment is negatively charged, [0] – electrode segment is in process of changing polarity.

Controlling the Current Density Distribution

In the case with a dynamic super-capacitor with k = 1 x 10^9, V = 2 volts, R = 1 meter, d = 5 microns as the exemplary example, C_A is about 5563 Farads for the entire disc, i.e., all segments of figure 20. Even dividing the disc into ten segments as shown in figure 20 leaves each segment with a capacitance of about 556 Farads. The fastest the polarity of the disc segment can be switched is limited by the well-known RC time constant . Even with a low intrinsic resistance R_{An} of one milliohm for the power supply and non-mercury part of the circuit, and one milliohm for the mercury resistance, R_{Hg}, it takes a little over two seconds for the polarity to reverse on a DSC segment, figure 21 shows a PSpice simulation of this configuration. The disc must be divided into much smaller segments such that the capacitance of any individual segment is much lower.

Figure 22 shows a disc electrode segmented into 1 cm^2 plates. As can be seen in figure 23, the capacitive segment polarities are now able to be switched in approximately 400 micro-seconds.

The major merit of the currently described design is the exclusion of a superconducting magnetic shield. The major challenge of the design is handling the large currents required to reverse the polarity at the high spin rates required to produce significant lift; needing reversal at least twice the frequency of rotation. The traces that supply charge to the plate segments through the central shaft can be made of high-conductivity materials such as graphene or in some cases superconductors. Unfortunately, the current necessarily flows through the mercury (unless the point contact slip method described in the previous disclosure and again later is implemented). While resistances can be minimized, there will always be a certain amount of resistance and ohmic loss that must be dealt with. Equation 26 and 27 describe electrical resistance and ohmic power loss respectively,

$$R = \frac{\rho L}{A} \qquad (26)$$

$$P_{ohmic} = I^2 R \qquad (27)$$

where *R* is the resistance of the conductor in question, ρ is the resistivity of the material the current is flowing through, *L* is the path length through the conductor, *A* is the cross-sectional area of the conductor, *I* is the current in the conductor, and P_{ohmic} is the ohmic power loss. The conductors here being the traces supplying the currents on the disc and shaft, the capacitive segment resistance, and the current path through the mercury.

The capacitive segments can be appropriately sized in order to compensate for circuit resistance, and/or inductance, in order to get charging time constants consistent with reversing the polarity at least two times per rotation. In order to produce maximum lift, the segments should be maximally charged as the tangential velocity of the capacitive segment's velocity vector runs perpendicular to the external magnetic field vector. A controller that operates the power supplies and ensures the plates are polarized and reverse-polarized in the correct timing sequence should be incorporated and can be external to the shaft and disc electrode system, though the signals could be transmitted on traces along the shaft and discs.

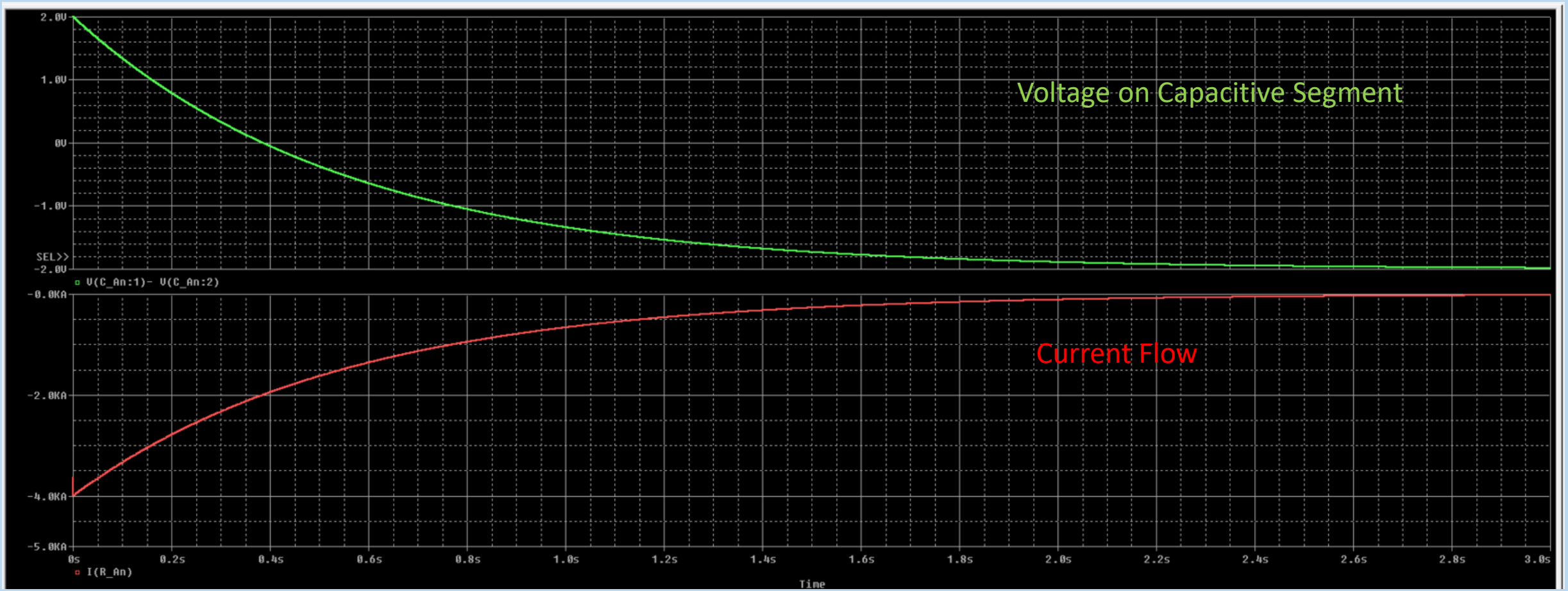

Figure 21. PSpice simulation of the equivalent circuit of one of the A_n capacitive segments shown in figure 20. With a total circuit resistance of 2 milliohm (R_{Hg} plus R_{An}) and intrinsic inductance of 100 nH. It requires about two seconds for the capacitive element to reverse polarity.

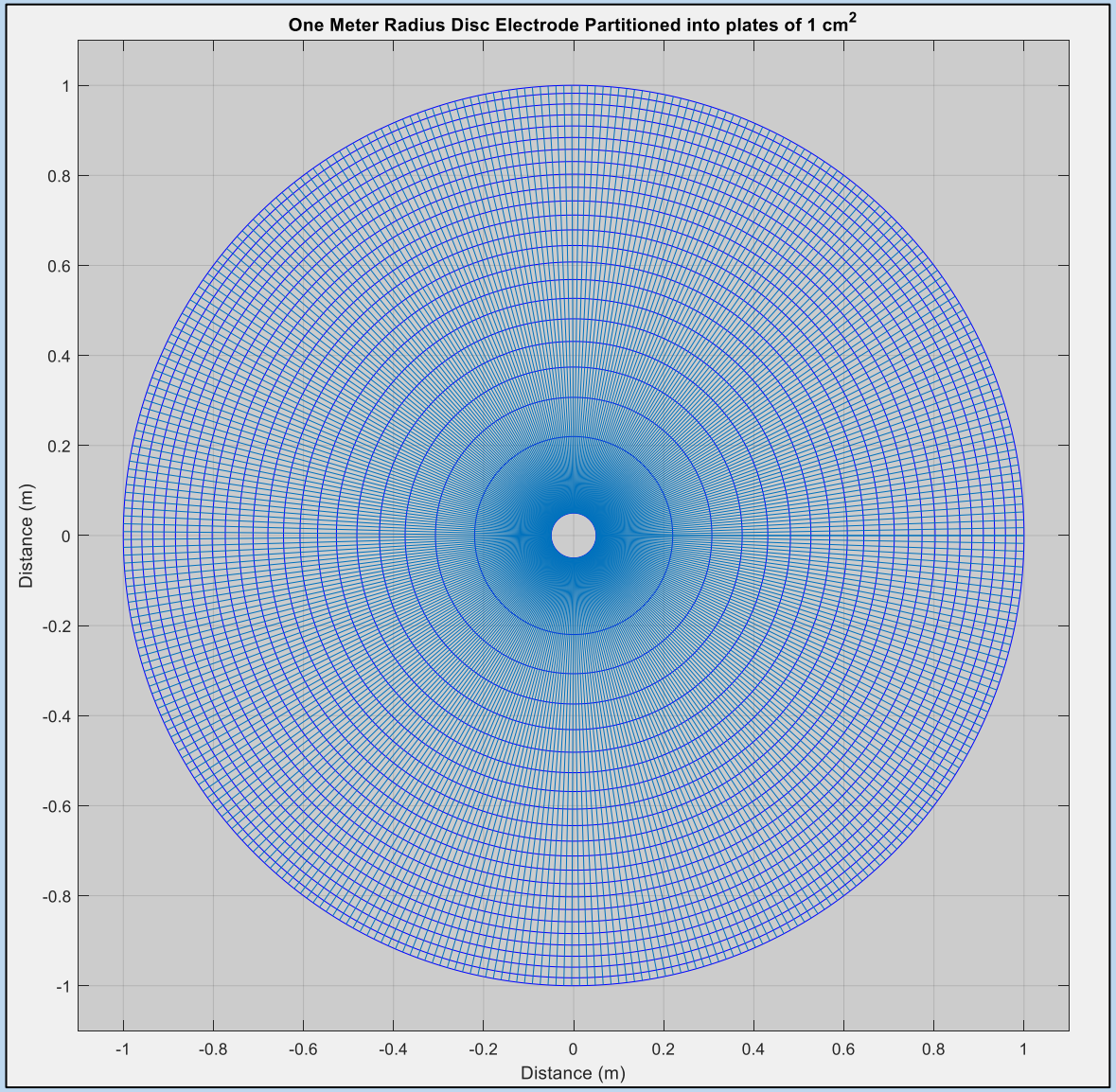

Figure 22. One meter radius disc electrode partitioned into 1 cm^2 capacitive segments. The outer radial segments truncated by the one-meter radial disc limit.

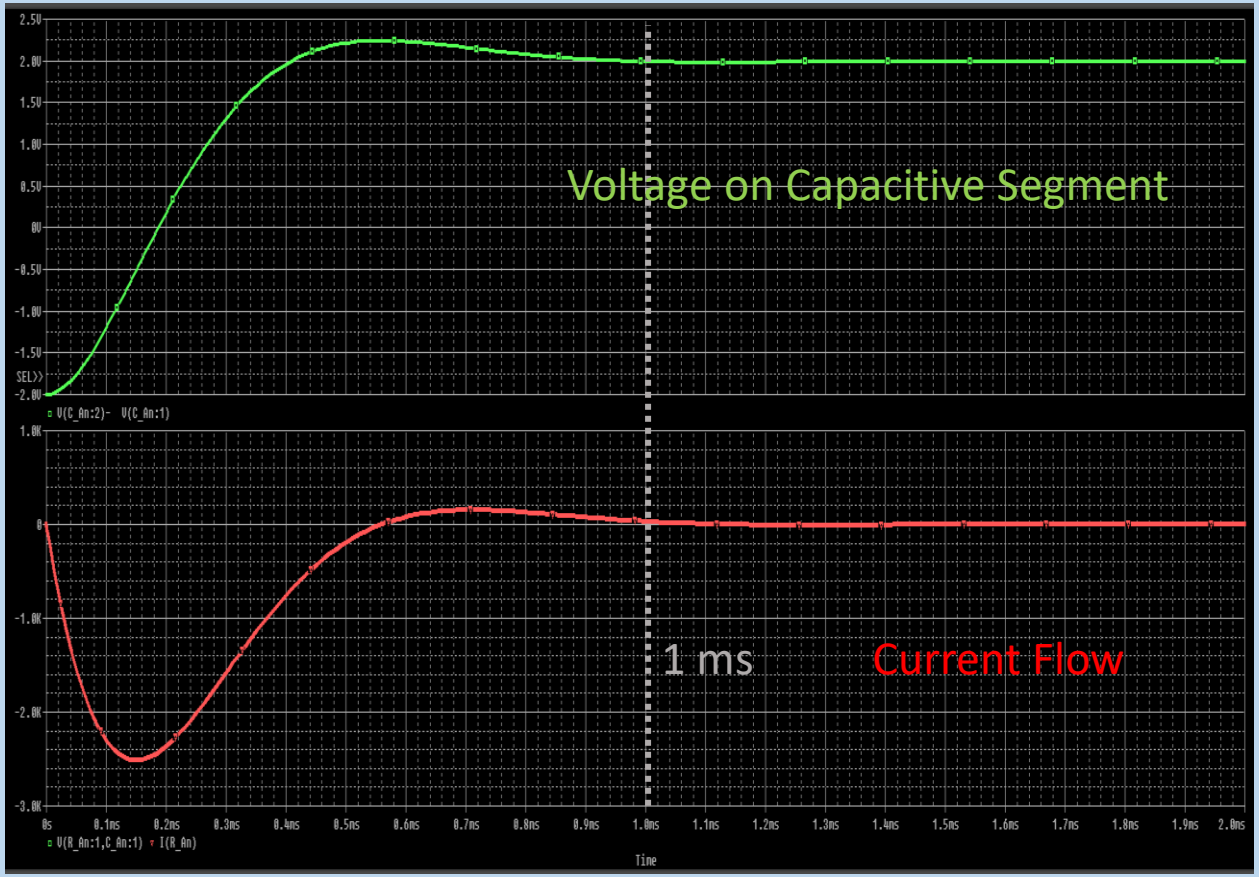

Figure 23. PSpice simulation of the equivalent circuit of one of the A_n capacitive segments shown in figure 22. With a total circuit resistance of 2 milliohm (R_{Hg} plus R_{An}) and intrinsic inductance of 100 nH per segment, it requires about one millisecond for the capacitive element to reverse polarity.

Manipulating the Mercury Fluid

Because of its fluidic nature and conductivity, the mercury slip join fluid can be manipulated in the presence of the magnetic field produced by the DSC, in other words the mercury can be made to flow in a desired manner using electromagnetic manipulation. One of the challenges discussed in serial no. 63/162,137 is preventing the mercury fluid from 'sticking' to the rotating electrodes and being dragged along with the electrode rotation, causing parasitic charge motions. In the breaking effective current, *J*, symmetry design just discussed, because there is conventional electrical current flowing through the mercury in the presence of magnetic fields produced by the DSC, the mercury will experience magnetohydrodynamic forces. The electron currents and corresponding Lorentz forces can be configured to mitigate the drag the mercury may experience at the contact between the super-dielectric layer (SD) on the disc electrode and the mercury; further mitigating charges in the mercury close to the mercury-SD interface from being dragged along with the rotating disc - which would diminish the total effective current, i.e., parasitic charge motion. Figure 24 shows the simulated magnetic field vector between the two plates, i.e., in the mercury slip-joint fluid layer. As can be seen, for the most part, the magnetic field vector inside the mercury runs perpendicular to the plane of the discs. As a reminder, the effective current is the current produced by the charges on the electrodes being in mechanical motion. The electron current used to exert force on the mercury is a conventional electron current as is commonly encountered in any common electrical circuit, e.g., current in a wire. The flow of the electron current can be configured such that magnetohydrodynamic forces can be exerted on the mercury in a controlled and desirable way. Electrical traces can be patterned on the disc(s) and come into contact with the mercury where desired, allowing current to flow through the mercury in a controlled and patterned way. Due to the Lorentz force, equation 6 and 12, a force is locally exerted on the mercury proportional to the perpendicular component of the local magnetic field and electron current density flow, figure 25. The force of equations 6 and 12 is the force exerted on the electrons, the electrons will then transfer their acquired momentum to the fluid through electron-atom collisions. In this way the mercury can be made to experience a force counter to the motion of the rotating disc, or discs if two or more discs are counter-rotated. The mercury fluid can potentially be made to move counter to the rotation of the electrodes or in just about any other motional path desired. In the simulations and calculations of the present disclosure, the charges accumulated in the mercury due to the capacitive nature of the DSC are assumed to be stationary. While it is clear that the conventional current used to reverse the polarity of the capacitive segments in the symmetry breaking method described prior can be used in this way to manipulate the motion of the mercury, an electron current can be applied as described to control mercury movement and mitigate movement of charge accumulation in the mercury close to the SD-mercury interface for any design, e.g., the previously described superconductor shielded design as well.

As an additional way to throttle the lift of the propulsion system, the mercury can be made to rotate with the electrodes using these magnetohydrodynamic forces. In this way, the charge stored in the mercury will move along with its oppositely charged counterpart charge on the electrode thus reducing the overall net charge in motion, thus reducing the effective current and thusly the experienced lift in the external magnetic field. For example, an electron and proton closely spaced moving along together in space will produce no net magnetic field at a distance. If that same electron and proton were moving with opposite velocity vectors they will produce twice the magnetic field as would have been experienced by a single charged particle moving by itself. If the charged mercury layer at the SD-mercury interface and the charged electrode were moving in perfect unison, the $\vec{J}_{eff}$ in equation 12 would equal zero and no lift would be experienced. This is another method of potentially throttling the lift/thrust electrically as opposed to the mechanical methods described previously, e.g., rotating the magnetic superconductor shields.

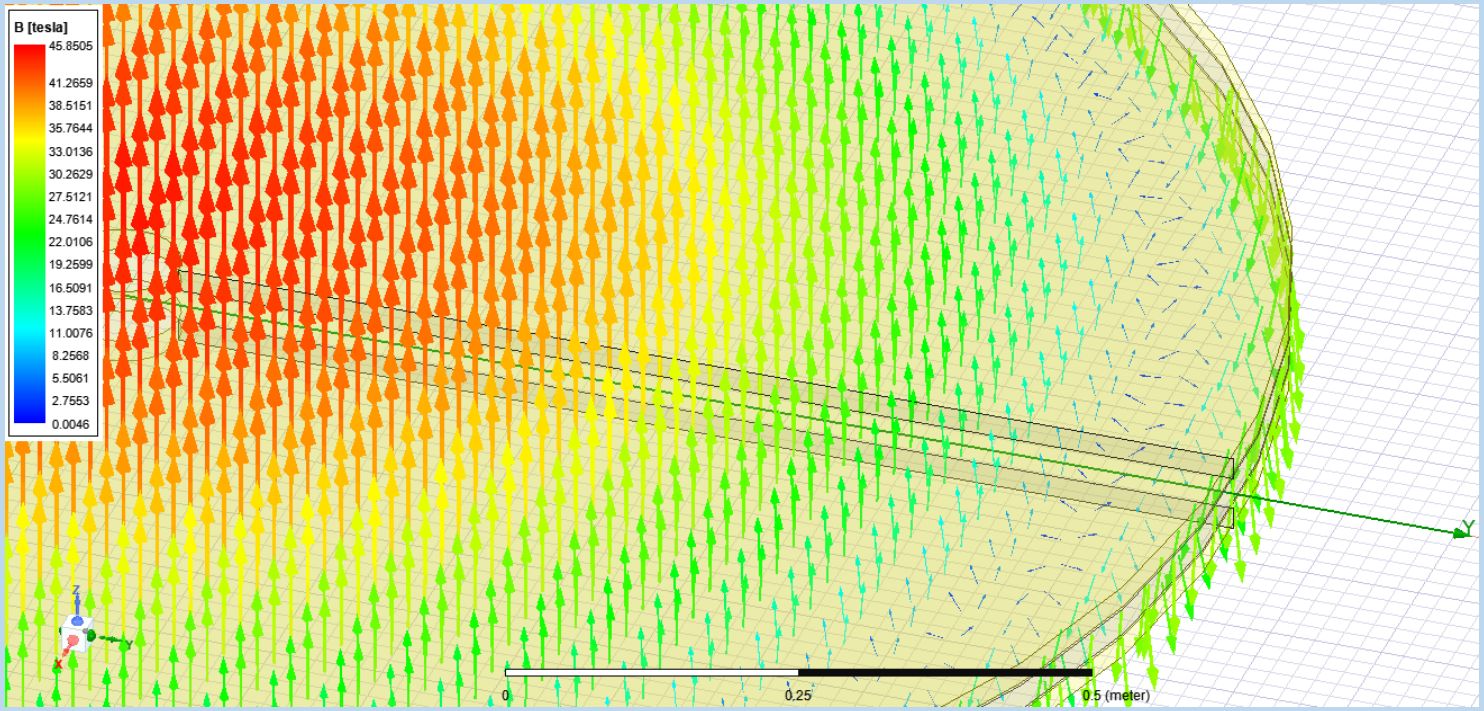

Figure 24. Simulated magnetic field vector in the mercury layer between the two discs in a counter-rotating DSC design, i.e., in the mercury slip-joint layer.

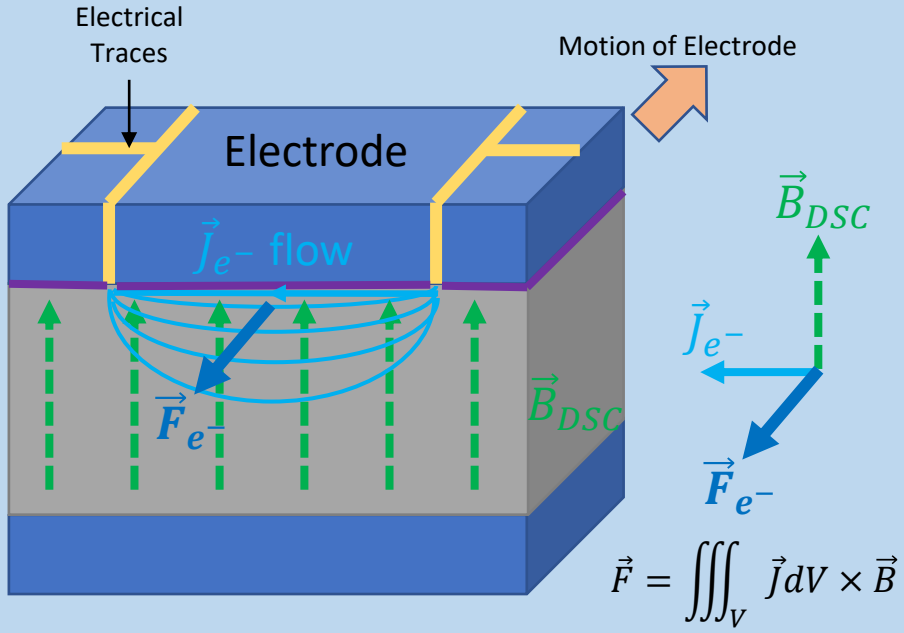

Figure 25. A volumetric segment of electrode and mercury slip layer in the DSC's magnetic field. The electron current, $\vec{J}_{e^-}$, can be configured as to produce a force, and thus motion, in the mercury that is counter to the motion of the electrodes themselves.

While tailoring the $\vec{J}_{eff}$ vector to produce lift is a technical possibility, it presents some challenges; large conventional currents must oscillate which introduce ohmic losses. These ohmic losses must be dealt with from a power loss perspective and heat management perspective. Additionally, Faraday's law (equation 2) dictates that changing magnetic fields will induce an electromotive force which may induce eddy currents within conducting volumes in the propulsion system and surrounding structures. While ohmic losses and eddy currents may be mitigated, due to the static field nature of the superconductor magnetic shielding method, the shielding method remains the preferred embodiment.

Type III Propulsion

Type I propulsion described the lift generated close to the magnetic poles of the Earth through the magnetic force generated by two magnetic dipoles - repelling or attracting one another. Type II propulsion described the magnetic Lorentz force generated by charged spinning discs in a uniform magnetic field with the plane of the discs oriented parallel to the magnetic field, such as close to the equator of the Earth; with the symmetry of the external magnetic field or the effective current on the discs being broken as previously described. Type III propulsion is when the charged spinning electrodes are oriented perpendicular to the locally uniform magnetic field, symmetry breaking is still required to generate net lift/thrust. The only substantive difference between Type II and Type III propulsion is the force vector component is directed perpendicular to the plane of the disc in Type II and the force vector component lies in the plane of the disc with Type III propulsion; both types work on the principle of magnetic Lorentz forces acting on moving charges in an external magnetic field, in the exemplary case the Earth's magnetic field.

Force on a Spinning Charged Disc II

Calculating the force on a spinning charged disc in a uniform magnetic field with the magnetic field being perpendicular to the plane of the disc, figure 26; the differential area, *dS*, in cylindrical coordinates is

$dS = rd\varphi dr$.

The differential charge is given by

$dQ = \sigma dS = \sigma r d\varphi dr$.

Plugging *dQ* and *v* in terms of the rotational velocity, $\mathrm{v} = \mathrm{r}\omega$, into equation 11 yields

$$d\vec{F} = dQ\vec{v} \times \vec{B} = (\sigma r d\varphi dr)(r\omega)\left(\hat{v} \times \vec{B}\right) = (\omega \sigma r^2 d\varphi dr)(\hat{\varphi} \times B_0 \hat{z})$$

$$d\vec{F} = dQ\vec{v} \times \vec{B} = B_0\, \sigma\, \omega\, r^2 d\varphi dr\, \hat{r} \qquad (28)$$

or written in Cartesian coordinates,

$$d\vec{F} = dQ\vec{v} \times \vec{B} = B_0\, \sigma\, \omega\, r^2 d\varphi dr\, (cos\varphi\, \hat{x} + sin\varphi\, \hat{y}) \qquad (28)$$

The force on a wedge of the disc, caused by the magnetic field, can be calculated as

$$\vec{F} = B_0\, \sigma\omega \int_{\varphi_1}^{\varphi_2} \int_{R_1}^{R_2} r^2 (\cos\varphi \hat{x} + sin\varphi \hat{y}) d\varphi dr \qquad (29)$$

where φ_1 is the angular start of the wedge and φ_2 is the angular ending of the wedge and R_1 and R_2 are the starting and ending radius of the wedge, see figure 26. Evaluation of equation 29 leads to

$$\vec{F} = \tfrac{1}{3} B_0\, \sigma\omega (R_2^3 - R_1^3)[(sin\varphi_2 - sin\varphi_1)\, \hat{x} + (cos\varphi_1 - cos\varphi_2)\, \hat{y}] \qquad (30) \text{ or}$$

$$\vec{F} = \tfrac{1}{3} B_0\, \omega (\tfrac{Q}{\pi R^2})(R_2^3 - R_1^3)[(sin\varphi_2 - sin\varphi_1)\, \hat{x} + (cos\varphi_1 - cos\varphi_2)\, \hat{y}] \qquad (31)$$

if written in terms of the total charge on the disc $Q = \sigma(\pi R^2)$.

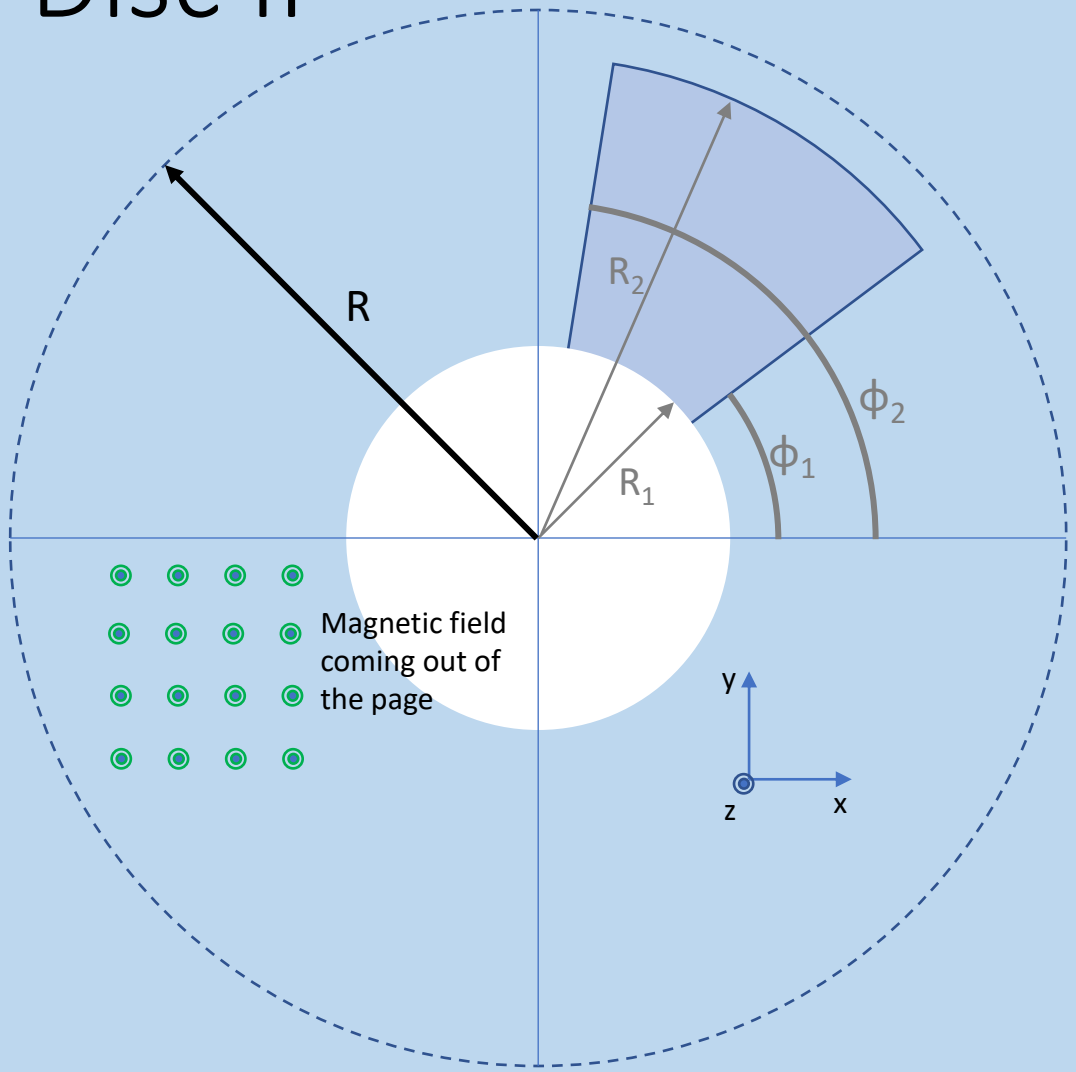

Figure 26. Geometric set up to derive force equations.

Force on a Spinning Charged Disc II

Examining equation 31, it can be discerned that the force vector can be directed in any desired direction in the plane of the disc when there is a magnetic field component perpendicular to the plane of the disc; using any of the symmetry breaking techniques discussed previously. Note, equation 31 has a very similar form to equation 19. The Lift/Thrust vs RPM vs Disc Radius results of figure 10 apply to Type III propulsion similarly. With quadrants I and IV exposed to the external magnetic field, a one-meter radius disc spinning at 100,000 RPM, with $k = 1 \times 10^9$, V = 2 volts, and d = 2 microns at the Earth's equator yields a force of about 3700 Newtons (835 lbs) in the positive z-direction. An ANSYS Maxwell™ simulation, figure 27, of the same system using a superconductor magnetic shield predicts 3880 Newtons (870 lbs) in the z-direction, in reasonable agreement.

With Type III propulsion the forces are directed along the radial plane of the discs as can be seen from equation 28. Mobile charges will have the tendency to migrate to the edges of the discs, the Hall effect. Unwanted voltage potentials may be produced, i.e., the degradation voltage potential of the super-dielectric may be reached or exceeded. In order to hinder the migration of charges and mitigate the Hall effect and limit potential eddy currents as well, the electrode may be electrically segmented similar to that shown in figure 22 to limit charge mobility and eddy current path lengths. Conversely, the charges have their maximum tangential velocity at the rim of the disc. Forcing the charge distribution to the outer rim of the discs would enhance thrust/lift over the uniform charge distribution assumed. Super dielectrics with higher breakdown/degradation voltage potentials would benefit from the Hall effect.

While disc electrodes for the DSCs have been covered, any rotationally symmetric electrodes may be used, such as cylinders or spheres. Figure 28 shows a cylindrical DSC superconductor shielded model; length = 2 meters, diameter = 1 meter, d = 2 microns, $k = 1 \times 10^9$, RPM = 100,000, V = 2 volts, with counter-rotating electrodes. Simulated lift is 256 Newtons (60 lbs). This is for a single cylinder configuration, of course several concentric cylindrical DSCs could be used to amplify the performance; see "Methods and Apparatuses for Producing Ultra-strong Magnetic Fields" serial no. 63/162,137 for more information on Multi-Electrode Cylindrical Ultra-magnets (MCUs).

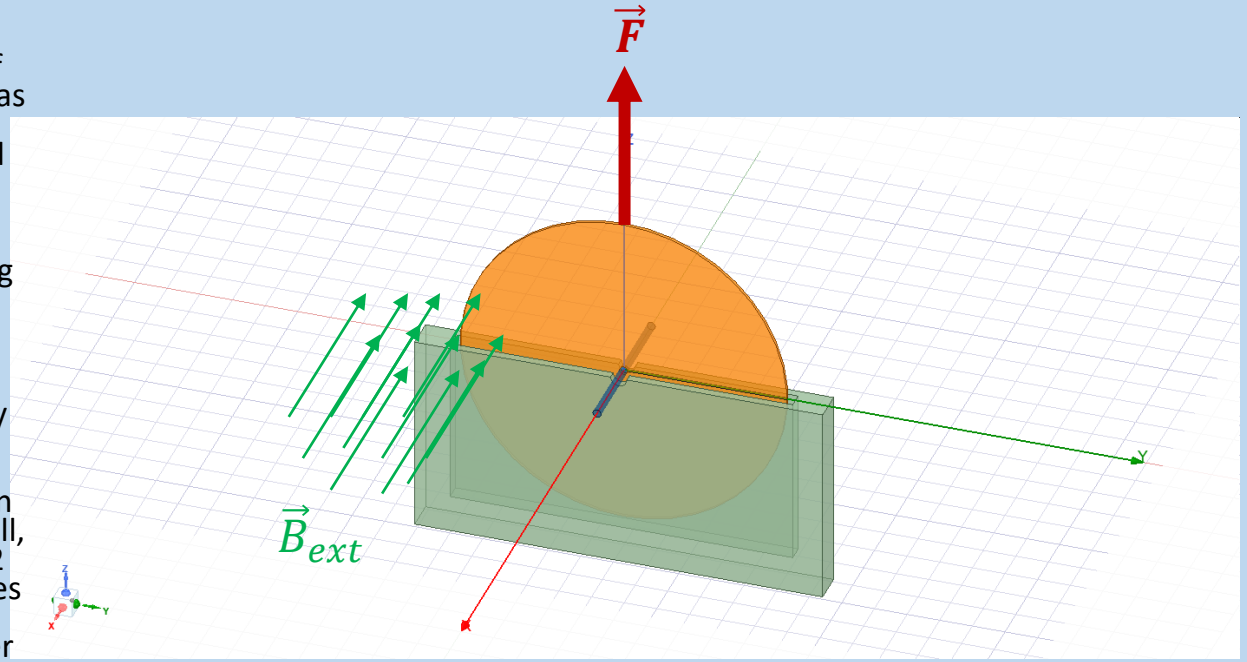

Figure 27. ANSYS Maxwell™ model of shielded DSC system with magnetic field perpendicular to the disc electrode.

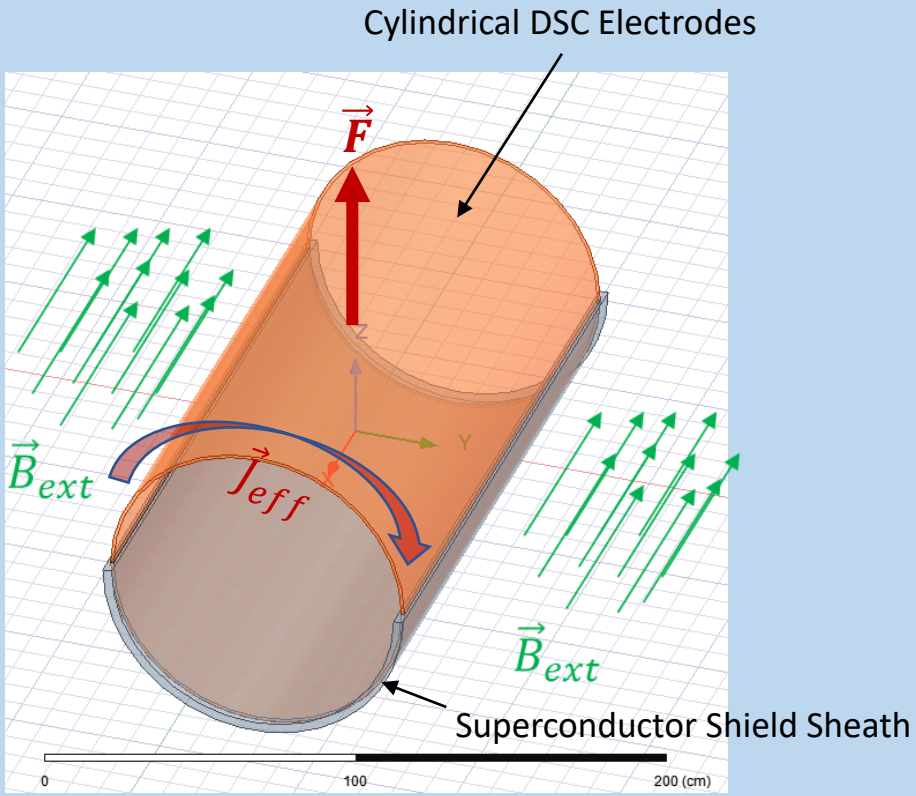

(a)

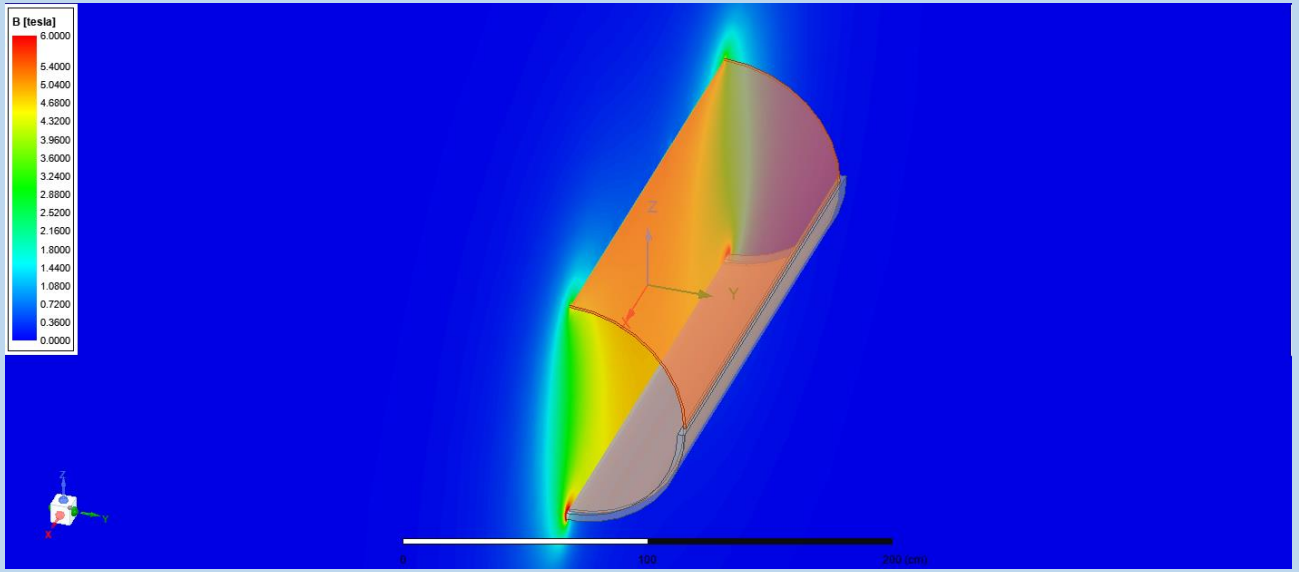

(b)

Figure 28. Cylindrical dynamic super-capacitor ANSYS Maxwell™ model. (a) layout of model with external magnetic field direction shown (B_{ext} ~ 30 micro-Tesla at Earth's equator). (b) magnetic field intensity profile generated by cylindrical DSC. Length = 2 meters, Diameter = 1 meter, k = 1 x 10^9, d = 2 microns, RPM = 100,000, Voltage = 2 V. Counter-rotating electrodes assumed.

Magnetic Field Orientation and Thrust

Type II and Type III propulsion work on the principle of magnetic Lorentz forces. Due to the nature of the cross-product operation in the Lorentz force equation (equation 6), neither Type II nor Type III propulsion can produce thrust components parallel to the external magnetic field lines. However, using Type II and/or Type III propulsion, thrust can be generated in any direction perpendicular to the lines of the magnetic field. Table 2 shows the results of a large number of simulations in which the external magnetic field vector direction is varied; the magnitude remains at ~30 μTesla. The reference configuration is as shown in figure 9 with the $-\hat{x}$ field direction. The magnetic field vector is first rotated about the x-axis, followed by a rotation about the y-axis, finally followed by a rotation about the z-axis. Figure 29 shows the (0 deg, 0 deg, 0 deg) field and the (5 deg, 5 deg, 5 deg) field for reference. The resultant force (thrust) vector is referenced to a local x, y, z cartesian frame of reference sitting on the surface of the planet; x-north/south, y-east/west, z-up/down. This can be thought of as sitting in a craft on the surface of the planet with a planetary magnetic field penetrating the surface of the planet at that point at a certain azimuthal and polar angle. Of course, this may also be interpreted as the relative inclination of the magnetic field to a magnetic propulsion system in arbitrary orientation, though the prior interpretation is easier to visualize and understand. Figure 30 shows a force field vector plot of table 2. For clarity of understanding and comparison of propulsion system orientation, the same force field vector plot with the propulsion system rotated 90 degrees around the x-axis is shown in figure 31.

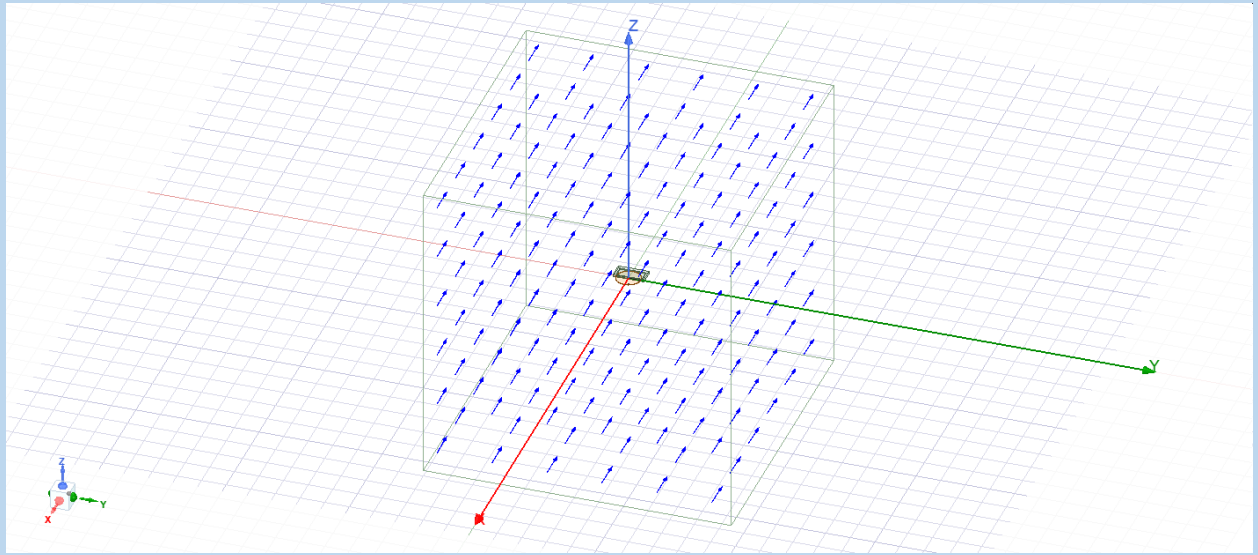

(a)

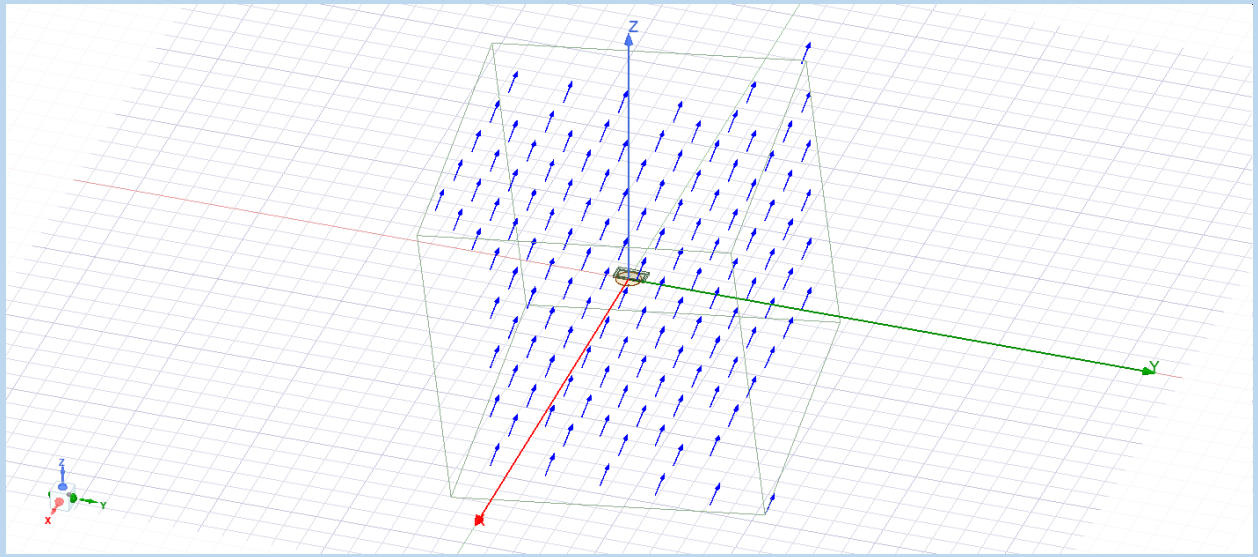

(b)

Figure 29. Aid in visualizing magnetic field orientation thrust simulations. (a) Reference external magnetic field (0 deg, 0 deg, 0 deg). (b) External magnetic field tilted by 5 degrees (x), 5 degrees (y), and 5 degrees (z).

B_Rot_X [deg]	B_Rot_Y [deg]	B_Rot_Z [deg]	F_x (lbs)	F_y (lbs)	F_z (lbs)	B_Rot_X [deg]	B_Rot_Y [deg]	B_Rot_Z [deg]	F_x (lbs)	F_y (lbs)	F_z (lbs)	B_Rot_X [deg]	B_Rot_Y [deg]	B_Rot_Z [deg]	F_x (lbs)	F_y (lbs)	F_z (lbs)
-180	-180	-180	0	0	747	-135	-180	-180	0	0	750	-90	-180	-180	0	0	750
-180	-180	-135	0	0	533	-135	-180	-135	0	0	535	-90	-180	-135	0	0	535
-180	-180	-90	0	0	0	-135	-180	-90	0	0	0	-90	-180	-90	0	0	0
-180	-180	-45	0	0	-527	-135	-180	-45	0	0	-534	-90	-180	-45	0	0	-524
-180	-180	0	0	0	-749	-135	-180	0	0	0	-749	-90	-180	0	0	0	-746
-180	-180	45	0	0	-532	-135	-180	45	0	0	-538	-90	-180	45	0	0	-535
-180	-180	90	0	0	0	-135	-180	90	0	0	0	-90	-180	90	0	0	0
-180	-180	135	0	0	526	-135	-180	135	0	0	523	-90	-180	135	0	0	522
-180	-180	180	0	0	747	-135	-180	180	0	0	750	-90	-180	180	0	0	749
-180	-135	-180	-675	0	532	-135	-135	-180	-672	0	535	-90	-135	-180	-667	0	539
-180	-135	-135	-688	0	370	-135	-135	-135	-676	0	377	-90	-135	-135	-677	0	378
-180	-135	-90	-688	0	0	-135	-135	-90	-674	0	0	-90	-135	-90	-677	0	0
-180	-135	-45	-680	0	-371	-135	-135	-45	-673	0	-376	-90	-135	-45	-677	0	-373
-180	-135	0	-676	0	-534	-135	-135	0	-685	0	-524	-90	-135	0	-675	0	-533
-180	-135	45	-680	0	-380	-135	-135	45	-684	0	-380	-90	-135	45	-664	0	-382
-180	-135	90	-669	0	0	-135	-135	90	-665	0	0	-90	-135	90	-667	0	0
-180	-135	135	-667	0	378	-135	-135	135	-669	0	385	-90	-135	135	-665	0	373
-180	-135	180	-685	0	527	-135	-135	180	-672	0	535	-90	-135	180	-667	0	539
-180	-90	-180	-967	0	0	-135	-90	-180	-965	0	0	-90	-90	-180	-967	0	0
-180	-90	-135	-965	0	0	-135	-90	-135	-964	0	0	-90	-90	-135	-966	0	0
-180	-90	-90	-967	0	0	-135	-90	-90	-966	0	0	-90	-90	-90	-966	0	0
-180	-90	-45	-966	0	0	-135	-90	-45	-966	0	0	-90	-90	-45	-967	0	0
-180	-90	0	-966	0	0	-135	-90	0	-967	0	0	-90	-90	0	-965	0	0
-180	-90	45	-967	0	0	-135	-90	45	-966	0	0	-90	-90	45	-963	0	0
-180	-90	90	-966	0	0	-135	-90	90	-963	0	0	-90	-90	90	-967	0	0
-180	-90	135	-963	0	0	-135	-90	135	-967	0	0	-90	-90	135	-965	0	0
-180	-90	180	-967	0	0	-135	-90	180	-965	0	0	-90	-90	180	-966	0	0
-180	-45	-180	-680	0	-532	-135	-45	-180	-674	0	-533	-90	-45	-180	-683	0	-527
-180	-45	-135	-678	0	-368	-135	-45	-135	-684	0	-370	-90	-45	-135	-681	0	-381
-180	-45	-90	-666	0	0	-135	-45	-90	-680	0	0	-90	-45	-90	-683	0	0
-180	-45	-45	-687	0	373	-135	-45	-45	-688	0	375	-90	-45	-45	-683	0	379
-180	-45	0	-676	0	532	-135	-45	0	-682	0	529	-90	-45	0	-690	0	519
-180	-45	45	-677	0	369	-135	-45	45	-688	0	373	-90	-45	45	-686	0	367
-180	-45	90	-661	0	0	-135	-45	90	-685	0	0	-90	-45	90	-689	0	0
-180	-45	135	-674	0	-382	-135	-45	135	-681	0	-377	-90	-45	135	-684	0	-378
-180	-45	180	-691	0	-521	-135	-45	180	-674	0	-533	-90	-45	180	-683	0	-527
-180	0	-180	0	0	-747	-135	0	-180	0	0	-750	-90	0	-180	0	0	-748
-180	0	-135	0	0	-525	-135	0	-135	0	0	-515	-90	0	-135	0	0	-536
-180	0	-90	0	0	0	-135	0	-90	0	0	0	-90	0	-90	0	0	0
-180	0	-45	0	0	533	-135	0	-45	0	0	535	-90	0	-45	0	0	531
-180	0	0	0	0	748	-135	0	0	0	0	748	-90	0	0	0	0	750

Table 2. Simulated force vector vs orientation of the external magnetic field, referenced to a $\vec{B} = -B_0\hat{x}$ magnetic field. Force is for the set up shown in Figure 9.

B_Rot_X [deg]	B_Rot_Y [deg]	B_Rot_Z [deg]	F_x (lbs)	F_y (lbs)	F_z (lbs)	B_Rot_X [deg]	B_Rot_Y [deg]	B_Rot_Z [deg]	F_x (lbs)	F_y (lbs)	F_z (lbs)	B_Rot_X [deg]	B_Rot_Y [deg]	B_Rot_Z [deg]	F_x (lbs)	F_y (lbs)	F_z (lbs)
-180	0	45	0	0	-534	-135	0	45	0	0	-527	-90	0	45	0	0	-526
-180	0	90	0	0	-750	-135	0	90	0	0	-750	-90	0	90	0	0	-749
-180	0	135	707	0	-524	-135	0	135	691	0	-537	-90	0	135	697	0	-532
-180	0	180	700	0	-373	-135	0	180	695	0	-369	-90	0	180	698	0	-374
-180	45	-180	705	0	0	-135	45	-180	701	0	0	-90	45	-180	699	0	0
-180	45	-135	702	0	382	-135	45	-135	693	0	383	-90	45	-135	699	0	376
-180	45	-90	688	0	539	-135	45	-90	706	0	525	-90	45	-90	698	0	531
-180	45	-45	701	0	371	-135	45	-45	708	0	363	-90	45	-45	691	0	366
-180	45	0	701	0	0	-135	45	0	690	0	0	-90	45	0	698	0	0
-180	45	45	698	0	-382	-135	45	45	697	0	-388	-90	45	45	697	0	-377
-180	45	90	707	0	-524	-135	45	90	691	0	-537	-90	45	90	697	0	-532
-180	45	135	988	0	0	-135	45	135	987	0	0	-90	45	135	990	0	0
-180	45	180	988	0	0	-135	45	180	988	0	0	-90	45	180	987	0	0
-180	90	-180	985	0	0	-135	90	-180	988	0	0	-90	90	-180	988	0	0
-180	90	-135	988	0	0	-135	90	-135	985	0	0	-90	90	-135	988	0	0
-180	90	-90	991	0	0	-135	90	-90	988	0	0	-90	90	-90	985	0	0
-180	90	-45	989	0	0	-135	90	-45	991	0	0	-90	90	-45	988	0	0
-180	90	0	988	0	0	-135	90	0	989	0	0	-90	90	0	990	0	0
-180	90	45	987	0	0	-135	90	45	988	0	0	-90	90	45	989	0	0
-180	90	90	988	0	0	-135	90	90	987	0	0	-90	90	90	988	0	0
-180	90	135	704	0	525	-135	90	135	701	0	529	-90	90	135	705	0	527
-180	90	180	707	0	374	-135	90	180	700	0	385	-90	90	180	708	0	363
-180	135	-180	693	0	0	-135	135	-180	705	0	0	-90	135	-180	708	0	0
-180	135	-135	709	0	-367	-135	135	-135	707	0	-361	-90	135	-135	706	0	-367
-180	135	-90	699	0	-530	-135	135	-90	706	0	-527	-90	135	-90	708	0	-524
-180	135	-45	700	0	-378	-135	135	-45	711	0	-366	-90	135	-45	711	0	-367
-180	135	0	696	0	0	-135	135	0	715	0	0	-90	135	0	715	0	0
-180	135	45	697	0	373	-135	135	45	698	0	370	-90	135	45	710	0	364
-180	135	90	689	0	538	-135	135	90	701	0	529	-90	135	90	705	0	527
-180	135	135	0	0	747	-135	135	135	0	0	750	-90	135	135	0	0	749
-180	135	180	0	0	533	-135	135	180	0	0	535	-90	135	180	0	0	535
-180	180	-180	0	0	0	-135	180	-180	0	0	0	-90	180	-180	0	0	0
-180	180	-135	0	0	-527	-135	180	-135	0	0	-534	-90	180	-135	0	0	-524
-180	180	-90	0	0	-749	-135	180	-90	0	0	-749	-90	180	-90	0	0	-748
-180	180	-45	0	0	-532	-135	180	-45	0	0	-538	-90	180	-45	0	0	-535
-180	180	0	0	0	0	-135	180	0	0	0	0	-90	180	0	0	0	0
-180	180	45	0	0	526	-135	180	45	0	0	523	-90	180	45	0	0	522
-180	180	90	0	0	747	-135	180	90	0	0	750	-90	180	90	0	0	749
-180	180	135	0	0	0	-135	180	135	0	0	0	-90	180	135	0	0	0
-180	180	180	0	0	0	-135	180	180	0	0	0	-90	180	180	0	0	0

Table 2. Continued

B_Rot_X [deg]	B_Rot_Y [deg]	B_Rot_Z [deg]	F_x (lbs)	F_y (lbs)	F_z (lbs)		B_Rot_X [deg]	B_Rot_Y [deg]	B_Rot_Z [deg]	F_x (lbs)	F_y (lbs)	F_z (lbs)		B_Rot_X [deg]	B_Rot_Y [deg]	B_Rot_Z [deg]	F_x (lbs)	F_y (lbs)	F_z (lbs)
-45	-180	-180	0	0	749		0	-180	-180	0	0	746		45	-180	-180	0	0	748
-45	-180	-135	0	0	529		0	-180	-135	0	0	524		45	-180	-135	0	0	530
-45	-180	-90	0	0	0		0	-180	-90	0	0	0		45	-180	-90	0	0	0
-45	-180	-45	0	0	-532		0	-180	-45	0	0	-534		45	-180	-45	0	0	-527
-45	-180	0	0	0	-748		0	-180	0	0	0	-750		45	-180	0	0	0	-750
-45	-180	45	0	0	-532		0	-180	45	0	0	-525		45	-180	45	0	0	-515
-45	-180	90	0	0	0		0	-180	90	0	0	0		45	-180	90	0	0	0
-45	-180	135	0	0	530		0	-180	135	0	0	533		45	-180	135	0	0	535
-45	-180	180	0	0	749		0	-180	180	0	0	748		45	-180	180	0	0	748
-45	-135	-180	-667	0	538		0	-135	-180	-676	0	532		45	-135	-180	-682	0	529
-45	-135	-135	-678	0	366		0	-135	-135	-677	0	369		45	-135	-135	-688	0	373
-45	-135	-90	-669	0	0		0	-135	-90	-661	0	0		45	-135	-90	-685	0	0
-45	-135	-45	-683	0	-378		0	-135	-45	-674	0	-382		45	-135	-45	-681	0	-377
-45	-135	0	-674	0	-537		0	-135	0	-691	0	-521		45	-135	0	-674	0	-533
-45	-135	45	-674	0	-376		0	-135	45	-678	0	-368		45	-135	45	-684	0	-370
-45	-135	90	-669	0	0		0	-135	90	-666	0	0		45	-135	90	-680	0	0
-45	-135	135	-682	0	378		0	-135	135	-687	0	373		45	-135	135	-688	0	375
-45	-135	180	-667	0	538		0	-135	180	-676	0	532		45	-135	180	-682	0	529
-45	-90	-180	-966	0	0		0	-90	-180	-966	0	0		45	-90	-180	-967	0	0
-45	-90	-135	-966	0	0		0	-90	-135	-967	0	0		45	-90	-135	-966	0	0
-45	-90	-90	-967	0	0		0	-90	-90	-966	0	0		45	-90	-90	-963	0	0
-45	-90	-45	-965	0	0		0	-90	-45	-963	0	0		45	-90	-45	-967	0	0
-45	-90	0	-963	0	0		0	-90	0	-967	0	0		45	-90	0	-965	0	0
-45	-90	45	-967	0	0		0	-90	45	-965	0	0		45	-90	45	-966	0	0
-45	-90	90	-965	0	0		0	-90	90	-966	0	0		45	-90	90	-966	0	0
-45	-90	135	-969	0	0		0	-90	135	-966	0	0		45	-90	135	-966	0	0
-45	-90	180	-966	0	0		0	-90	180	-966	0	0		45	-90	180	-967	0	0
-45	-45	-180	-686	0	-525		0	-45	-180	-676	0	-534		45	-45	-180	-685	0	-524
-45	-45	-135	-685	0	-371		0	-45	-135	-680	0	-380		45	-45	-135	-684	0	-380
-45	-45	-90	-689	0	0		0	-45	-90	-669	0	0		45	-45	-90	-665	0	0
-45	-45	-45	-685	0	370		0	-45	-45	-667	0	378		45	-45	-45	-669	0	385
-45	-45	0	-675	0	534		0	-45	0	-685	0	527		45	-45	0	-672	0	535
-45	-45	45	-689	0	367		0	-45	45	-688	0	370		45	-45	45	-676	0	377
-45	-45	90	-675	0	0		0	-45	90	-688	0	0		45	-45	90	-674	0	0
-45	-45	135	-680	0	-371		0	-45	135	-680	0	-371		45	-45	135	-673	0	-376
-45	-45	180	-686	0	-525		0	-45	180	-676	0	-534		45	-45	180	-685	0	-524
-45	0	-180	0	0	-748		0	0	-180	0	0	-749		45	0	-180	0	0	-749
-45	0	-135	0	0	-529		0	0	-135	0	0	-532		45	0	-135	0	0	-538
-45	0	-90	0	0	0		0	0	-90	0	0	0		45	0	-90	0	0	0
-45	0	-45	0	0	526		0	0	-45	0	0	526		45	0	-45	0	0	523
-45	0	0	0	0	750		0	0	0	0	0	747		45	0	0	0	0	750

Table 2. Continued

B_Rot_X [deg]	B_Rot_Y [deg]	B_Rot_Z [deg]	F_x (lbs)	F_y (lbs)	F_z (lbs)	B_Rot_X [deg]	B_Rot_Y [deg]	B_Rot_Z [deg]	F_x (lbs)	F_y (lbs)	F_z (lbs)	B_Rot_X [deg]	B_Rot_Y [deg]	B_Rot_Z [deg]	F_x (lbs)	F_y (lbs)	F_z (lbs)
-45	0	45	0	0	-530	0	0	45	0	0	-527	45	0	45	0	0	-534
-45	0	90	0	0	-747	0	0	90	0	0	-748	45	0	90	0	0	-749
-45	0	135	706	0	-527	0	0	135	699	0	-530	45	0	135	706	0	-527
-45	0	180	694	0	-378	0	0	180	700	0	-378	45	0	180	711	0	-366
-45	45	-180	693	0	0	0	45	-180	696	0	0	45	45	-180	715	0	0
-45	45	-135	695	0	370	0	45	-135	697	0	373	45	45	-135	698	0	370
-45	45	-90	696	0	533	0	45	-90	689	0	538	45	45	-90	701	0	529
-45	45	-45	696	0	378	0	45	-45	707	0	374	45	45	-45	700	0	385
-45	45	0	701	0	0	0	45	0	693	0	0	45	45	0	705	0	0
-45	45	45	696	0	-378	0	45	45	709	0	-367	45	45	45	707	0	-361
-45	45	90	706	0	-527	0	45	90	699	0	-530	45	45	90	706	0	-527
-45	45	135	989	0	0	0	45	135	991	0	0	45	45	135	988	0	0
-45	45	180	989	0	0	0	45	180	989	0	0	45	45	180	991	0	0
-45	90	-180	987	0	0	0	90	-180	989	0	0	45	90	-180	989	0	0
-45	90	-135	988	0	0	0	90	-135	987	0	0	45	90	-135	989	0	0
-45	90	-90	988	0	0	0	90	-90	988	0	0	45	90	-90	987	0	0
-45	90	-45	985	0	0	0	90	-45	988	0	0	45	90	-45	988	0	0
-45	90	0	988	0	0	0	90	0	985	0	0	45	90	0	988	0	0
-45	90	45	991	0	0	0	90	45	988	0	0	45	90	45	985	0	0
-45	90	90	989	0	0	0	90	90	991	0	0	45	90	90	988	0	0
-45	90	135	704	0	528	0	90	135	710	0	524	45	90	135	706	0	525
-45	90	180	705	0	372	0	90	180	701	0	371	45	90	180	708	0	363
-45	135	-180	703	0	0	0	135	-180	701	0	0	45	135	-180	690	0	0
-45	135	-135	702	0	-380	0	135	-135	698	0	-382	45	135	-135	697	0	-388
-45	135	-90	696	0	-528	0	135	-90	707	0	-524	45	135	-90	691	0	-537
-45	135	-45	705	0	-358	0	135	-45	700	0	-373	45	135	-45	695	0	-369
-45	135	0	708	0	0	0	135	0	705	0	0	45	135	0	701	0	0
-45	135	45	711	0	372	0	135	45	702	0	382	45	135	45	693	0	383
-45	135	90	704	0	528	0	135	90	710	0	524	45	135	90	706	0	525
-45	135	135	0	0	749	0	135	135	0	0	748	45	135	135	0	0	748
-45	135	180	0	0	529	0	135	180	0	0	524	45	135	180	0	0	530
-45	180	-180	0	0	0	0	180	-180	0	0	0	45	180	-180	0	0	0
-45	180	-135	0	0	-532	0	180	-135	0	0	-534	45	180	-135	0	0	-527
-45	180	-90	0	0	-748	0	180	-90	0	0	-747	45	180	-90	0	0	-750
-45	180	-45	0	0	-532	0	180	-45	0	0	-525	45	180	-45	0	0	-515
-45	180	0	0	0	0	0	180	0	0	0	0	45	180	0	0	0	0
-45	180	45	0	0	530	0	180	45	0	0	533	45	180	45	0	0	535
-45	180	90	0	0	749	0	180	90	0	0	748	45	180	90	0	0	748
-45	180	135	0	0	0	0	180	135	0	0	0	45	180	135	0	0	0
-45	180	180	0	0	0	0	180	180	0	0	0	45	180	180	0	0	0

Table 2. Continued

B_Rot_X [deg]	B_Rot_Y [deg]	B_Rot_Z [deg]	F_x (lbs)	F_y (lbs)	F_z (lbs)	B_Rot_X [deg]	B_Rot_Y [deg]	B_Rot_Z [deg]	F_x (lbs)	F_y (lbs)	F_z (lbs)	B_Rot_X [deg]	B_Rot_Y [deg]	B_Rot_Z [deg]	F_x (lbs)	F_y (lbs)	F_z (lbs)
90	-180	-180	0	0	748	135	-180	-180	0	0	750	180	-180	-180	0	0	748
90	-180	-135	0	0	526	135	-180	-135	0	0	532	180	-180	-135	0	0	533
90	-180	-90	0	0	0	135	-180	-90	0	0	0	180	-180	-90	0	0	0
90	-180	-45	0	0	-526	135	-180	-45	0	0	-530	180	-180	-45	0	0	-527
90	-180	0	0	0	-749	135	-180	0	0	0	-747	180	-180	0	0	0	-748
90	-180	45	0	0	-536	135	-180	45	0	0	-529	180	-180	45	0	0	-532
90	-180	90	0	0	0	135	-180	90	0	0	0	180	-180	90	0	0	0
90	-180	135	0	0	531	135	-180	135	0	0	526	180	-180	135	0	0	526
90	-180	180	0	0	749	135	-180	180	0	0	750	180	-180	180	0	0	747
90	-135	-180	-690	0	519	135	-135	-180	-675	0	534	180	-135	-180	-685	0	527
90	-135	-135	-686	0	367	135	-135	-135	-689	0	367	180	-135	-135	-688	0	370
90	-135	-90	-689	0	0	135	-135	-90	-675	0	0	180	-135	-90	-688	0	0
90	-135	-45	-684	0	-378	135	-135	-45	-680	0	-371	180	-135	-45	-680	0	-371
90	-135	0	-683	0	-527	135	-135	0	-686	0	-525	180	-135	0	-676	0	-534
90	-135	45	-681	0	-381	135	-135	45	-685	0	-371	180	-135	45	-680	0	-380
90	-135	90	-683	0	0	135	-135	90	-689	0	0	180	-135	90	-669	0	0
90	-135	135	-683	0	379	135	-135	135	-685	0	370	180	-135	135	-667	0	378
90	-135	180	-690	0	519	135	-135	180	-675	0	534	180	-135	180	-675	0	532
90	-90	-180	-966	0	0	135	-90	-180	-963	0	0	180	-90	-180	-967	0	0
90	-90	-135	-963	0	0	135	-90	-135	-967	0	0	180	-90	-135	-965	0	0
90	-90	-90	-967	0	0	135	-90	-90	-965	0	0	180	-90	-90	-966	0	0
90	-90	-45	-965	0	0	135	-90	-45	-966	0	0	180	-90	-45	-966	0	0
90	-90	0	-966	0	0	135	-90	0	-966	0	0	180	-90	0	-966	0	0
90	-90	45	-966	0	0	135	-90	45	-966	0	0	180	-90	45	-967	0	0
90	-90	90	-966	0	0	135	-90	90	-967	0	0	180	-90	90	-966	0	0
90	-90	135	-967	0	0	135	-90	135	-966	0	0	180	-90	135	-963	0	0
90	-90	180	-965	0	0	135	-90	180	-963	0	0	180	-90	180	-967	0	0
90	-45	-180	-675	0	-533	135	-45	-180	-674	0	-537	180	-45	-180	-680	0	-532
90	-45	-135	-664	0	-382	135	-45	-135	-674	0	-376	180	-45	-135	-678	0	-368
90	-45	-90	-667	0	0	135	-45	-90	-669	0	0	180	-45	-90	-666	0	0
90	-45	-45	-665	0	373	135	-45	-45	-682	0	378	180	-45	-45	-687	0	373
90	-45	0	-667	0	539	135	-45	0	-667	0	538	180	-45	0	-676	0	532
90	-45	45	-677	0	378	135	-45	45	-678	0	366	180	-45	45	-677	0	369
90	-45	90	-677	0	0	135	-45	90	-669	0	0	180	-45	90	-661	0	0
90	-45	135	-677	0	-373	135	-45	135	-683	0	-378	180	-45	135	-674	0	-382
90	-45	180	-675	0	-533	135	-45	180	-674	0	-537	180	-45	180	-680	0	-532
90	0	-180	0	0	-747	135	0	-180	0	0	-748	180	0	-180	0	0	-747
90	0	-135	0	0	-535	135	0	-135	0	0	-532	180	0	-135	0	0	-525
90	0	-90	0	0	0	135	0	-90	0	0	0	180	0	-90	0	0	0
90	0	-45	0	0	522	135	0	-45	0	0	530	180	0	-45	0	0	533
90	0	0	0	0	749	135	0	0	0	0	749	180	0	0	0	0	747

Table 2. Continued

B_Rot_X [deg]	B_Rot_Y [deg]	B_Rot_Z [deg]	F_x (lbs)	F_y (lbs)	F_z (lbs)	B_Rot_X [deg]	B_Rot_Y [deg]	B_Rot_Z [deg]	F_x (lbs)	F_y (lbs)	F_z (lbs)	B_Rot_X [deg]	B_Rot_Y [deg]	B_Rot_Z [deg]	F_x (lbs)	F_y (lbs)	F_z (lbs)
90	0	45	0	0	-524	135	0	45	0	0	-532	180	0	45	0	0	-534
90	0	90	0	0	-747	135	0	90	0	0	-748	180	0	90	0	0	-750
90	0	135	708	0	-524	135	0	135	696	0	-528	180	0	135	707	0	-524
90	0	180	711	0	-367	135	0	180	705	0	-358	180	0	180	700	0	-373
90	45	-180	715	0	0	135	45	-180	708	0	0	180	45	-180	705	0	0
90	45	-135	710	0	364	135	45	-135	711	0	372	180	45	-135	702	0	382
90	45	-90	705	0	527	135	45	-90	704	0	528	180	45	-90	710	0	524
90	45	-45	708	0	363	135	45	-45	705	0	372	180	45	-45	701	0	371
90	45	0	708	0	0	135	45	0	703	0	0	180	45	0	701	0	0
90	45	45	706	0	-367	135	45	45	702	0	-380	180	45	45	698	0	-382
90	45	90	708	0	-524	135	45	90	696	0	-528	180	45	90	707	0	-524
90	45	135	985	0	0	135	45	135	988	0	0	180	45	135	988	0	0
90	45	180	988	0	0	135	45	180	985	0	0	180	45	180	988	0	0
90	90	-180	989	0	0	135	90	-180	988	0	0	180	90	-180	985	0	0
90	90	-135	989	0	0	135	90	-135	991	0	0	180	90	-135	988	0	0
90	90	-90	988	0	0	135	90	-90	989	0	0	180	90	-90	989	0	0
90	90	-45	987	0	0	135	90	-45	990	0	0	180	90	-45	989	0	0
90	90	0	988	0	0	135	90	0	987	0	0	180	90	0	989	0	0
90	90	45	988	0	0	135	90	45	988	0	0	180	90	45	987	0	0
90	90	90	985	0	0	135	90	90	988	0	0	180	90	90	988	0	0
90	90	135	698	0	532	135	90	135	696	0	533	180	90	135	709	0	522
90	90	180	691	0	366	135	90	180	696	0	378	180	90	180	707	0	374
90	135	-180	698	0	0	135	135	-180	701	0	0	180	135	-180	693	0	0
90	135	-135	697	0	-377	135	135	-135	696	0	-378	180	135	-135	709	0	-367
90	135	-90	697	0	-532	135	135	-90	706	0	-527	180	135	-90	699	0	-530
90	135	-45	698	0	-374	135	135	-45	694	0	-378	180	135	-45	700	0	-378
90	135	0	699	0	0	135	135	0	693	0	0	180	135	0	696	0	0
90	135	45	699	0	376	135	135	45	695	0	370	180	135	45	697	0	373
90	135	90	698	0	531	135	135	90	696	0	533	180	135	90	707	0	524
90	135	135	0	0	748	135	135	135	0	0	750	180	135	135	0	0	747
90	135	180	0	0	526	135	135	180	0	0	532	180	135	180	0	0	533
90	180	-180	0	0	0	135	180	-180	0	0	0	180	180	-180	0	0	0
90	180	-135	0	0	-526	135	180	-135	0	0	-530	180	180	-135	0	0	-527
90	180	-90	0	0	-749	135	180	-90	0	0	-748	180	180	-90	0	0	-748
90	180	-45	0	0	-536	135	180	-45	0	0	-529	180	180	-45	0	0	-532
90	180	0	0	0	0	135	180	0	0	0	0	180	180	0	0	0	0
90	180	45	0	0	531	135	180	45	0	0	526	180	180	45	0	0	526
90	180	90	0	0	748	135	180	90	0	0	750	180	180	90	0	0	749
90	180	135	0	0	0	135	180	135	0	0	0	180	180	135	0	0	0
90	180	180	0	0	0	135	180	180	0	0	0	180	180	180	0	0	0

Table 2. Continued

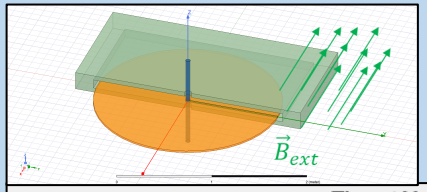

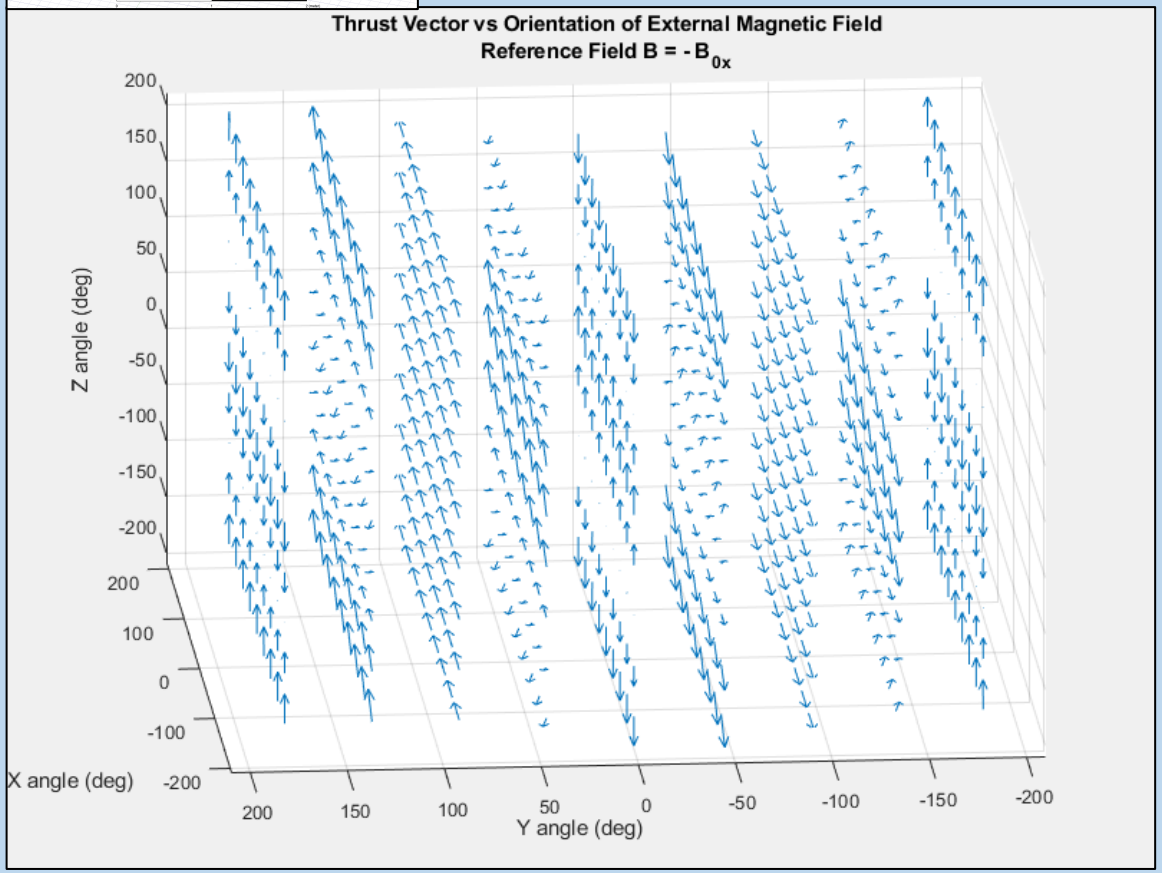

(a)

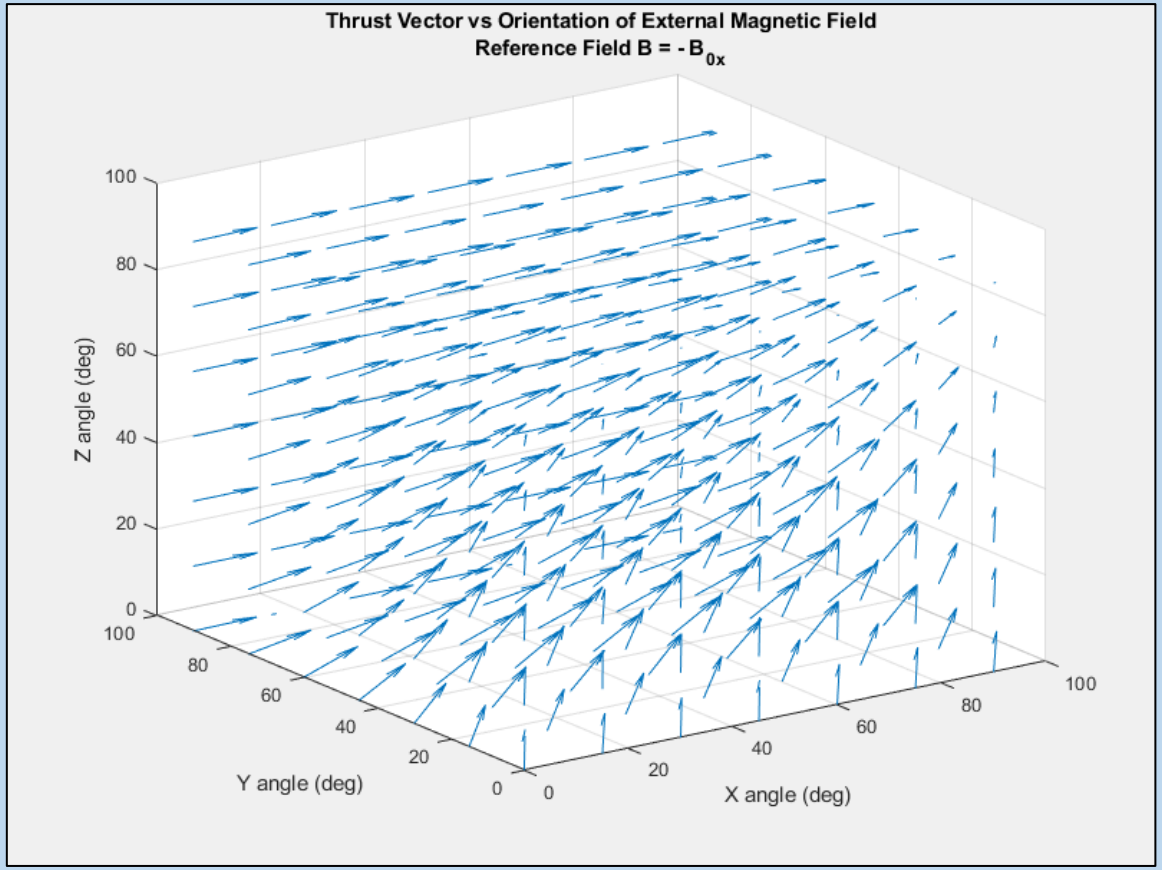

(b)

Figure 30. Simulated force vector vs orientation of the external magnetic field, referenced to a $\vec{B} = -B_0\hat{x}$ magnetic field. Force is for the set up shown in Figure 9; disc radius = 1 meter, k = 1 x 10^9, Voltage = 2 V, RPM = 100,000, d = 2 microns. (a) simulations at 45-degree increments from -180 degrees to 180 degrees on all axis. (b) simulations at 15-degree increments from 0 to 90 degrees.

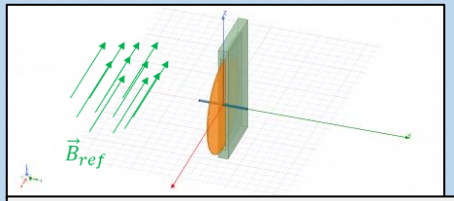

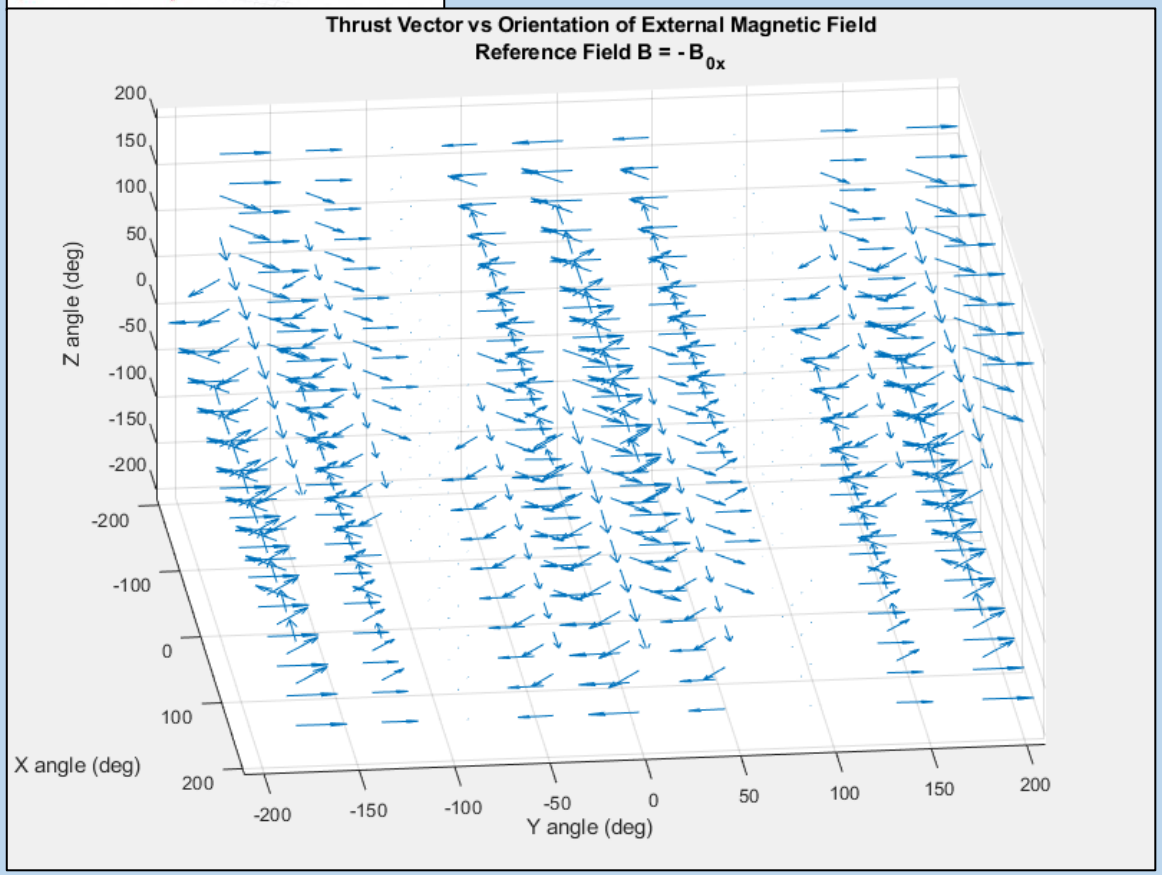

(a)

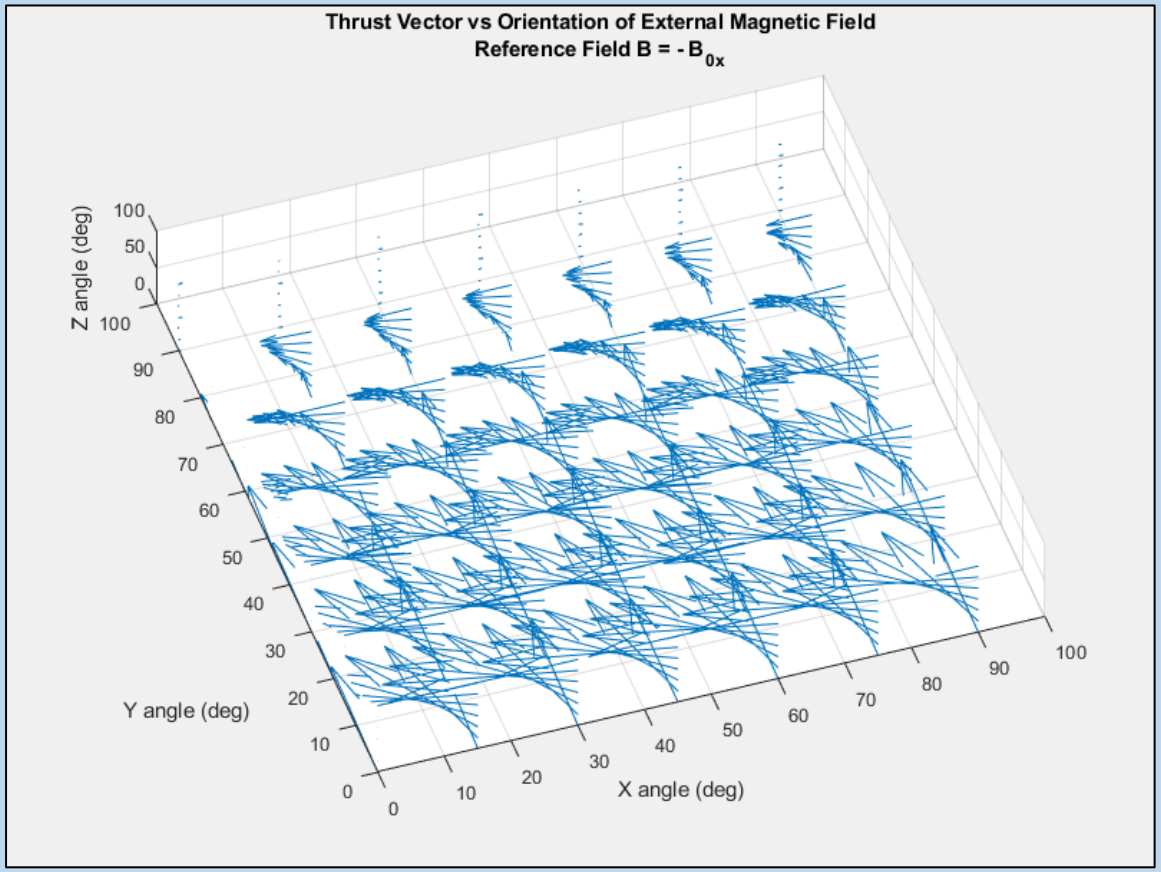

(b)

Figure 31. Alternate propulsion system orientation. Simulated force vector vs orientation of the external magnetic field, referenced to a $\vec{B} = -B_0\hat{x}$ magnetic field. Force is for the set up shown in Figure 9; disc radius = 1 meter, k = 1 x 10^9, Voltage = 2 V, RPM = 100,000, d = 2 microns. (a) simulations at 45-degree increments from -180 degrees to 180 degrees on all axis. (b) simulations at 15-degree increments from 0 to 90 degrees.

Micro-ultra magnet (MUM) system

To this point in the description of the current invention rather large dynamic supercapacitors (DSC) on the order of a meter to meters have been discussed. In “Methods and Apparatuses for Producing Ultra-strong Magnetic Fields”, serial no. 63/162,137 a small device abbreviated Micro Ultra-magnets (MUMs) was described in detail, see figure 32 for an illustration. The discs are made of diamond and sapphire, metal coated to provide conduction paths. The advantage of the MUM design is it allows for a high density of discs to be packed into a small diameter design giving a very high charge per unit volume which translates to a high thrust per unit volume when combined with the symmetry breaking methods described within the current invention. Additionally, the smaller size allows for a number of manufacturing and operational advantages as outlined in the prior patent, e.g., very good tolerances, mass production of a modular base unit, availability of exotic materials in smaller sizes, use of micro-fabrication technology, higher achievable rotation rates, etc.. The preferred embodiment of the MUM as described in serial no. 64/162,137 is 1-cm diameter discs. However, as was noted in equation 25, the thrust goes as the radius of the discs to the third power; the 1-cm MUM design can not practically produce lift greater than its own weight (as measured on the Earth). To this end, the MUM as previously described, can be scaled up to 10-cm discs which can provide lift well in excess of the modified MUM’s intrinsic weight. Ten centimeters is a size that still provides many of the manufacturing and operational benefits as described by the 1-cm MUM in serial no. 64/162,137.

Figure 33 shows a schematic of a modified MUM model with 10-cm diameter discs stacked to a 10-cm height. The inner discs are attached to the inner shaft. The outer discs are attached to the outer cylinder which is attached to the outer shaft. In this way, the inner and outer discs can be counter rotated independently, each having opposite charge polarity. The discs may also be made of extremely strong materials such as diamond, sapphire, silicon carbide, etc. to resist the high centrifugal forces as well as the internal electromagnetic stresses the device will experience during operation. A number of additional MUM construction details can be found in serial no. 64/162,137.

Micro Ultra-Magnet (Magnetic Core unit)

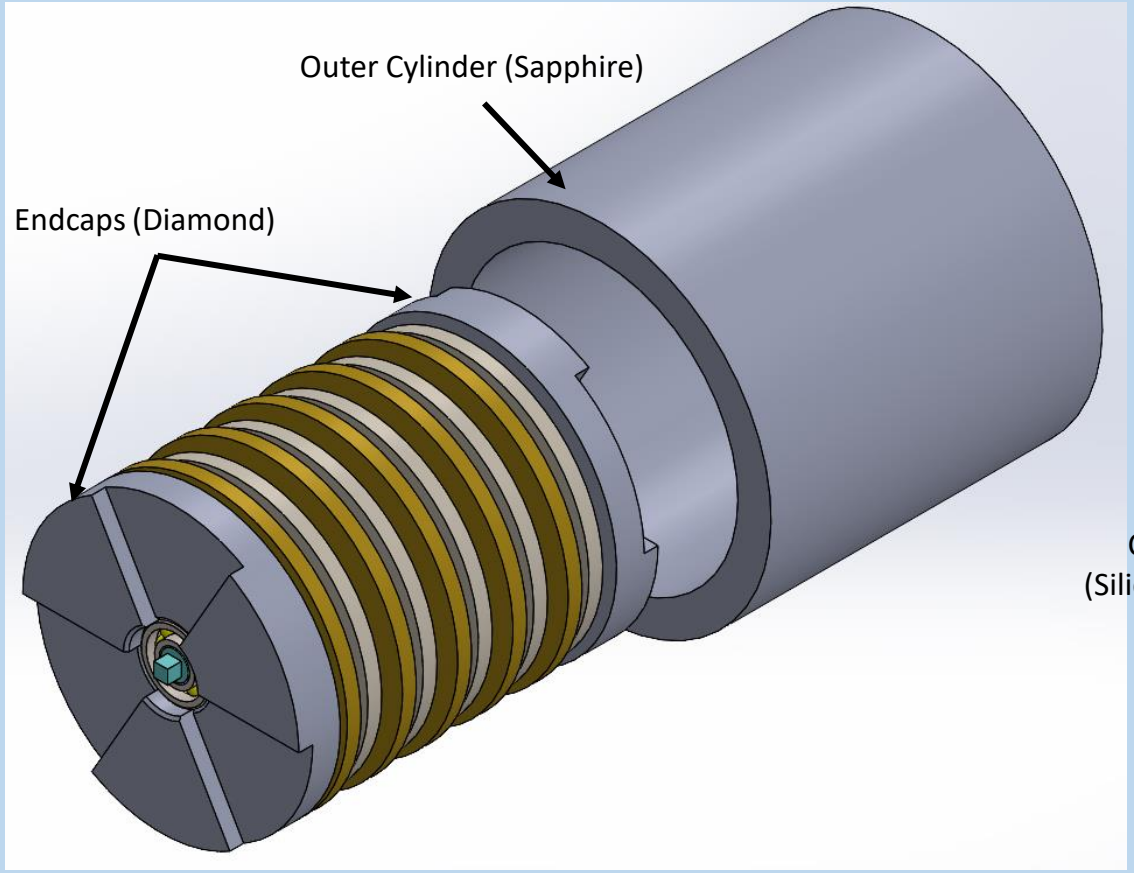

(a)

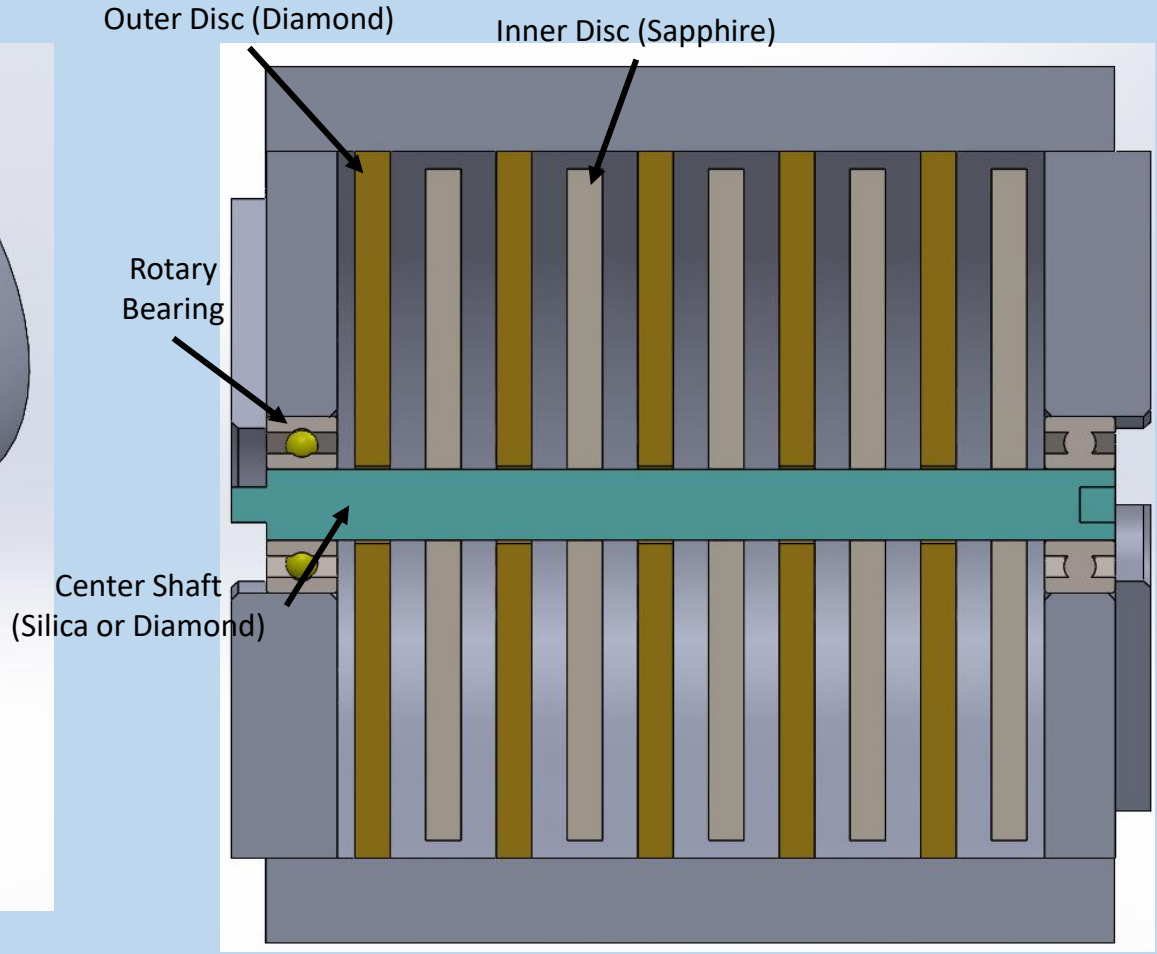

(b)

Figure 32. Micro Ultra-Magnet (MUM) Core. (a) an exploded view of the MUM core; (b) a cross-sectional view of the MUM core.

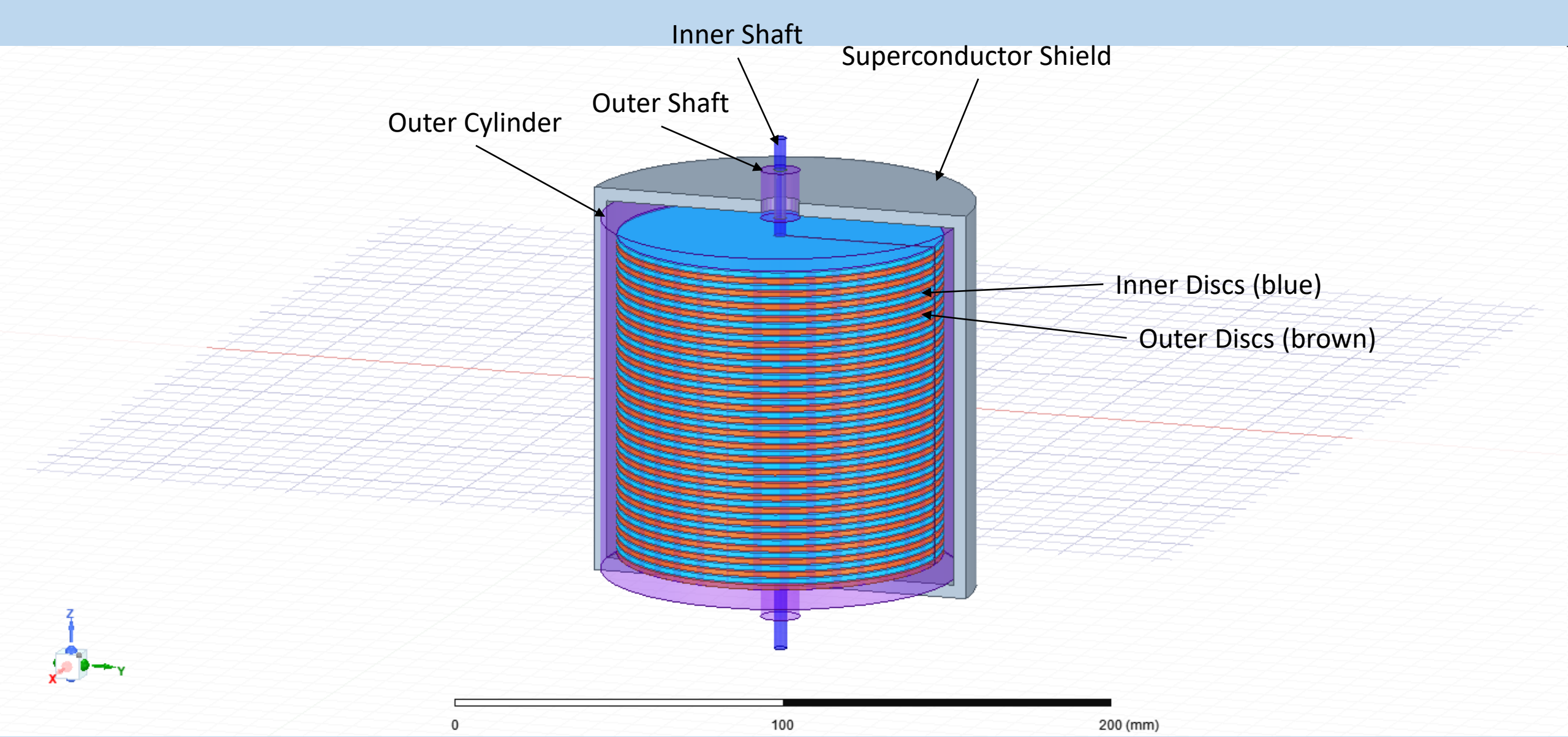

Figure 33. Modified Micro Ultra-Magnet (MUM) to provide lift in an external magnetic field. Discs are 10 cm in diameter.

MUM Propulsion Unit

With the large disc DSCs (MDU based) described so far (e.g., figure 9), the solid angle of the opening for the superconductor shielding is relatively small and is efficient at shadowing the external magnetic field from reaching portions of the DSC disc which would diminish the lift of the system. The MUM shown in figure 32 has a relatively large solid angle and is inefficient at shadowing the external magnetic field from unwanted portions of the disc. The superconductor shield shadowing is most efficient when the rotational axis of the discs is aligned with the magnetic field, figure 34.

There is a balance between the effective current exposed to the external magnetic field and the shadowing of the field reaching unwanted parts of the system (i.e., the lower part of the discs shown in figure 34). The maximum effective current runs at the outer portion of the rotating discs, see figure 13. The maximal force is exerted at the apex of the rotation, i.e., where the cross product of the tangential velocity vector and the external magnetic field produce the maximal z-directional force, shown on figure 33. This point is at 90 degrees from the x-axis on the configuration shown in figure 34. As one deviates from the 90-degree line, the contribution to the force in the z-axis diminishes; the magnitude of the force vector remains the same, but components of force are directed into the $\pm$y-direction which cancel due to the symmetry of the disc, manifesting as an internal tensile stress on the disc. At 0 and 180 degrees the force vector is fully in the y-direction; positive for 0 degrees and negative for 180 degrees which sum to a zero net force contribution overall.

Figure 35a shows the default configuration. With 10-cm diameter discs (~4 inches) with a 10-cm height, disc spacings of D = 0.1 mm, dielectric thickness d = 1 micron, k = 1 x 10^9, V = 2 volts, RPM = 100,000, the default configuration produces a lift of approximately 113 pounds at the Earth's equator. Figure 34b shows a modified configuration in which the optimal balance between external field shadowing and exposed effective current, this configuration produces a lift of approximately 124 pounds. Figure 34c shows a plot of the lift vs the angle of the wedge, showing a maximum around 130 degrees; the angle shown in figure 35b. The modified MUM, excluding the cryofluids to cool the superconductor, weighs approximately 20 lbs. This gives the MUM propulsion unit a net lift of about 100 lbs.

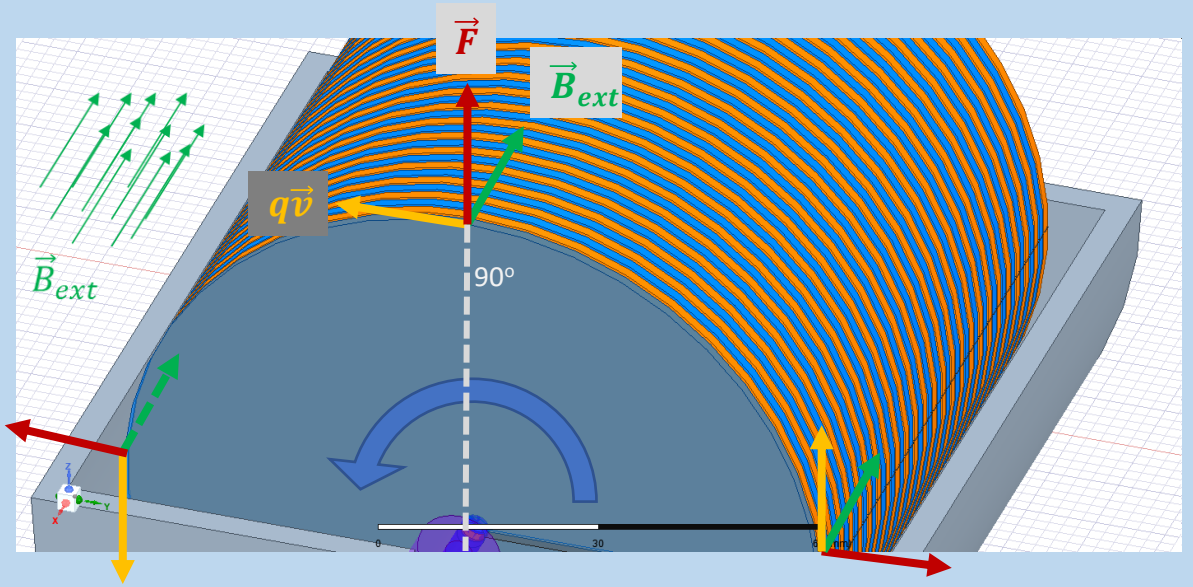

Figure 34. Modified Micro Ultra-Magnet (MUM) core illustrating force directions throughout the rotation process. Maximum lift (F_z) is at the apex of rotation.

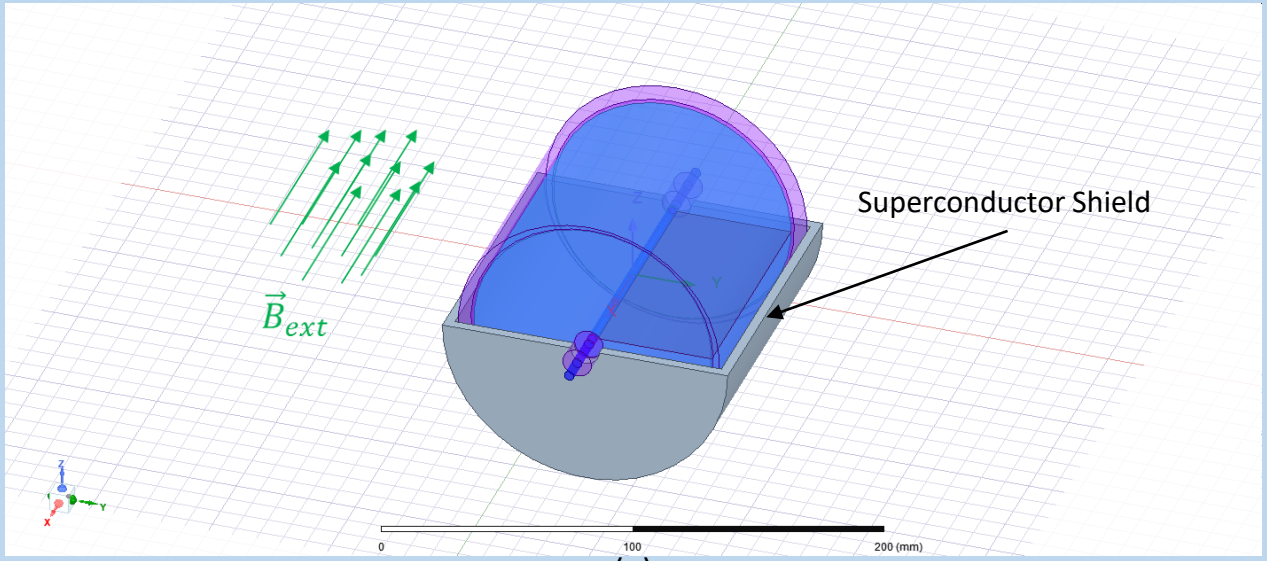

(a)

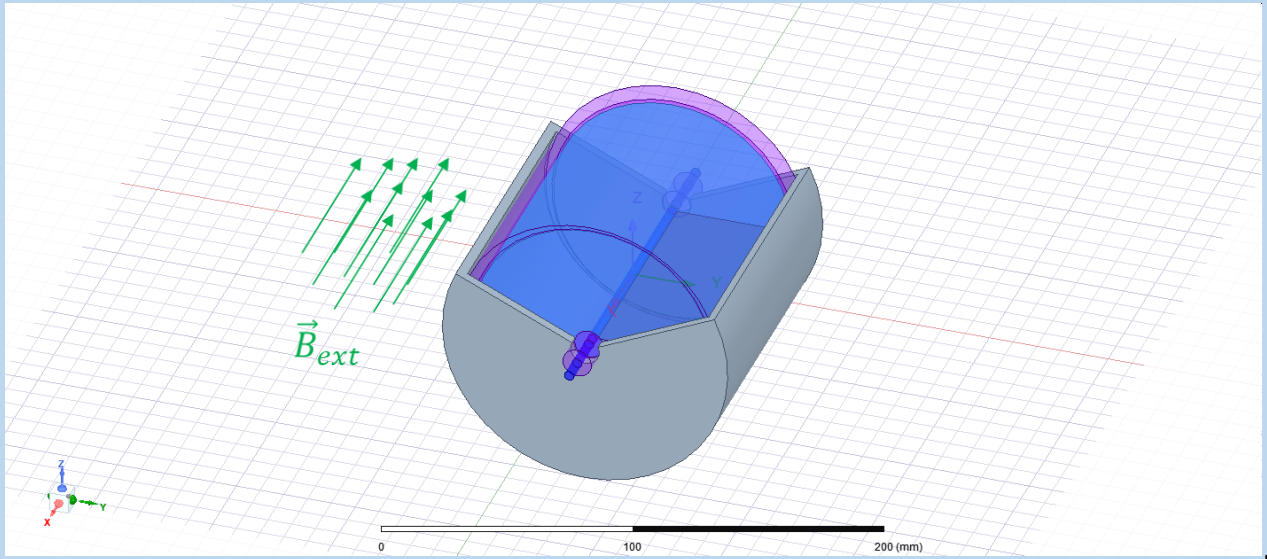

(b)

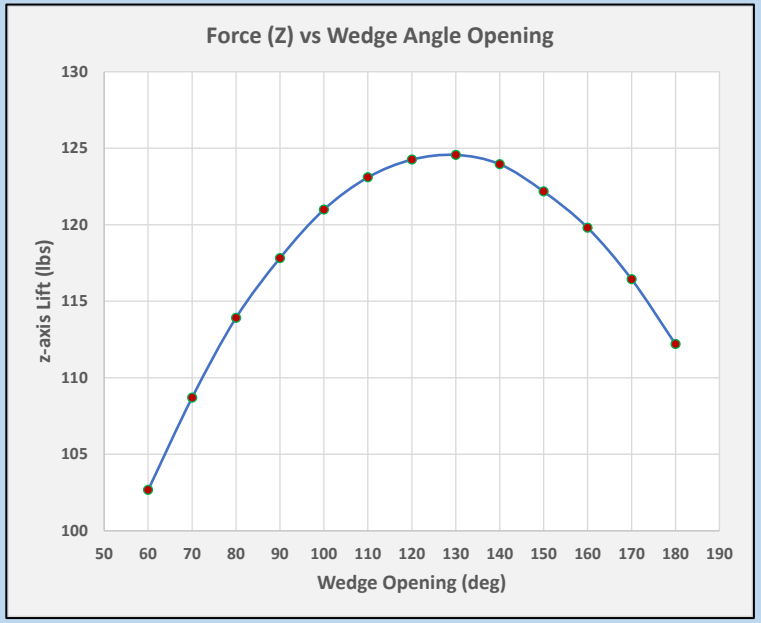

(c)

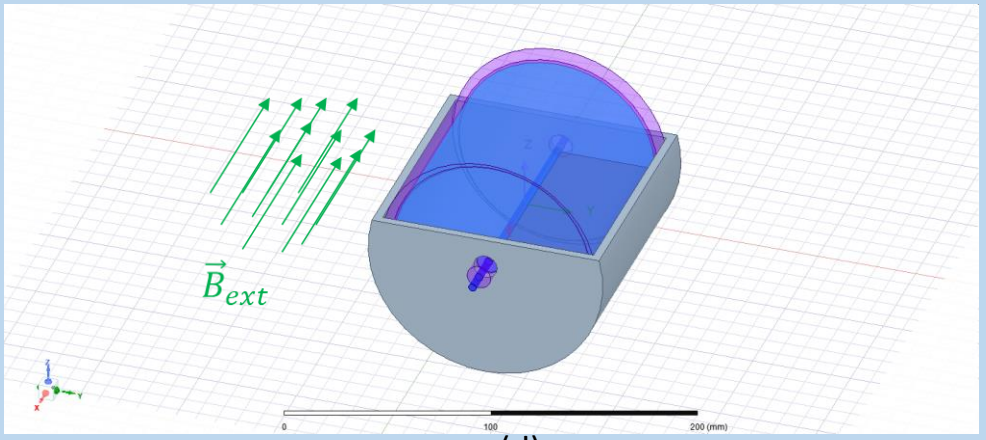

(d)

Figure 35. Optimal balance between occluding the external magnetic field from reaching the –z region of the rotating discs and exposing the effective current to produce optimal lift from a modified MUM. (a) default configuration, with a 180-degree exposure (F_z = 113 lbs); (b) with a 130-degree exposure (F_z = 124 lbs); (c) plot of F_z vs angle of exposure; (d) different geometry method of occluding the external field – produces similar optimum as (c).

Craft Design Considerations

When designing a craft around the propulsion technology described herein there are some considerations that should be taken into account. Firstly, the DSCs produce strong magnetic fields that can be dangerous to living organisms as well as electronic and electrical components. Fortunately, the magnetic fields drop off quickly, to the third power of distance for a magnetic dipole

$$\vec{B}_{dip} = \frac{\mu|\vec{m}|}{4\pi R^3}(2cos\theta\hat{R} + sin\theta\hat{\theta}) \quad (32).$$

Once the field drops to an acceptable level, conventional magnetic shielding can be used to shield people or equipment from the magnetic fields produced by the DSCs. Figure 36 shows the magnetic field distribution for the MUM propulsion unit described in figure 35. The field drops to one tesla within a distance of 60 centimeters. Conventional magnetic shielding can operate on the order of one Tesla [58]. If shielding is required in stronger fields, superconductor shielding may be used.

Space travel requires energy, especially to get into orbit or to escape the gravity well of a planet such as the Earth. A kilogram of mass in low Earth orbit (LEO), at the same altitude as the International Space Station in this case, has a total energy (kinetic plus gravitational potential) of about 33 megajoules, and a one-kilogram object in geosynchronous orbit (GSO) has a total energy of about 58 megajoules; both values above what they would have referenced to sitting stationary on the ground at the Earth's equator. A great deal of energy can be infused into the propulsion unit before launch. A single MUM propulsion unit previously described can be charged and set into motion before leaving the launch pad. At 100,000 RPM the previously described MUM unit can store approximately 1.2 gigajoules of electromagnetic energy. The propulsion unit is not ideal as the main source of power as it will lose energy over time to non-conservative forces such as friction and fluid drag on the electrodes in motion. This loss will occur even when the propulsion unit is not under load. Additionally, as the MUM propulsion unit loses stored energy, its thrust potential will diminish. However, the proposed propulsion systems herein operate on electricity instead of chemical fuel and can take advantage of any high-density, efficient, electrical power source, such as a nuclear reactor as an example, to restore lost energy to the system. Static high energy storage devices such as high-energy density batteries and super-capacitors are an active area of advancement and conceivably can be used as a power source for shorter missions. As a reference, a gallon of regular unleaded gasoline contains about 120 megajoules of energy. In the end, it becomes a matter of how efficiently one can utilize the energy sources at hand to go from the Earth's surface to orbit. In a one hundred percent efficient system, surprisingly little energy is needed to achieve orbit.

The propulsive efficiency of the current invention is not yet known; however, it is likely the proposed propulsion system is significantly more efficient than a rocket engine which depends on mass ejection to generate thrust. Due to conservation of momentum a great deal of kinetic energy is lost to the exhaust of the rocket. Additionally, combustion of the reactants creates high thermal energy molecular gases. These hot gas molecules experience significant excitation of vibrational and rotational molecular modes which diminishes their translational energy. Translational energy is the energetic mode necessary to provide the needed thrust. Overall, rocket engines are inefficient in converting chemical energy into mechanical, i.e. kinetic, energy of the craft. The current invention does not utilize any type of exhaust or mass ejection to achieve thrust. Additionally, rockets experience a great deal of aerodynamic drag due to the high velocities needed to escape the Earth's atmosphere and achieve orbit. The current invention does not require high velocities to rise out of the atmosphere, therefore, aerodynamic drag can be minimized; the craft can be accelerated to the translational velocity needed for orbit once the craft is above the drag of the atmosphere.

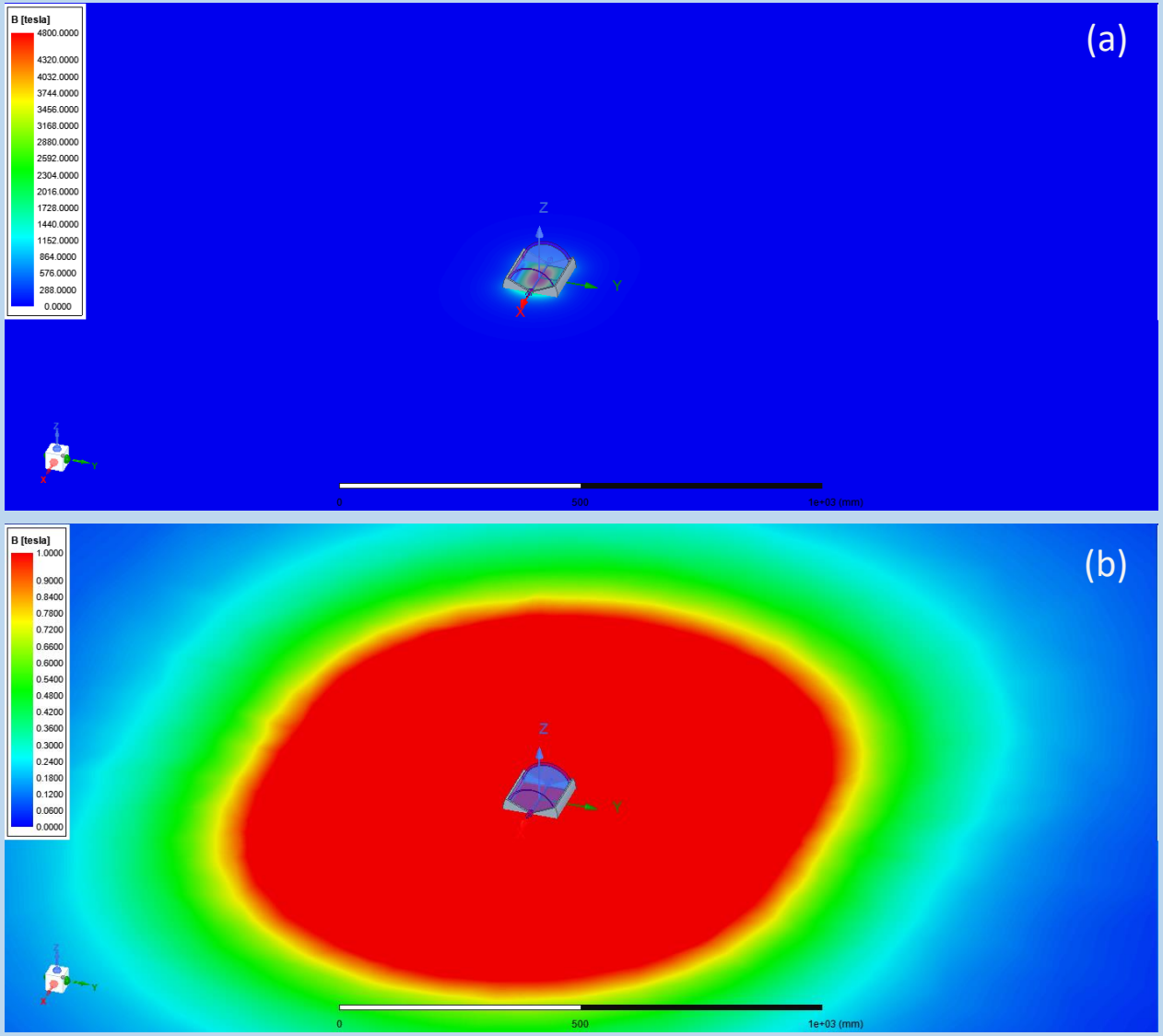

Figure 36. (a) Magnetic field strength distribution for the modified MUM propulsion unit. (b) Magnetic field strength distribution for the modified MUM propulsion unit; areas in red are greater than one Tesla, all other areas are less than one Tesla.

Craft Design Considerations

A single propulsion unit may not be sufficient to provide the desired lift and thrust forces. The base units described so far are designed to be modular such that a great number of individual base units can be assembled to provide greater overall performance. Figure 37 shows three such configurations, one a 2 m x 2 m planar layout of modified MUMs which, at the Earth's equator, produces a simulated lift of 74,180 Newtons (16,670 lbs). The second is a 2 m x 2 m x 2 m cubic volume which produces an estimated lift/thrust of approximately 810,000 Newtons (183,000 lbs) at the Earth's equator; about the weight of a fully loaded 737-800 commercial jet. The third is based on the stacking of propulsion units based on the multi-electrode disc ultra-magnet (MDU). As shown the assembly in figure 37c produces a simulated lift of 34,300 Newtons (7700 lbs). This lift is not as impressive as the MUMs unit assemblies; however, this configuration may provide implementation advantages. Additionally, the MDU's shown are only two counter-rotating discs per MDU base unit; more densely packed electrodes per base unit may be implemented to produce magnified lift (a factor of 10 to 20) as was described in MDU technology from the prior disclosure.

It is worth noting, due to the fields diminishing quickly from their source, the base propulsion units can be assembled and spaced such that the total magnetic field strength can be controlled as to not exceed the critical magnetic point of the superconductor shielding to avoid quenching, i.e., loss of superconductivity. In all regards, all attempts should be made to magnetically harden the superconductor shield as described by Wu et al [15] and Yoshizawa et al [16] to provide maximum lift per unit volume. The individual base propulsion units will also experience attractive and repulsive magnetic forces with the other base propulsion units as they are each powerful magnets. The geometry of the configurations shown are only examples; any number of geometrical configurations can be realized. The geometry and spacing of the propulsion system assemblies can be configured to control inter-unit field exposure from other units, e.g., to prevent magnetic superconductor quenching or exceeding mechanical structural limits. Ultimately ,it is a matter of packing density vs superconductor magnetic quenching threshold and mechanical stress integrity that limits the lift/thrust density achievable in any design.

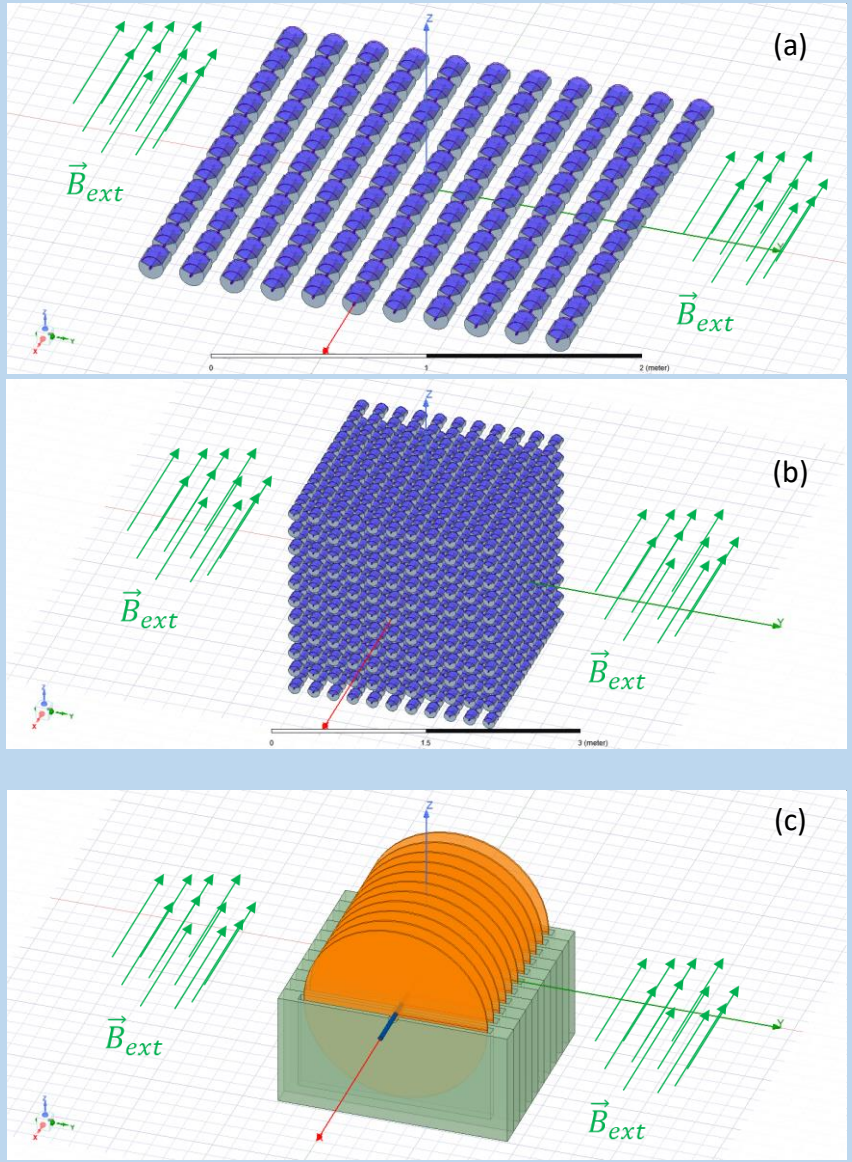

Figure 37. Expanded propulsion systems built from individual base propulsion units. (a) 121 MUM units in a four-square meter planar layout (d = 1 microns). (b) 1331 MUM units in a 2 m x 2 m x 2 m volumetric layout (d = 1 microns). (c) an 11 base propulsion unit assembly based on MDU units (d = 2 microns).

Craft Design Considerations

Finally, it should be apparent that it is advantageous to build the craft out of materials with very high weight to strength ratios; making the craft as light as possible while meeting mission or operational requirements. It is not necessary for the craft to travel at supersonic or hypersonic speeds inside the atmosphere in order to obtain orbit; liftoff and reentry can be accomplished in a highly controlled manner if desired. The skin and frame of the craft can be constructed of ceramics, polymers, composites, magnesium alloys, newer biomimetic ceramics [19], or any of the myriad of materials artificial satellites and space probes are currently constructed from today [20, 21, 22]. All these materials provide good strength to weight ratios. Of course, if the craft is outside the atmosphere, the materials must be capable of withstanding the harshness of space – meteorites, radiation, thermal cycles, vacuum, etc. The same environmental considerations should be adhered to if the craft is to operate underwater as well. The only structural components that strictly require extreme strength are the mechanical components of the extended propulsion system, e.g., the superstructure that holds the MUM units shown in figure 37 for example, the shafts that transfer the lift from the propulsion units to the body/frame of the craft, and the constituent components of the DSCs. Ideally, the materials used will be non-magnetic, as to not create unwanted forces, and largely non-conductive to minimize the potential of magnetically induced eddy currents. If conductors are to be used in the area of strong magnetic fields, such as the traces that supply charging to the DSCs and the electrodes of the DSCs, the conductor should be made as thin as is practically possible, such as vapor deposited thin metal films, and segmented and/or labyrinthine to break up potential eddy currents.

Lift Mechanism at the Quantum Level

So far lift/thrust has been described at the macroscopic level. Ultimately, the lift and thrust described is a quantum phenomenon. The positive charges are part of the material structure. The magnetic force for positive charges is imparted to the structure through the material's atomic lattice. The electrons however are free to move throughout the conductive materials of the DSC electrodes. As the electrons move, they will collide with the atoms in the conductors and impart some of their momentum to the atoms, however, the migrating electrons will reach the boundary edge of the conductor. Here the electrons will encounter the Schottky-Nordheim quantum barrier; the potential barrier between inside the metal and the outside world. Because the electrons have energy and are under the influence of strong Lorentz forces, they exert 'pressure' on this barrier, which provides aforementioned lift and thrust via pressure on the conductor's Schottyky-Nordheim barrier. Due to this, the electrons have a probability of quantum tunneling through the quantum barrier potential and escaping as field emission electrons. Building on the work of S.G. Christov [17] and cold field emission of electrons for electron microscopes [18], adding an electron moving in a magnetic field term to the aforementioned references it can be shown that the probability of the electron escaping, i.e., quantum tunneling through the quantum barrier, is

$$P = \exp[-\frac{4\sqrt{2m_e}}{\hbar}\int_0^{\frac{W}{e\left(E+|v|\left|B_{\|}\right|\right)}}\sqrt{W - ex\left(E + |v|\left|B_{\|}\right|\right)}\,dx] \qquad (33)$$

where ħ is the reduced Planck's constant, m_e is mass of the electron, e is the charge of the electron, W is the work function of the conductor, E is the electric field at the barrier, v is the velocity of the electron, and $B_{\|}$ is the component of the magnetic field parallel to the barrier.

Using a somewhat extreme example, a system with a two-micron disc spacing with a two-volt potential with a k = $1x10^9$ super-dielectric, an electron in a one-meter radius disc coated in silver (W = 4.74 eV) spinning at 100,000 RPM, with an internal B field of 5000 Tesla, at the edge of the disc, i.e., where the highest tangential velocity will be found, the electron has a 2.49×10^{-37} probability of escaping the conductor by quantum tunneling. It can be stated the lift/thrust can be generated by the propulsion system without worry of the atomic and particle scale lift components escaping their quantum confinement potential wells.

Energy Chain Considerations

As is well known, energy can not be created or destroyed (conservation of energy and the first law of thermodynamics). To this end, it may be instructive to describe how the internal energy, *U*, of the propulsion system is affected by a change in the potential or translational kinetic energy of the system, i.e., the craft changing altitude (potential energy) or changing velocity (translational kinetic energy).

The energy stored in the propulsion system is

$$U = Mechanical + Magnetic + Electrical \quad (34)$$

$$U = \frac{1}{2}\sum_i (I_i\omega_i^2 + \int_V \frac{1}{2\mu}B_i^2 dV + Q_i V_i) \quad (35)$$

where I_i is the moment of inertia of the *i*-th rotating element, ω_i is the rotational velocity of the *i-th* rotating element, B_i is the magnetic field produced by the *i-th* rotating electrode, μ is the magnetic permeability of the material in which the field exists, Q_i is the electrical charge stored on the *i-th* rotating electrode, V_i is the voltage potential between the *i-th* rotating electrode and the conductive slip joint fluid. The magnetic field, B_i, is integrated over all space to obtain the total magnetic energy stored in the magnetic field of the *i-th* element.

For illustrative purposes, a single spinning disc will be considered; one electrode being the spinning disc, the other electrode being the conductive slip-joint fluid in the exemplary case. More complex systems can be extrapolated and understood from this base example. When the potential or translational kinetic energy of the craft changes, the energy flow needed to affect those changes will come from the internal energy of the propulsion system. The primary question becomes how will the energy flow from the propulsion system to the potential and translational kinetic energy of the craft manifest itself. The magnetic field strength is directly proportional the rotational velocity of the disc. For a single spinning disc as described, equation 35 can be rewritten as

$$U = \frac{1}{2}I\omega^2 + \frac{1}{2}\omega^2 \int_V \frac{K_B^2}{\mu} dV + \frac{1}{2}QV \quad (36)$$

$$K_T = (I + \int_V \frac{K_B^2}{\mu} dV)$$

$$U = \frac{1}{2}K_T\omega^2 + \frac{1}{2}QV \quad (37)$$

where $\vec{K}_B$ is an intermediate resultant field after the rotational velocity variable has been factored out of the magnetic field, $\vec{B}$. It is assumed ω is constant with respect to spatial coordinates and can be factored out of the integral, as is the case for a rigid rotating disc.

Energy Chain Considerations

The system can be closed to charge transfer, i.e., the charge magnitude on the electrodes can be fixed. In this case, the term on the right in equation 37 is a constant and does not contribute to energy flow. The effective current for a charged spinning disc can be derived as

$$\vec{J}_{eff}(r) = \frac{Q\omega r}{\pi h R^2}\hat{\varphi} \qquad (38)$$

where h is the thickness of the conducting part of the disc. The charge used in the J_{eff} calculations is a constant, leaving only the ω term as a changeable variable under energy flow. Since B, K_B, and K_T are proportional to J_{eff}, the only variable term in energy flow is ω. This means that without external energy being supplied into the propulsion system (from a power supply for example), the energy that flows from the internal energy of the propulsion system to do work on the craft, i.e., affect a change in potential or kinetic energy of the craft, must come from a change in the rotational velocity of the charged discs. To get a change in rotational velocity there must be a reactionary torque on the spinning disc that acts to either speed up or slow down the rotation speed of the disc.

The microscopic source of this reactionary torque can be understood as follows, in the case of a potential energy increase, i.e., an increase in altitude. Referring to figure 38, the disc contains a large number of charges, in this case positive charges are shown in the disc. The disc sits at a position at time, t = 0. In a time Δt the disc moves higher in altitude by an amount Δz. As the charges pass through the external magnetic field, they experience a force in the z-direction due to the rotational motion of the disc in the external magnetic field, as has already been explained in detail. Additionally, as the craft moves in the z-direction and gains altitude, the charges on the disc now experience a velocity component in the z-direction as well. From equation 6, it can be seen that the charges now experience a force, $\vec{F}_{v_z}$, in the plane of the disc that, in the case of an increase in altitude (i.e., positive z velocity), results in a force that acts in the direction opposite to that of the tangential velocity of the charges in the rotating disc. Along the x-axis this force points in the negative y direction. As one moves away from the axis of rotation, a moment arm is produced by these forces and a torque, $\vec{\tau} = \vec{r} \times \vec{F}$, is exerted on the disc that is opposite to the rotational velocity, $\vec{\omega}$. Reactionary torque due to an increase in craft translational kinetic energy is similar to potential energy and is shown in figure 39.

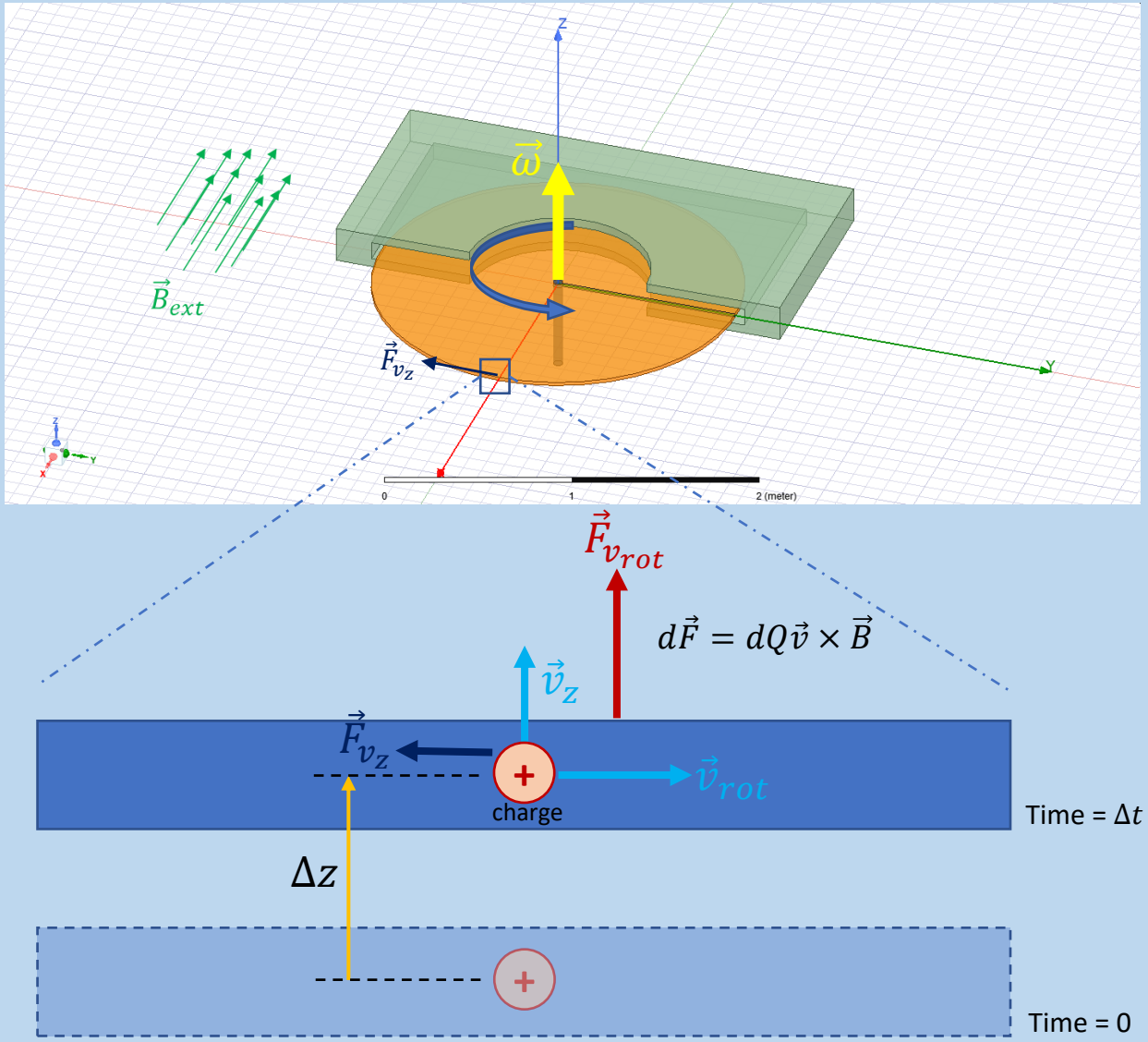

Figure 38. Schematic showing how reactionary torque is produced on spinning charged disc due to propulsion system rising in altitude, i.e., increase in potential energy.

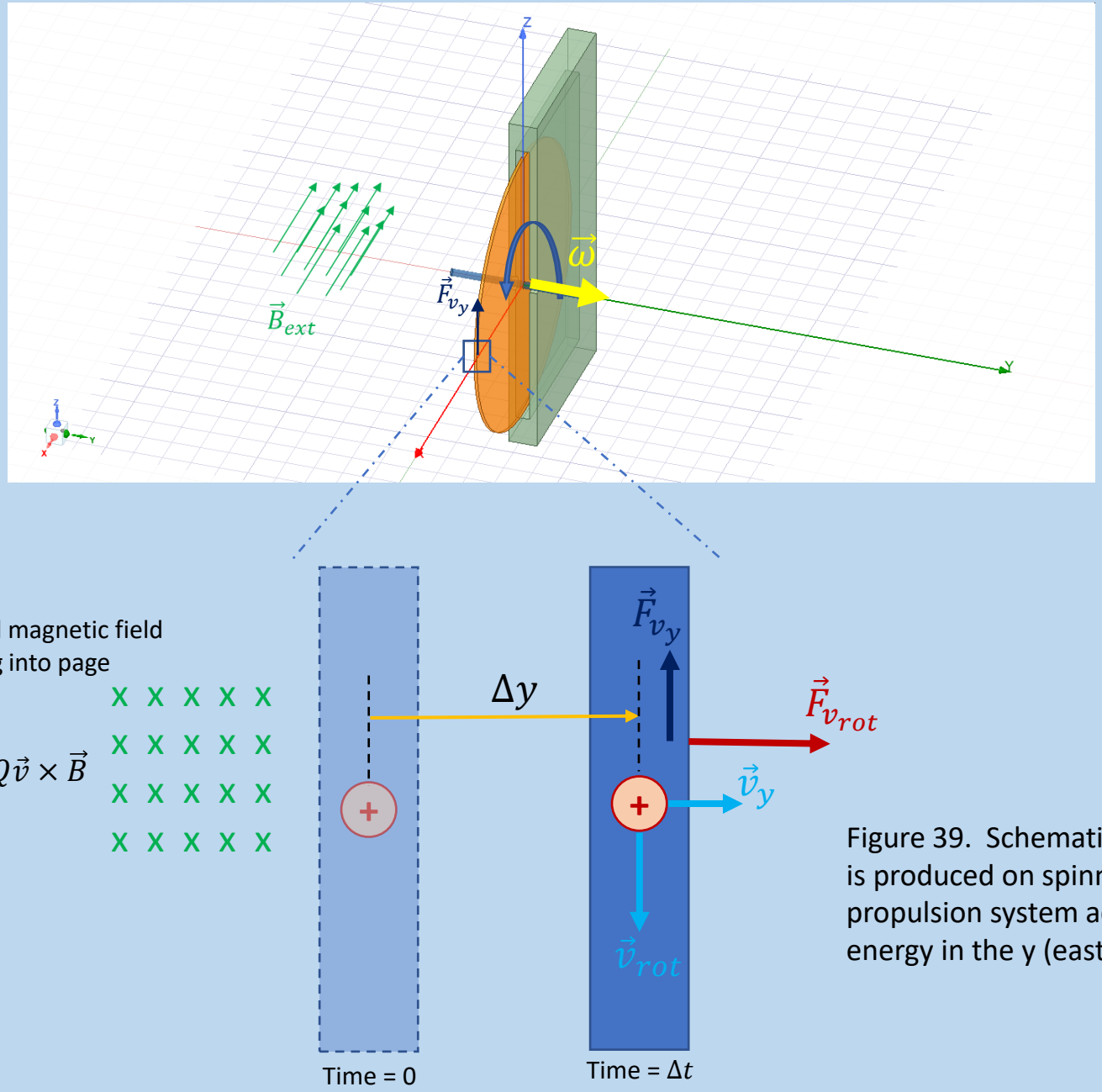

Figure 39. Schematic showing how reactionary torque is produced on spinning charged disc due to propulsion system acquiring translational kinetic energy in the y (eastwardly) direction.

Energy Chain Considerations

Figure 38 and 39 show how the reactionary torque is generated due to energy flow from the point at the edge of disc at r = (R, 0). A full torque calculation requires consideration across the entire disc or set of discs in the case of assemblies. The net reactionary torque may be calculated using energy methods.

To get an approximation on the magnitude of the reactionary torque, the differential work is the force times the differential displacement for the craft and the torque times the differential angular displacement for the propulsion system. Returning to the situation in figure 38,

$$dW = (F_{v_{rot}} - F_{grav})dz = \tau_{react} d\varphi \quad (39)$$

Taking the time derivative,

$$\frac{dW}{dt} = (F_{v_{rot}})\frac{dz}{dt} = \frac{d\varphi}{dt}$$

$$P = (F_{v_{rot}})v_z = \tau_{react}\omega \quad (40)$$

because there are forces and torques present, v_z and ω are time dependent. Assuming the forces and torques do not change significantly on the time scales we are interested in, we can substitute in the Galilean equations of motion for v_z and ω,

$$P = (F_{v_{rot}} - F_{grav})(v_0 + \frac{(F_{v_{rot}} - F_{grav})}{M}t) = \tau_{react}(\omega_0 + \frac{\tau_{react}}{I}t) \quad (41)$$

Taking the time derivative again to eliminate non-time dependent terms and solving for the reactionary torque,

$$\frac{dP}{dt} = \frac{(F_{v_{rot}} - F_{grav})^2}{M} = \frac{(\tau_{react})^2}{I} = \frac{(\tau_{react})^2}{\frac{1}{2}mR^2} \quad (42)$$

$$\tau_{react} = \pm(F_{v_{rot}} - F_{grav})R\sqrt{\frac{m}{2M}} \quad (43)$$

where τ_{react} is the reactionary torque produced by the energy flow, *m* is the mass of the disc, *I* is the moment of inertia of the disc, *M* is the mass of the entire craft, *R* is the radius of the disc, F_{grav} is the force on the craft due to gravity, *W* is work, and *P* is instantaneous power. As an example, using the system in figure 9 (F_{rot} = 3709 N), if the craft has a mass of 200 kg and the discs have a mass of 50 kg, and all other parameters (k, d, V, RPM) are as stated and the acceleration due to gravity is assumed to be 9.8 m/s^2, the reactionary torque on the propulsion unit is approximated to be 620 N-m (456 ft-lbs), about the torque of a Corvette C3 sportscar. It should be clear from equation 43 that the reactionary torque is directly proportional to the acceleration (a = F/M) one desires from the craft; a faster acceleration requires more torque. In order to hover at one altitude, from equation 43, $Fv_{rot} = F_{grav}$, which suggests zero reactionary torque is experienced. The equation for reactionary torque for translational kinetic energy changes is similar to equation 43 without the gravity term.

$$\tau_{react} = \pm(F_{v_{rot}})R\sqrt{\frac{m}{2M}} \quad (44)$$

It should be noted that there may be other forces such as aerodynamic drag on the craft, if the craft is in motion in a fluid such as water or the atmosphere. Those forces are not shown here but are easily added. Note that when the craft reduces its altitude or 'breaks' for translational motion, the torque reacts to increase the rotational velocity of the disc, putting energy back into the propulsion system.

Energy Losses

Since power expended is

$$P = (\tau_{react})\omega \quad (45),$$

from equation 43, theoretically a craft hovering in place will have zero reactionary torque which from equation 45 suggests it would expend no power to hover. This, of course, is only possible if the system in question is frictionless and lossless. In reality, there will be frictional losses from the rotary components (bearings and/or rotary seals). There will be ohmic losses where conventional currents flow. There will also be losses due to drag of the mercury, if mercury is used, or sliding contact friction, if the alternate point contact super-dielectric method is used. These energy losses will need to be replenished to keep the propulsion system operating. Many of these losses are difficult to approximate, therefore, what follows are only rough approximations.

Bearing and seal losses are complex; depending on construction material, bearing size, bearing design, rotational speed, and lubrication. High speed rotary bearings can lose tens of watts to thousands of watts (joules/second) of power due to friction [28, 61, 62], relatively small values compared to other potential sources of power loss in the system. Regarding ohmic losses, if the current breaking symmetry method is used, massive currents must be circulated. These currents can reach on the order of a million amps or more. Even if the resistance is a small value of one milliohm, with one million amps of current the ohmic power loss would be on the order of ten gigawatts. This suggests that using the electrical current oscillation method of breaking symmetry is not a realistic way of producing lift/thrust unless superconductors are used to bring the resistance close to zero. However, superconductors undergoing large time varying currents do not always behave as perfect superconductors [29] but are nonetheless an improvement over typical resistive elements.

In the case of the superconductor shield used to shield part of the spinning charged discs(s) from the external magnetic field, the propulsion unit does not need conventional electrical current for its fundamental operation and does not experience ohmic losses. The exception to this may be if electron current is injected into the mercury in order to create magnetohydrodynamic forces on the mercury and put the mercury into a desired motion. These currents may be in the hundreds to thousands of amps and result in ohmic losses on the order of tens of kilowatts. Another possible ohmic power loss may occur due to eddy currents. Equation 2 says that changing magnetic fields induce circulating electric fields. These circulating electric fields can induce eddy currents in conductive elements in the propulsion system and craft structure. These eddy currents experience ohmic losses similar to conventional currents. Strong eddy currents only occur in rapidly time varying magnetic fields. The magnetic fields need not be rapidly varying and only need to vary at all in order to change lift/thrust force which can be done gradually in most cases. Additionally, mitigating eddy currents through system design is a well-known art in the design of transformers and motors where strong fluctuating magnetic fields are common. With proper design considerations, eddy currents are not likely to be a leading contributor to energy loss of the propulsion system.

Energy Losses

By far the largest frictional energy losses to the system will come from the frictional drag between the spinning disc electrodes and the mercury fluid.

Traditionally, the skin friction drag of the mercury on the walls of the spinning plates would be estimated as [26, 27]

$$F_{Hg} = \int_S C_f \frac{\rho v^2}{2} dA \quad (46),$$

where C_f is the skin friction coefficient, ρ is the mercury density, v is the tangential plate velocity (assumes fluid is stationary far from the plate wall), *S* is the area of the electrode (disc) in question to be integrated over.

$$C_f = \frac{0.664}{\sqrt{Re}} \quad \text{, for Laminar flows} \quad (47)$$

$$C_f = \frac{0.027}{(Re)^{1/7}} \quad \text{, for Turbulent flows} \quad (47)$$

where *Re* is the Reynolds number,

$$Re = \frac{\rho v L}{\mu} \quad (48)$$

where ρ is the density of the mercury, *L* is the characteristic linear dimension of the system, and μ is the dynamic viscosity of the mercury.

The power loss due to the frictional drag of the mercury can be written as

$$P_{Hg}(r) = F_{Hg}\, \omega\, r \quad (49)$$

where r is the distance from the axis of rotation.

Integrating over the entire disc, spinning at 100,000 RPM, gives nonsensical results of losses of tens of billions of watts whether turbulent or laminar. Unfortunately, the system operates well outside the validity range of these traditional methods and no method exists today to accurately estimate the drag losses the spinning discs would experience in the mercury. At the heart of these calculations and indeed computational fluid dynamics as a whole is the 'no-slip' boundary condition in which the fluid is assumed to stick to the wall boundary. As the field of micro-fluidics has grown, deeper research into the no-slip boundary condition has been undertaken. Research has shown that under certain conditions the no-slip assumption is invalid [30, 31, 32]. In fact, the drag from the fluid has been shown to be two to four orders of magnitude less than predicted by the Navier Stokes Dirichlet Boundary Condition (the no-slip boundary condition) [30, 31, 32]. The conditions under which the fluid does not obey the no-slip boundary condition are 1) the fluid does not wet the wall material, 2) the wall surface is smooth, and 3) there is a high shear rate. All three of these conditions are abundantly met in the current invention. The mercury does not wet the super-dielectric matrix material, the walls have nanometer scale smoothness, and due to the counter-rotation nature of the design there will be very high counter-shear rates in the mercury. The discs should readily slip through the mercury and the fluid drag will be greatly reduced. Additionally, adding a counteracting magnetohydrodynamic force to the mercury, as discussed earlier, may cause the mercury to not only not stick to the super-dielectric coated disc walls, but to move against the natural angular momentum that would otherwise be imparted into the mercury fluid. An accurate picture of the mercury's interaction with the electrode wall is complex and not fully known at this time.

Mercury-less Design

While it is believed the discs will slip through the mercury fluid for the reasons previously stated, due to some of the inherent uncertainties associated with how the discs will mechanically interact with the mercury and the importance of power loss at this interface, an alternate design will be discussed which eliminates the need for a conductive slip-joint fluid.

One of the major advantages to the use of a liquid conductor, i.e., mercury, as one of the electrodes is the propulsion system components may be constructed and operated with relatively lax tolerances as these tolerances can be taken up in the mercury. If great care is taken with tolerances in the design and operation of the propulsion system, the use of mercury may be foregone.

The alternative being the super-dielectric layer between electrodes affixed to one electrode and in dynamic/sliding contact with the other electrode, figure 40. The super-dielectric matrix material can be made of super hard materials such as a variety of hard ceramics as stated previously. Additionally, graphene based super-dielectrics are a plausible future alternative [33], graphene being one of the strongest materials known, being stronger than diamond. The point contact slip method was previously described in disclosure serial number 63/162,137. Figure 41 shows the dimpled MUMs super-dielectric layer described in 63/162,137.

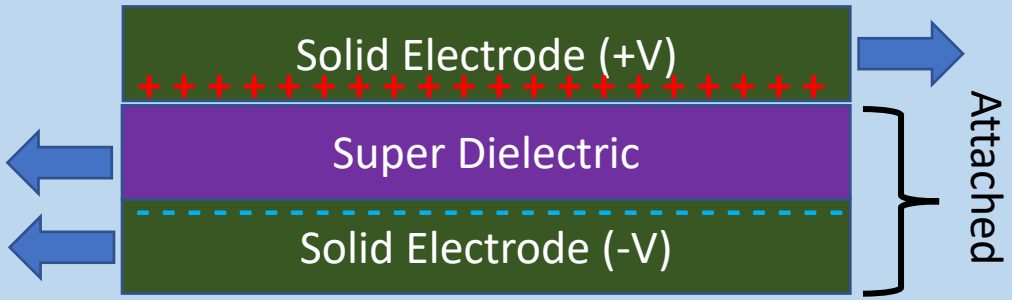

Figure 40. Schematic of interface geometry of mercury-less design. Super-dielectric is attached to the bottom electrode. The top electrode slides on the super-dielectric.

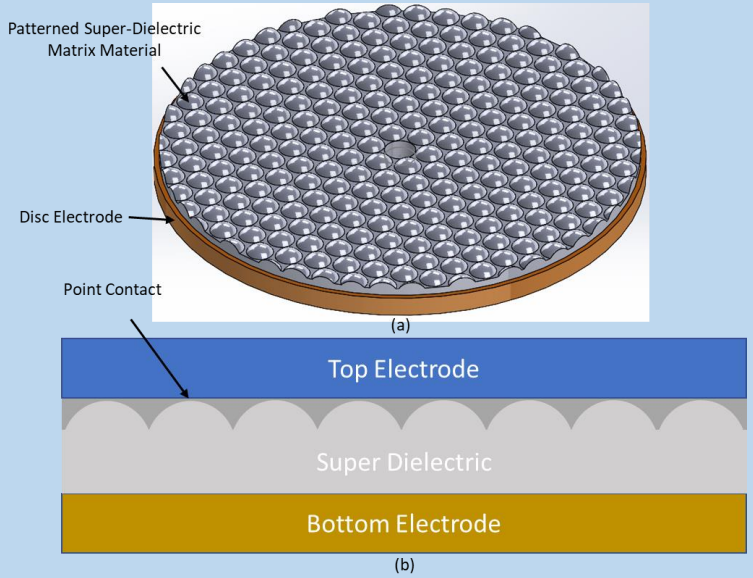

Figure 41. Dimpled super-dielectric matrix layer.

Mercury-less Design

The friction between two sliding surfaces is known from Amonton's Law of Friction to be

$$F_{friction} = \mu_k N \quad (50).$$

where μ_k is the coefficient of kinetic friction, and *N* is the normal force between the two surfaces.

The differential torque on the discs due to rotational friction can be stated as,

$$d\tau = r\, F_{friction} = r\mu_k dN = r\mu_k N(r,\varphi)\, r dr d\varphi$$

The frictional power loss will be ,

$$dP_{friction} = \omega d\tau = \omega \mu_k r^2 N(r,\varphi) dr d\varphi$$

$$P_{friction} = \omega \mu_k \int_{\varphi_1}^{\varphi_2} \int_{R_1}^{R_2} N(r,\varphi)\, r^2\, dr d\varphi \quad (51)$$

, if N varies (non-uniform contact).

$$P_{friction} = \frac{2\pi}{3} \omega\, \mu_k\, N(R_2^3 - R_1^3) \quad (52)$$

, if N is uniform. ω is the relative angular velocity between the two discs, τ is the torque on the discs.

It is well known the friction force is independent of the contact area between the two surface, as is evidenced by equation 50. However, equation 50 is an approximation of the true frictional force. Friction is caused by inter-molecular forces. If the surfaces are smooth and flat, to the order of one nanometer, and in close contact, also to the order of one nanometer, the intermolecular forces will cause the two surfaces to strongly adhere to one another [34], a process known as optical contacting. The dimpling process ensures the optical contacting process does not take place. It should be understood that the super-dielectric may be flat and the electrode dimpled conversely, whichever provides for easier implementation and operation. It may not always be necessary to dimple the surfaces as the super-dielectric matrix itself may provide sufficient surface roughness to prevent optical contacting, as the super-dielectric matrix contains porous structures much larger than one nanometer. The dimpling is accomplished through a MEMs fabrication process known as grayscale etching or grayscale lithography [59]. A potential method that negates the need for grayscale patterning, i.e., dimpling, will be discussed shortly, though both techniques may be used in tandem.

Mercury-less Design

The normal force, N, in equation 50 warrants attention as this is the primary driver for the frictional force the spinning discs will experience during operation. The discs, containing large oppositely polarized electric charges, will experience a large electrostatic attraction, making N large if unmanaged. A Quickfield™ FEM simulation of this electrostatic attraction, figure 42, estimates the electrostatic pressure between the two plates of the system shown in figure 9 (d = 2 microns, ΔV = 2 volts) to be 4.4 GPa at full lift; full lift being 3709 Newtons (834 lbs) for a 1-meter radius disc. Analytically, the electrostatic force between two charged, flat capacitor plate electrodes is derived to be [35], ignoring fringe fields

$$F_C = \frac{k\epsilon_0 A\,(\Delta V)^2}{2d^2} = \frac{k\epsilon_0 \pi R^2 (\Delta V)^2}{2d^2} \qquad (53)$$

where A is the area of the plates, which gives an electrostatic pressure of

$$P_C = \frac{k\epsilon_0 (\Delta V)^2}{2d^2} \qquad (54).$$

Solving equation 54 for the system described in figure 9 also gives a result of 4.4 GPa, in exact agreement with simulation.

The lift goes proportionally with the voltage, equation 25, and the electrostatic pressure goes as the square of the voltage, equation 54. A similar relationship exists for the electrode spacing (i.e., super-dielectric thickness). A tradeoff can be made between lift/thrust force and electrostatic pressure. Figure 43 graphically illustrates these tradeoffs. As can be seen, this is a non-linear relationship, thus, it is possible to sacrifice some lift for a significant reduction in electrostatic pressure. The lift goes to the cube of the radius and electrostatic pressure does not depend on the radius of the disc, equation 54. Counterintuitively, if the discs can be made large enough, the electrostatic pressure to lift/thrust ratio can be made small, Figure 43d.

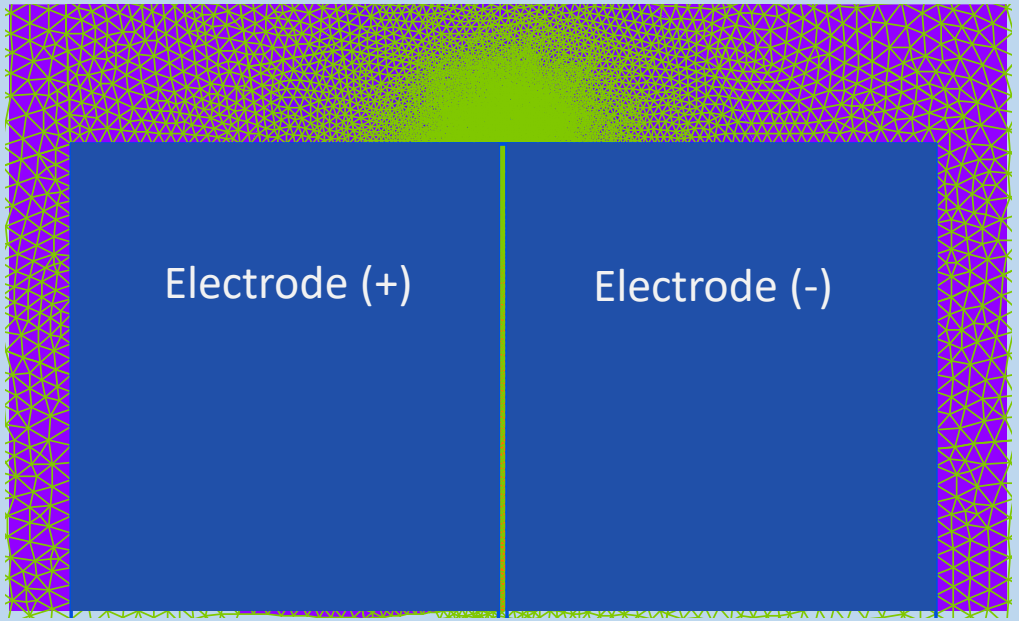

Figure 42. Quickfield™ simulation of electrostatic pressure between the DSC plates of the system shown in figure 9. (d = 2 microns, ΔV = 2 volts, R = 1 meter) . Electrostatic pressure = 4.4 GPa.

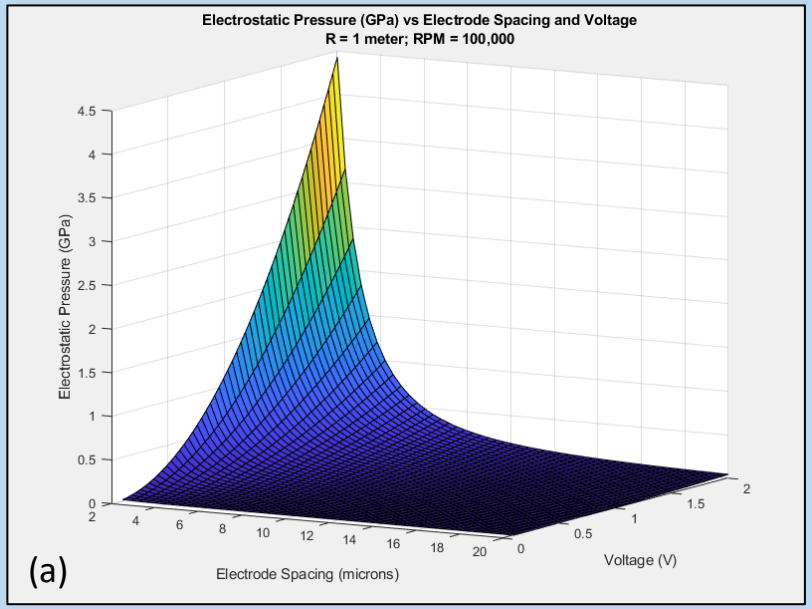

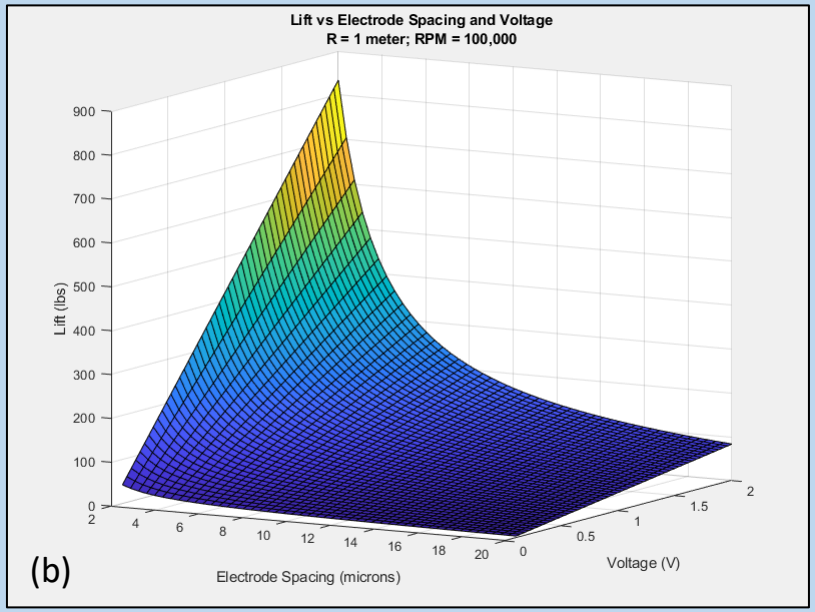

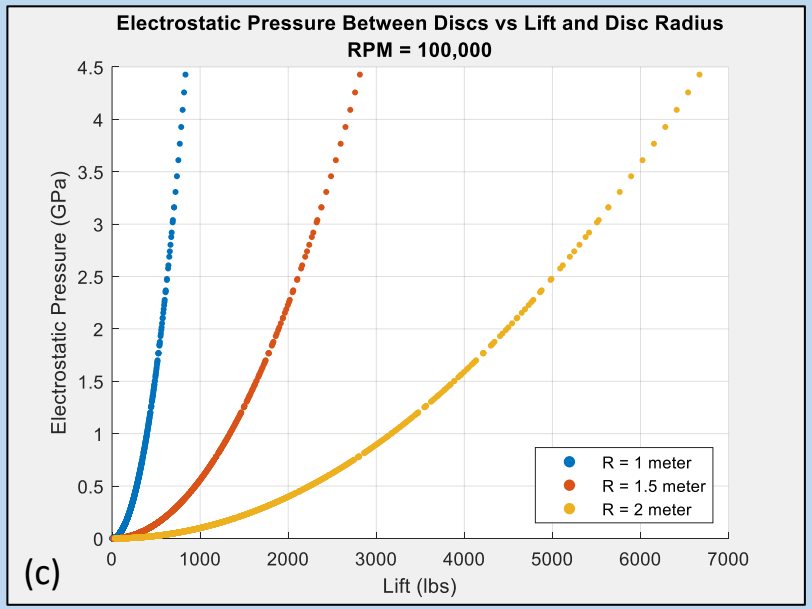

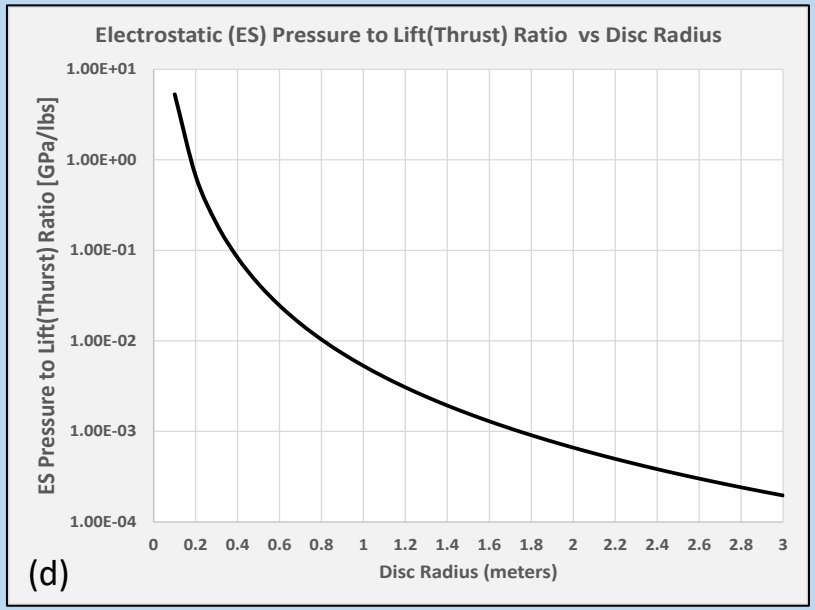

Figure 43. Electrostatic Disc Pressure and Lift/Thrust design tradeoffs. (a) Electrostatic pressure vs electrode spacing and voltage. (b) Lift vs electrode spacing and voltage. (c) Trade off between Electrostatic Pressure and Lift/Thrust and Disc Radius. (d) Electrostatic Pressure to Lift/Thrust ratio vs Disc Radius. For configuration shown in figure 9; RPM = 100,000, discs oriented in x-y plane.

Material Strength Considerations

Gigapascals of pressure is an immense amount of pressure which would likely crush any structure or device made of typical materials such as aluminum or steel. To this end, more exotic materials should be employed in the construction of the propulsion systems. Table 3 lists some candidate materials with the necessary strength and are in existence today. The list of materials is by no means complete but demonstrates materials are available that can handle the pressures and forces the propulsion system may generate internally. Graphene as well as aluminum and steel are listed for reference. The 2010 Nobel Prize in Physics was awarded to Andre Geim and Konstantin Novoselov for their work with graphene. It is widely believed that graphene will be the wonder material of the 21st century, ushering in new technologies , being highly conductive and stronger than diamond. Currently, lighter, stronger, more resilient materials are being researched by combining graphene with metals, epoxies, and polymers [36-43]. The point being that while the current invention will operate with currently attainable materials, the achievable performance of the propulsion system may be limited by the mechanical strength of those materials. As new materials are pioneered and material strengths are pushed into new regimes, so will the capabilities of the proposed propulsion system be expanded.

Material	Compressive Strength (GPa)	Tensile Strength (GPa)	Young's Modulus (GPa)	Bulk Modulus (GPa)	Poisson Ratio	Thermal Expansion (ppm/deg K)
Synthetic Diamond	110	1.2	1220	548	0.2	1.1
Synthetic Sapphire	2	0.4	400	240	0.29	4.5-9.0
Alumina	5.5	0.6	413	324	0.3	4.5-10.9
Silicon Carbide	1.4	1.6	137	176	0.37	7.9-11
Tungsten Carbide	6.8	0.5	686	680	0.22	4.4-7.1
Boron Carbide	5.6	0.5	472	271	0.21	3.2-9.4
Carbon Fiber	2.5	4.9	700	500	0.27	-0.38
Nickle-Graphene Matrix	-	1.1	-	222	-	-
Pure Graphene	500-1000	130	1040	500-1000	-	-8.0
Aluminum	*0.28*	*0.3*	*88.5*	*88*	*0.36*	*16-24*
Stainless Steel (316)	*0.3*	*0.6*	*205*	*205*	*0.27*	*15-18*

Table 3. List of super strong materials and some of their properties. Aluminum and stainless steel are included for reference. Dashes indicate data has not yet been published or is unknown. Ref [44-55, 62, 71-73]. The properties of carbon fiber can vary considerably based on the manufacturing process.

Reducing Rotational Friction

Materials are typically stronger under compressive loads than tensile loads. The shafts holding the discs will experience large forces. In one potential embodiment, figure 44, the top disc shaft passes through the bottom disc. The top disc is attracted to the bottom disc due to electrostatic attraction. The bottom disc is affixed to a rigid, fixed support structure and does not rotate. The bottom disc is attracted to the top disc through the same electrostatic attraction. The load from the attraction of the top disc to the bottom disc is transferred through the shaft. In this configuration the shaft is now under compressive stress, a stronger state for most materials. The bottom disc being rigid and stationary can be made as structurally strong as needed. Since only one disc rotates, the disc in the complementary propulsion unit (described earlier) should be configured to rotate oppositely to the base unit so that no unwanted angular momentum is imparted into the craft.

Returning to reducing the frictional losses between the two rotating discs; in order to reduce the force between the discs resulting from the electrostatic pressure, it may not be necessary to charge the entire disc. The lift/thrust force contribution on the disc is small near the center of the disc and large at the outer portions of the disc, as can be ascertained from looking at the J_{eff} distribution in figure 13. This relationship can also be directly understood by looking at equation 21, where R_2 is the radius of the outside radius of the ring and R_1 is the inner radius of the ring. This radial dependence is a cubic relationship. The electrostatic force between the discs goes as the square of the radius, equation 53. Since the lift goes as the cube and the electrostatic force goes as the square of the radii, if a significant portion of the disc is not charged this can result in a reduction in electrostatic force with a minor loss in overall lift/thrust performance. As an example, figure 45, for a 1-meter radius disc, if the center 0.5 meters of the disc is not charged, the lift is reduced by 12.5% as calculated using equation 21 but reduces the electrostatic force caused to the electrostatic pressure by 25%, a highly favorable result.

Additionally, examining equation 52, having part of the discs out of contact will also reduce the frictional power loss, here the uncharged parts of the discs. The frictional reduction with the central 0.5 meters out of contact will reduce the frictional power losses by 12.5%, in addition to the reduction in electrostatic pressure.

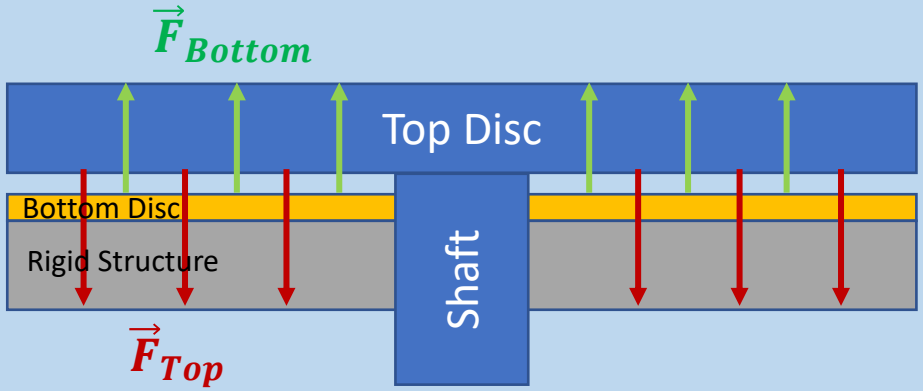

Figure 44. Embodiment in which the shaft is put into compressive stress as opposed to tensile stress due to internal electrostatic pressure. Top disc rotates, bottom disc is stationary and attached to a rigid support structure (or the disc can be made as thick as needed for structural integrity).

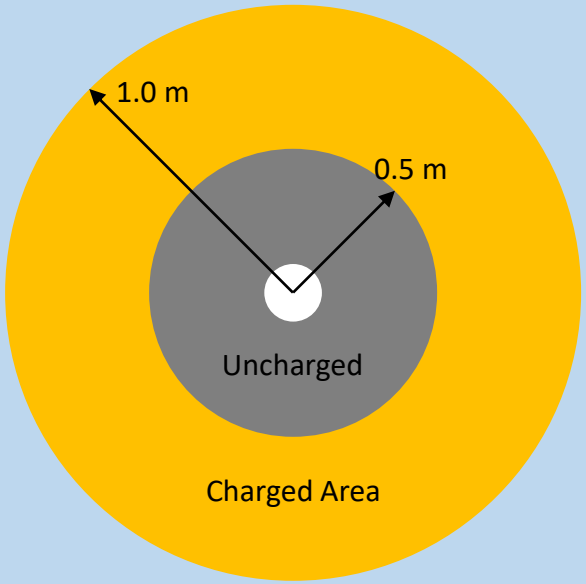

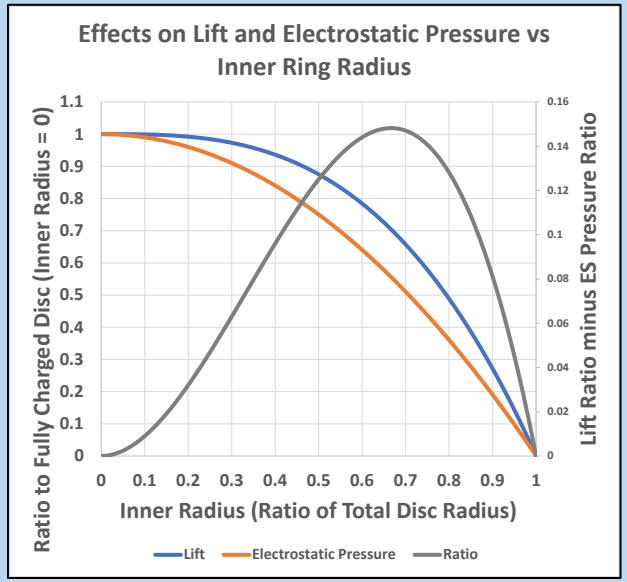

Figure 45. Partially charged disc (ring configuration). A favorable tradeoff can be made between lift and forces generated by the electrostatic pressure between the discs by not electrically charging the entire disc.

Reducing Rotational Friction

It can be ascertained that the frictional force, equation 50, can be minimized or even eliminated by applying a force to the disc that counters the normal force, N, generated by the electromagnetic stresses. As pointed out, super strong materials may be necessary to handle such forces. In order to reduce the kinetic friction between the spinning discs, the normal force in equation 50 should be reduced. Reducing N by not charging the entire disc has been discussed, figure 45. A reduction in the normal force can be additionally accomplished by applying a counter force through the shaft or shafts depending on the design of the propulsion system. Figure 46 shows a two-shaft system in which the shafts are in tensile stress. It should be clear that an upward force can be applied to the shaft in figure 44 to counter the attractive forces caused by the electrostatic pressure. In the latter case, the shaft is in compressive stress.

The separation forces needed to reduce the frictional normal force can be very large. One potential way of producing these forces is through the use of thermal expansion/contraction. Platens at the base of the shafts, or the shafts themselves, can be made of super-strong materials, like those listed in table 3, and heated or cooled as necessary to produce expansion or contraction as needed. For instance, the shafts in figure 46 could be cooled in a controlled way to produce a contraction of the shafts. The shaft in figure 44 could similarly be heated to produce the needed expansion. Depending on the materials used and the temperature change induced, the existing strains in the system, i.e., the strains causing the normal force, will be mitigated by exchanging deformation strain at the disc interface to axial deformation strain in the shaft; or the discs will experience a prescribed displacement if the discs are already in separation. These thermal expansions/contractions are capable of producing massive forces depending on the thermo-mechanical properties of the materials used. Another advantage of this method is the forces and displacements can be precisely controlled with accurate temperature controls.

Presented are only two simple exemplary layouts, figure 44 and 46. A great number of other configurations and mechanical designs can be realized. Indeed, the details of the many potential mechanical designs can no doubt be a source for future disclosures.

It is instructive to estimate the rotational frictional losses. Equation 52 is only a rough approximation of the power loss due to rotational friction since the contact stresses throughout the discs are likely to be nonuniform. However, to get a rough approximation of the rotational friction power loss, if the normal force can be reduced to 1000 newtons (225 lbs), and only the outer 1/3 of the discs are used for lift (a ring configuration – reducing the lift to 2630 N [592 lbs]), and a coefficient of kinetic friction of 0.03 is used, the rotational frictional power losses are estimated to be roughly 0.5 Megawatts. If the normal force can be reduced to 100 newtons, the power loss reduces to 50 kW. This illustrates the importance of reducing the normal force between the discs.

Since the rotational frictional power loss goes as the radius cubed, equation 52, it is worth running an approximation of the MUMs unit since it is a small diameter version of the propulsion system, 1/10th the diameter of the exemplary example. Due to the small diameter, the starting electrostatic force is 1/100th that of the exemplary example, if the dielectric layer thickness remains the same. If the normal force can be reduced to 100 N between each pair of discs in the MUM (the MUMs consists of a large stack of discs), the sliding frictional power loss is approximately 50 kW for the whole MUMs unit described earlier. However, since the MUM's discs are small, resulting in a much smaller starting electrostatic force, and there are many discs, the force can be better distributed. It may be possible to lower the resultant normal force between disc pairs to a lower number, for instance a 10 N normal force per disc pair would result in a MUMs base unit only consuming 5 kilowatts of power to overcome rotational sliding friction losses. The choice of whether to use smaller radii MUMs or larger radii disc electrodes is a design choice, there are pros and cons to both.

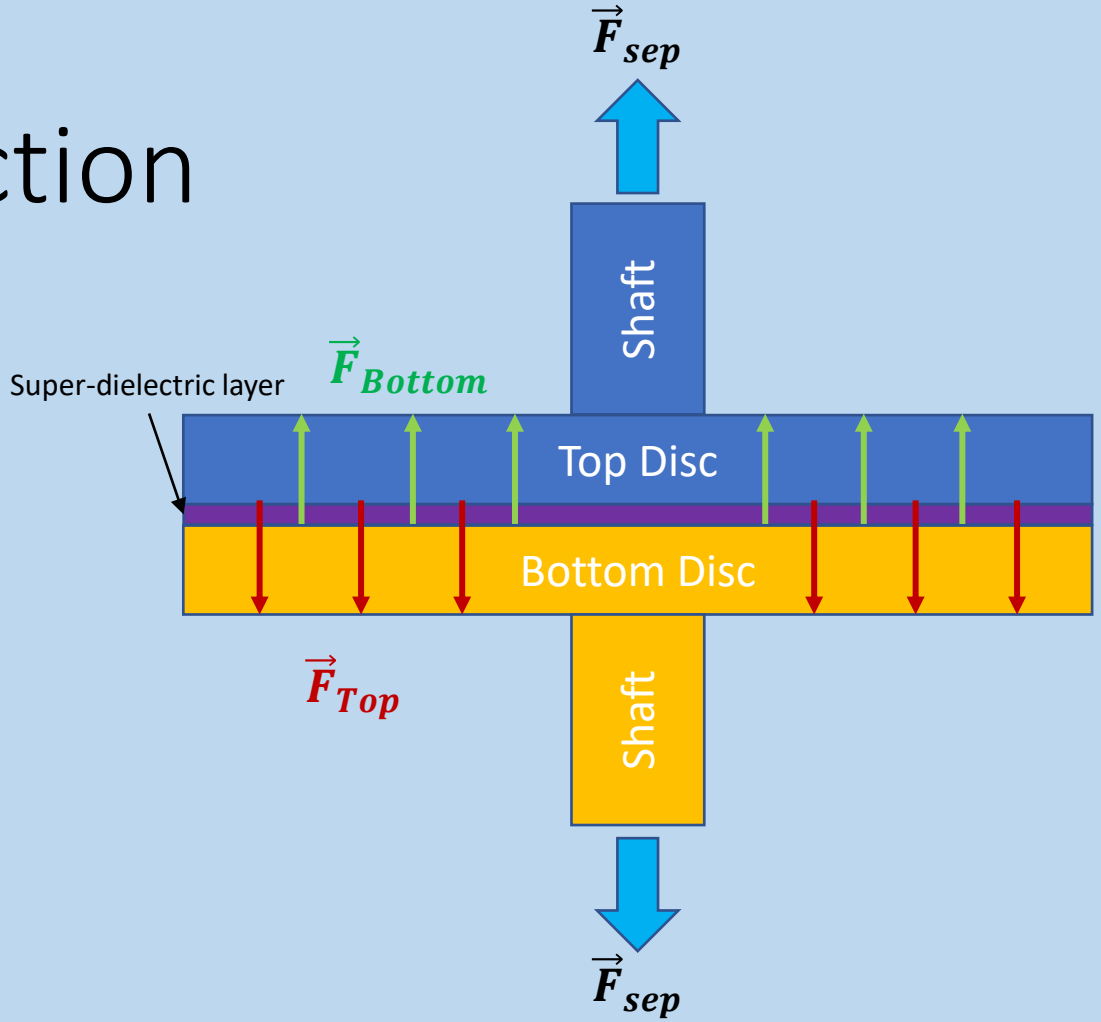

Figure 46. Force, F_{sep}, applied to shafts to counter the normal force created by the forces, F_{Bottom} and F_{Top}, generated by the electrostatic pressure between the charged discs.

Eliminating Sliding Friction

The reduction of the frictional normal force can be taken to the extreme; the discs can be separated. If the discs are separated beyond the range of the Van der Waals forces (~10 nm), the normal force will essentially drop to zero. This is a tricky proposition; first due to keeping such tight tolerances. Secondly, the electric circuit between the discs will need to be severed before disc separation takes place. If an air gap forms while the discs are still in electrical communication, i.e., part of a closed circuit, the supercapacitor will become a heterogenous capacitor with a super-dielectric layer and an air gap layer as the dielectric gap. The DSC will cease to be a supercapacitor at this point. The discs must be charged and then isolated (electrically disconnected). The discs now will retain their charge during the separation process. The charge on the discs is given by Q = CV. The voltage between the electrodes is V = Q/C. With Q now fixed, the voltage will rapidly increase as the discs are separated, since the capacitance, C, will drop rapidly as the discs are separated. The separation must be kept small, on the order of nanometers to tens of nanometers, or the voltage will rapidly increase to levels to which coronal discharge or field emission will take place. As a point of reference, if the super-dielectric were to be completely removed after the charge is fixed on the discs, or the discs were separated by an amount equal to the thickness of super-dielectric layer (for k >> 1), the voltage between the disc electrodes would increase by an amount equal to the dielectric constant of the super-dielectric, k. An air gap separation would be easier to achieve in a MUMs unit due to its smaller disc size and inherently better tolerances, though still a difficult task. At the time of this writing, the exemplary super-dielectric contains ionic fluids [24,25]. In the near future, ionic fluids may not be necessary as graphene, graphene oxide, and other super-dielectric materials make progress. Without ionic fluid, the air in the formed gap may be evacuated, eliminating any potential air molecule drag on the spinning discs in the formed gap as well.

Controlled separation of the discs would be an extremely challenging engineering task but is included here because, while extraordinarily challenging, is not impossible, and the benefits may be well worth the effort since near elimination of the disc interface sliding friction would make the craft extremely energetically efficient, allowing orbit to be achieved with very little energy. Orbit could be obtained using surprisingly little energy; the system using tens to hundreds of kilowatts of power to overcome intrinsic losses (bearings, dynamic seals, and ohmic losses, if any). Plus, the energy needed to achieve orbit, which as described earlier is 58 megajoules per kilogram to achieve geosynchronous orbit, about half the total energy contained in a gallon of gasoline. A calculated balance should be struck between time to achieve orbit, as energy is being expended to overcome intrinsic losses, $E_{loss} = P_{loss}\Delta t$, and aerodynamic energy losses. A shorter time to orbit may mean higher velocities inside the atmosphere which would increase aerodynamic drag energy losses; aerodynamic drag above the critical velocity goes as the velocity squared. A very doable orbital mechanics efficiency optimization problem. However, this is not a disclosure on orbital mechanics, only the propulsion system that enables new and novel orbital mechanics possibilities.

Premanufacture of the Electrodes

Due to the electrostatic pressure between the discs, the electromagnetic stresses predicted by equation 15, and the centrifugal forces of rotation, the discs will strain under operation. The discs should be premanufactured to compensate for the strain/distortion they will experience when stressed such that they will be as close to flat as possible under operation. This will help in ensuring a more uniform and controllable reduction of the normal force, N. Figure 47 shows the simulated pre-manufacture shape of the discs needed to compensate for the intrinsic electromagnetic forces of the system; centrifugal forces are not included here. The blue outline is the discs as they should be manufactured; exaggerated scale. The solid models are as under operation.

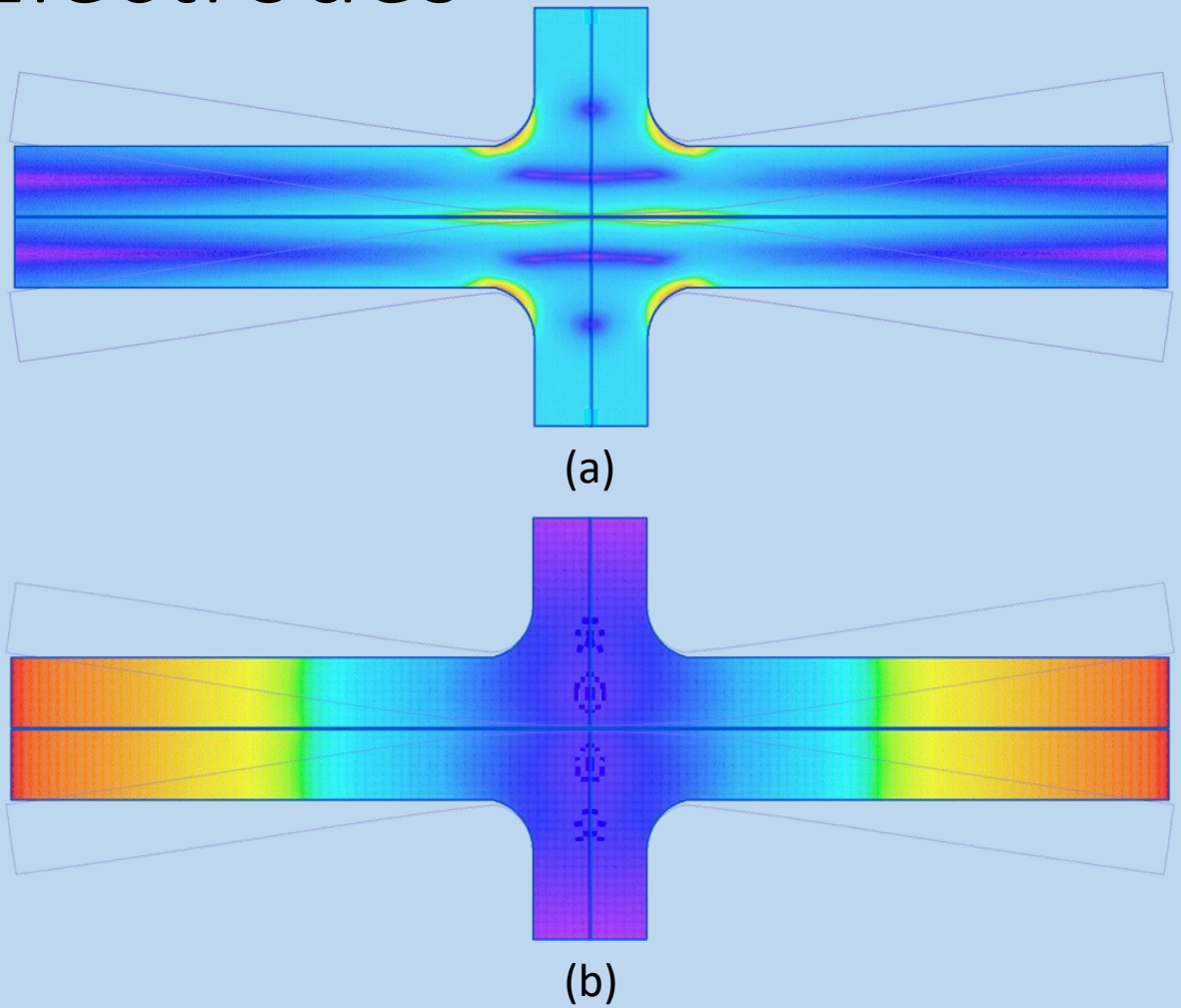

Figure 47. Discs should be premanufactured so that they are flat under operational stresses. Blue outline are profiles of how discs should be manufactured. Solid are discs' shape under operation. Not to scale. (a) stress profile on discs, (b) displacement from nominal profile. QuickField™.

Wrap-up

A one-meter radius dual disc dynamic super capacitor spinning at 100,000 RPM has been used throughout as the exemplary example. This base configuration is an instructional example as there are many parameters that can be varied as the design requirements and engineering tradeoffs require. For instance, smaller diameter electrodes provide higher packing densities, higher maximum electrode rotational speeds, and manufacturing advantages; the MUMs being the exemplary example. On the other side of the spectrum, larger diameter electrode DSC's can provide the equivalent lift/thrust at much lower rotational speeds. While there is a wide parameter design space that can be realized, as the design requirements and engineering tradeoffs require, at the fundamental level of the invention is the interaction of dynamic supercapacitors (DSCs) with external magnetic fields to generate usable torque and force; in this embodiment as a propulsion system for craft that can operate underwater, on water, in the atmosphere, and in outer space. These torques and forces may find other applications other than for craft propulsion alone.

Conclusion

The invention herein describes a new and novel propulsion system which provides lift and thrust by the interaction of dynamic super capacitors (DSCs) with external magnetic fields. The exemplary external magnetic field used throughout this writing is the Earth's magnetic field, however, it should be clear the propulsion system described will operate in any external magnetic field. For instance, Jupiter's magnetosphere is approximately twenty times stronger than that of the Earth's and has a volume about a million times that of the Earth's, figure 48. Propulsion within the vicinity of Jupiter and its moons is highly feasible. Any planet possessing a magnetic field, or celestial body such as the sun, can be used as the source of the external magnetic field.

Additionally, the solar system possesses an interplanetary magnetic field (IMF). Figure 49 shows our solar system's heliospheric current sheet generated by the sun, which plays a major role in generating the IMF. The IMF extends past the outer planets; however, the strength and distribution of the IMF is not well understood other than its strength is known to follow the rotation of the sun and varies with space weather [63]. The Advanced Composition Explorer (ACE) satellite monitors the IMF near Earth's orbital radial position from the sun. ACE has measured an average IMF strength of 6 nanotesla (37 nT at its peak) [64]. The MUM propulsion cube assembly shown in figure 37b would produce a thrust of approximately 162 Newtons (36 lbs) in a 6 nT IMF. While 162 N is not a large amount of thrust in terms of achieving Earth orbit, 162 N is a considerable amount of thrust in interplanetary (or interstellar) space where gravity is weaker. For comparison, state of the art ion thrusters used by NASA produce about 0.5 Newtons (0.1 lbs) of force [23]. As a point of reference, if 162 N of force could be maintained continuously for 764 days, a craft with a mass of 100 kg would reach a velocity of 100,000 km/sec (one-third the speed of light) in flat gravity space, i.e., far from large mass bodies such as planets. At this speed, on a direct course, it would take approximately 12 days to go from Earth to Neptune, and 12 and a half years to go from Earth to Proxima Centauri, our closest stellar neighbor. Of course, this is just a theoretical example as the craft would require the presence of an external magnetic field source during the acceleration period and a substantial power source. More practically, magnetically driven craft could use the powerful magnetic fields of bodies like Jupiter or the sun to gain velocity in the vicinity of the magnetic body and then sling shot away from those bodies at high velocities, not unlike the gravity assist technique used today for space probes. However, this is not an invention about orbital mechanics, it is an invention about the propulsion systems that make those orbital mechanics more feasible and attractive for achieving Earth orbit and reaching out into the solar system in an efficient and practical way. Interestingly, as a final point, galaxies like our Milky Way do posses strong, ordered magnetic fields throughout their volumes [65-69], potentially providing the needed external magnetic field source to drive craft through interstellar space and explore neighboring star systems on a more attractive timescale than what can be achieved today.

The author acknowledges the present invention pushes the limits of human engineering and material science technology. However, everything presented herein is within the scope of currently achievable technology. With the right expertise and appropriate effort, the described invention can be realized. The enablement of humankind to practically and efficiently leave the confines of Earth and explore and colonize the solar system as well as access the abundant resources of our solar system on greatly abbreviated timescales warrants the effort to build such propulsion systems as are described herein.

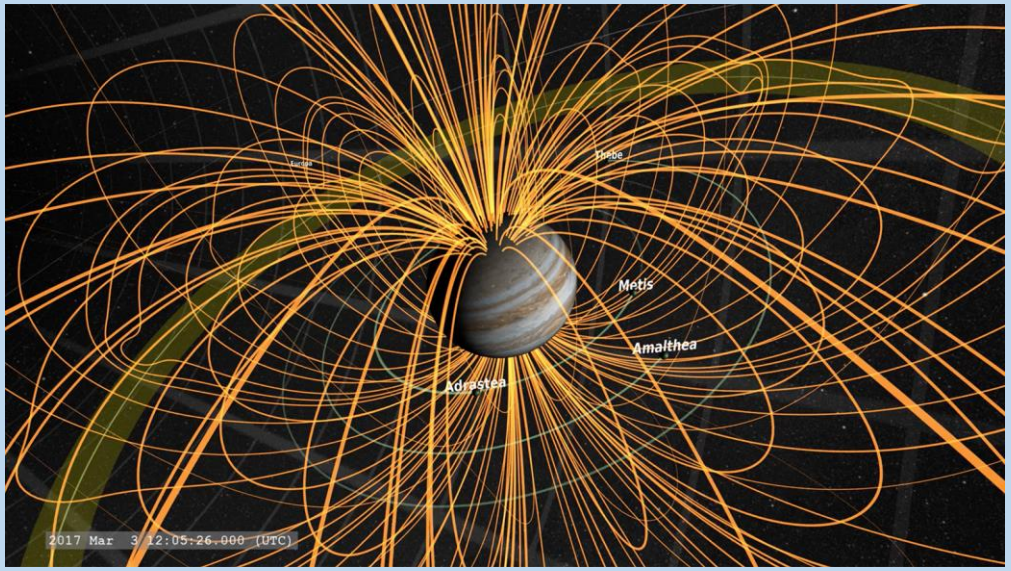

Figure 48. Jupiter's magnetosphere. **Source:** NASA's Scientific Visualization Studio.

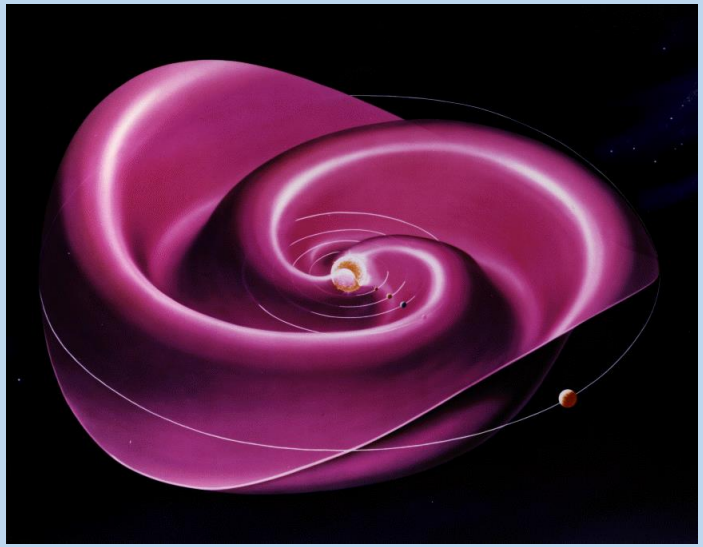

Figure 49. Our solar system's heliospheric current sheet. **Source**: Wikipedia.

References

1. NASA: This Rare Metal Asteroid Is Worth More Than the Global Economy – Robb Report
2. Geomagnetic field - Dipolar field | Britannica
3. Force between magnets – Wikipedia
4. Yung, et al. “An Analytic Solution for the Force Between Two Magnetic Dipoles”. Magnetic and Electrical Separation; Vol 9, pp 39-52, 1998.
5. Griffiths, David. Introduction to Electromagnetics, Cambridge University Press, 2017.
6. Woodson, Herbert H., and James R. Melcher. Electromechanical Dynamics. 3 vols. (Massachusetts Institute of Technology: MIT OpenCourseWare). http://ocw.mit.edu. License: Creative Commons Attribution-NonCommercial-Share Alike.
7. Kelly, Michael. The Earth’s Electric Field: Sources from Sun to Mud. Elsevier Press, 2021.
8. Ion-propelled aircraft – Wikipedia
9. NASA - Ion Propulsion | NASA
10. Wärtsilä-Sulzer RTA96-C – Wikipedia
11. How Much Torque Does a Train Have - Locomotive, Engine (trainconductorhq.com)
12. Superconductors for Electrical Power (stanford.edu)
13. D. Larbalestier et al., "High-Tc Superconducting Materials for Electric Power Applications," Nature 141, 368 (2001).
14. A. Gurevich, "To Use or Not to Use Cool Superconductors?," Nature Mat. 10, 255, (2011).
15. X. S. Wu, P. W. Adams, Y. Yang, and R. L. McCarley. Spin Proximity Effect in Ultrathin Superconducting Be-Au Bilayers. Phys. Rev. Lett. 96, 127002 (2006).
16. Shunsuke Yoshizawa, Takahiro Kobayashi, Yoshitaka Nakata, Koichiro Yaji, Kenta Yokota, Fumio Komori, Shik Shin, Kazuyuki Sakamoto, Takashi Uchihashi. Atomic-layer Rashba-type superconductor protected by dynamic spin-momentum locking. Nature Communications, 2021; 12 (1) DOI: 10.1038/s41467-021-21642-1
17. S.G. Christov. General Theory of Electron Emission from Metals. Phys stat. sol. 17, 11 (1966).

References

18. Fitzpatrick, R. (2020, September 25). Cold Emission. from https://phys.libretexts.org/@go/page/15746
19. Ceramics That Won't Shatter | MIT Technology Review
20. https://www.nasa.gov/centers/johnson/pdf/584729main_Wings-ch4c-pgs200-225.pdf
21. Rawal, Suraj. "Materials and structures technology insertion into spacecraft systems: Successes and challenges." Acta Astronautica, Volume 146, p. 151-160. May 2018.
22. The Materials Used in Artificial Satellites and Space Structures (azom.com)
23. NASA - Ion Propulsion: Farther, Faster, Cheaper
24. Cortes, F.J.Q.; Phillips, J. Novel materials with effective super dielectric constants for energy storage. J. Electron. Mater. 2015, 44, 1367–1376.
25. Cortes, F.J.Q.; Phillips, Tube-Super Dielectric Materials: Electrostatic Capacitors with Energy Density Greater than 200 J cm3, Materials 2015, 8, 6208-6227.
26. White, Frank (2011). Fluid Mechanics. New York City, NY: McGraw-Hill. pp. 477–485.
27. Sommerfeld 1908, pp. 116–124.
28. D.Nelias, J.Seabra, L.Flamand, G.Dalmaz. Power Loss in High-Speed Roller Bearings. Tribology Series. Volume 27. pp 465-478. V. Steinberg; Introduction to Micro-fluidics. SMR1670-10. The Abdus Salam International Centre for Theoretical Physics. August 2005.
29. FIGGINS, B., SHEPHERD, T. Alternating Current Losses in Superconductors. Nature 202, 890 (1964). https://doi.org/10.1038/202890a0
30. V. Steinberg; Introduction to Micro-fluidics. SMR1670-10. The Abdus Salam International Centre for Theoretical Physics. August 2005.
31. Roman S. Voronov, Dimitrios V. Papavassiliou, and Lloyd L. Lee; Boundary slip and wetting properties of interfaces: Correlation of the contact angle with the slip length. The Journal of Chemical Physics 124, 204701 (2006); doi: 10.1063/1.2194019
32. Yingxi Zhu and Steve Granick; Rate-Dependent Slip of Newtonian Liquid at Smooth Surfaces. Physical Review Letters Volume 87, Number 9, 27 August 2001.
33. Lionginas Liudvinavičius. Supercapacitors: Theoretical and Practical Solutions. June 27, 2018. Intech Open. ISBN-10- 1789233526
34. Optical Contacting: Changing the Interface of Optics. Chris Myatt, Nick Traggis and Kathy Li Dessau. Precision Photonics Corporation precisionphotonics.com
35. Force Acting on Capacitor Plates — Collection of Solved Problems (physicstasks.eu)

References

36. Graphene and the Most Popular Advanced Alloys (azom.com)

37. Anthony, S. (2013). Graphene used to make graphene-copper composite that's 500 times stronger. https://www.extremetech.com/extreme/164961-graphene-used-to-make-graphene-copper-composite-thats-500-times-stronger

38. Processing of graphene/CNT-metal powder. Prashantha Kumar HG and Anthony Xavior M. Powder Technology, Alberto Adriano Cavalheiro, IntechOpen, DOI: 10.5772/intechopen.76897. https://www.intechopen.com/books/powder-technology/processing-of-graphene-cnt-metal-powder

39. First report on high entropy alloy nanoparticle decorated graphene. M. Y. Rekha, Nitin Mallik, and Chandan Srivastava. Scientific Reports 2018; 8: 8737. doi: 10.1038/s41598-018-27096-8. https://www.ncbi.nlm.nih.gov/pmc/articles/PMC5992158/

40. Bioinspired, graphene-enabled Ni composites with high strength and toughness. Yunya Zhang, Frederick M. Heim, Jamison L. Bartlett, Ningning Song, Dieter Isheim, and Xiaodong Li. Science Advances 31 May 2019: Vol. 5, no. 5, eaav5577. DOI: 10.1126/sciadv.aav5577. https://advances.sciencemag.org/content/5/5/eaav5577.full

41. Investigating aluminum alloy reinforced by graphene nanoflakes. S.J.Yan, S.L.Dai, X.Y.Zhang, C.Yang, Q.H.Hong, J.Z.Chen, and Z.M.Lin. Materials Science and Engineering. https://doi.org/10.1016/j.msea.2014.06.077. https://www.sciencedirect.com/science/article/abs/pii/S092150931400803X

42. Copper/graphene composites: a review. Paloma Hidalgo-Manrique, Xianzhang Lei, Ruoyu Xu, Mingyu Zhou, Ian A. Kinloch & Robert J. Young. Journal of Materials Science volume 54, pages12236–12289(2019). https://doi.org/10.1007/s10853-019-03703-5. https://link.springer.com/article/10.1007/s10853-019-03703-5#Sec43

43. Graphene in composites and polymers (firstgraphene.net)

44. Diamond Properties (bris.ac.uk)

45. Sapphire Properties | Guild Optical Associates (guildoptics.com)

46. Properties: Alumina - Aluminium Oxide - Al2O3 - A Refractory Ceramic Oxide (azom.com)

47. Properties: Silicon Carbide (SiC) Properties and Applications (azom.com)

48. Properties: Tungsten Carbide - An Overview (azom.com)

49. Properties: Boron Carbide (B4C) - Properties and Information about Boron Carbide (azom.com)

50. Bioinspired, graphene-enabled Ni composites with high strength and toughness. Yunya Zhang, Frederick M. Heim, Jamison L. Bartlett, Ningning Song, Dieter Isheim, and Xiaodong Li. Science Advances 31 May 2019: Vol. 5, no. 5, eaav5577. DOI: 10.1126/sciadv.aav5577.

51. A short review on mechanical properties of graphene reinforced metal matrix composites - ScienceDirect

52. Properties of Graphene – Graphenea

53. Properties: Aluminum - Advantages and Properties of Aluminum (azom.com)

54. Properties: Stainless Steel - Grade 316 (UNS S31600) (azom.com)

References

55. Mahmood M. Shokrieh, Roham Rafiee. Prediction of Young's modulus of graphene sheets and carbon nanotubes using nanoscale continuum mechanics approach. Materials and Design. Volume 31, Issue 2, February 2010, Pages 790-795.

56. Working with turbomolecular vacuum pumps (vacuumscienceworld.com)

57. Waumans, T.; Vleugels, P.; Peirs, J.; Al-Bender, F.; Reynaerts, D. (2006). Rotordynamic behaviour of a micro-turbine rotor on air bearings: modelling techniques and experimental verification, p. 182 (PDF). ISMA. International Conference on Noise and Vibration Engineering.

58. Magnetic Shielding | How Does It Work? (magneticshields.co.uk)

59. a447924.pdf (dtic.mil). https://apps.dtic.mil/dtic/tr/fulltext/u2/a447924.pdf

60. G Ianu et al. Power loss in grease lubricated ball bearings. 2020 IOP Conf. Ser.: Mater. Sci. Eng. 724 012009

61. Simon Söndgen and Wolfgang Predki. Power Loss and Axial Load Carrying Capacity of Radial Cylindrical Roller Bearings. Power Transmission Engineering. June 2013.

62. Duhee Yoon, Young-Woo Son, and Hyeonsik Cheong. Negative Thermal Expansion Coefficient of Graphene Measured by Raman Spectroscopy. Nano Letters 2011 11 (8), 3227-3231

63. Interplanetary magnetic field – Wikipedia

64. Glossary, interplanetary magnetic field (IMF), Southwest Research Institute. Retrieved 11 February 2020.

65. http://www.scholarpedia.org/article/Galactic_magnetic_fields

References

66. http://www.scholarpedia.org/article/Galactic_magnetic_fields

67. Bührke, T.: Forces that Rule in Galaxies, Max Planck Research 1/2015, p.34-41 (http://www.mpg.de/9093617/F003_Focus_034-041.pdf)

68. Klein, U., Fletcher, A.: Galactic and Intergalactic Magnetic Fields, Springer, Heidelberg 2015

69. Rüdiger, G., Hollerbach, R.: The Magnetic Universe, Wiley-VCH, Weinheim 2004

70. Wielebinski, R., Beck, R.: Cosmic Magnetic Fields, Springer, Heidelberg 2005 (http://www.mpifr-bonn.mpg.de/staff/rbeck/springer.pdf)

71. http://nguyen.hong.hai.free.fr/EBOOKS/SCIENCE%20AND%20ENGINEERING/MECANIQUE/MATERIAUX/COMPOSITES/Carbon%20Fiber%20Composites/91697_04.pdf 91697_04.pdf (free.fr)

72. Direct measurement of the axial poisson's ratio of single carbon fibres - ScienceDirect

73. T700SDataSheet.pdf (rockwestcomposites.com)

ADDENDUMS

Super-Dielectric

Empirical Results

Super-dielectric Empirical Performance

The super dielectric is an integral component in the performance of ultra-magnets and the corresponding magnetic propulsion systems as described herein. Throughout the current invention a super dielectric constant of 1×10^9 is used as the baseline value of the dielectric constant for calculation and simulation. It is important to empirically validate the achievability of such a colossal dielectric constant value.

To this end, several super-capacitors of the type of geometry described herein were built and tested using the preferred embodiment of the super-dielectric material mentioned herein. As described, a ceramic or ceramic-like matrix material is used as the container of the ionic electrolyte which allows the electric dipoles to form inside the super-dielectric matrix. In the current embodiment, an alumina matrix was created using alumina powders which are subsequently saturated with a sodium chloride aqueous solution. As the electrolyte solution is partially conductive it is important to fill the matrix with electrolyte solution without excess electrolyte solution overfilling the matrix and making the dielectric 'wet'. If excess electrolyte solution is added, this can create an unwanted ohmic loss between the electrodes.

Three different alumina powders were used to create the super-dielectric matrix for the supercapacitors. Figure 1 shows scanning electron microscope (SEM) images of the morphology of the matrices created with these powders. The first powder (associated with Sample A) is advertised as a high surface area (100-200 m^2/g) nano-powder with an average 20 nm grain size. The second powder (associated with Sample B and Sample C) is advertised as a high effective surface area (80-120 m^2/g) powder with an average 3-micron grain size. The third powder is advertised as a high surface area (100-150 m^2/g) powder with an average 2.5-micron grain size.

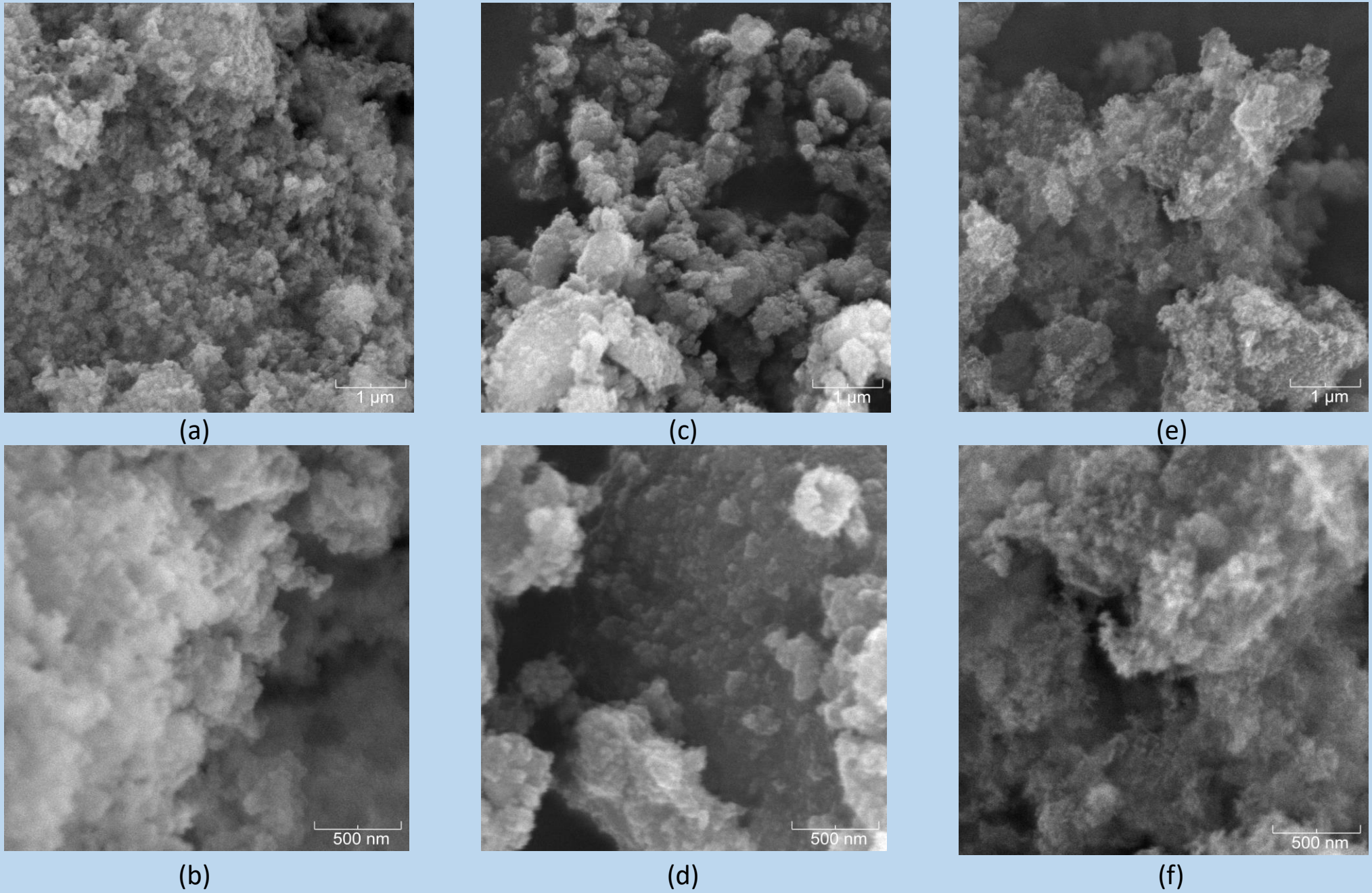

Figure 1. Scanning electron micrographs of the super-dielectric matrix. (a) and (b) Sample A, (c) and (d) Sample B and Sample C, (e) and (f) Sample D.

In general, the electric displacement field, $\vec{D}$, is described as

$$\vec{D} = \varepsilon_0 \vec{E} + \vec{P} \qquad (1)$$

, where ε_0 is the free space permittivity and $\vec{P}$ is the polarizability of the material the $\vec{E}$ field exists in, here the super-dielectric material. $\vec{P}$ is measured as the dipole moment per unit volume and in linear media can be expressed as,

$$\vec{P} = (\overleftrightarrow{\varepsilon_r} - \overleftrightarrow{I})\varepsilon_0 \vec{E} \qquad (2)$$

,where $\overleftrightarrow{\varepsilon_r}$ is the electric permittivity tensor and $\overleftrightarrow{I}$ is the unit tensor. In isotropic media $\overleftrightarrow{\varepsilon_r}$ reduces to a scalar value equal to the dielectric constant, *k*, $k = \varepsilon_r$. The electric dipole moment, $\vec{p}$, of two equal and opposite electric charges of charge magnitude, *q*, and distance of separation, *d*, is given by

$$\vec{p} = q\vec{d} \qquad (3)$$

In a conventional dielectric, the molecules of the media are stretched in the applied electric field. In this case, the molecular stretch may be on the order of angstroms or fractions of an angstrom. In addition, the electrons are shared within the molecule, so the magnitude of q in equation (3) is typically a fraction of a single electronic charge. Therefore, in a conventional dielectric both the magnitude of q and *d* in equation (3) are small and since $\vec{P}$ is the electric dipole moment per unit volume, this results in relatively tiny dielectric constants. For example, the electric dipole moment of a water molecule is 6.2×10^{-30} C-m [1]. The colossal super-dielectric constants described herein can be partially explained by the fact that electric dipoles can form in the pores and cavities formed via the electrolytic fluid in the super-dielectric matrix. The pores and cavities can be many tens of nano-meters or larger and the ions carry a substantial electronic charge. For instance, a sodium and chlorine ion separated by 100 nanometers of will have a dipole moment of approximately 1.6×10^{-26} C-m, about four orders of magnitude larger than a water molecule. Water is considered a high dielectric constant material in relation to conventional dielectrics.

Four super-capacitors were prepared with a flat, smooth parallel plate geometry as described in the ultra-magnet embodiments described herein. These supercapacitors were labeled Sample A, Sample B, Sample C, and Sample D. Table 1 shows the various configurations.

Supercapacitor	Electrode Material	Super Dielectric Thickness	Matrix Material	Matrix Average Grain Size	Effective Surface Area
SAMPLE A	Graphite	1.0 mm	Alumina	20 nm	100-200 m^2/g
SAMPLE B	Graphite	1.0 mm	Alumina	3 um	80-120 m^2/g
SAMPLE C	Aluminum	1.0 mm	Alumina	3 um	80-120 m^2/g
SAMPLE D	Graphite	1.0 mm	Alumina	2.5 um	100-150 m^2/g

Each supercapacitor was charged through a 1 kΩ resistor with a 5.2 volt drive voltage. The supercapacitors where then discharged through a 10 kΩ resistor. The voltage on the supercapacitor electrodes was monitored using a National Instruments DAQ6289 18-bit data acquisition system. The capacitance was determined by examining the total remaining charge on the electrodes at each voltage, C = Q/V. The dielectric constant as a function of voltage was then inferred using the parallel plate capacitor equation,

$$k = \frac{Cd}{\varepsilon_0 A} \qquad (4)$$

, where *C* is the capacitance, *d* is the spacing between the electrodes, and *A* is the area of the plates. The spacing between the electrodes was precisely controlled by the use of 1.0 mm diameter silicon nitride precision ball bearings inserted with periodic spacing between the electrodes. Figure 2 shows an assembled supercapacitor with graphite electrodes. Since it may take several days for a supercapacitor to discharge through a 10 kΩ resistance, the supercapacitor was sealed with epoxy before testing to prevent loss of the electrolyte during the test cycle.

(a)

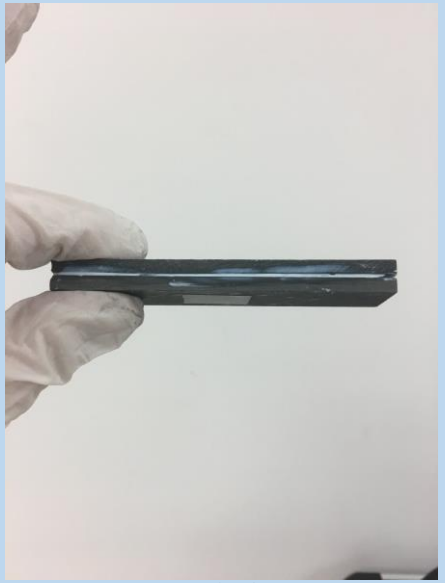

(b)

Figure 2. (a) graphite electrodes used in supercapacitor construction (100.7 mm x 21.0 mm x 4.0 mm). (b) Finished supercapacitor before encapsulation.

As an example of the charge and discharge dynamics, figure 3 shows the charge and discharge profile for Sample D. Figure 4 shows the resulting dielectric constant, k, for each of the four supercapacitor samples as a function of voltage. The base value of $k = 1 \times 10^9$ is shown for reference on the plots. As can be seen, in every case, the super-dielectric far exceeds the base value of 1×10^9, reaching dielectric values of 6×10^{11} in Supercapacitor Sample D.

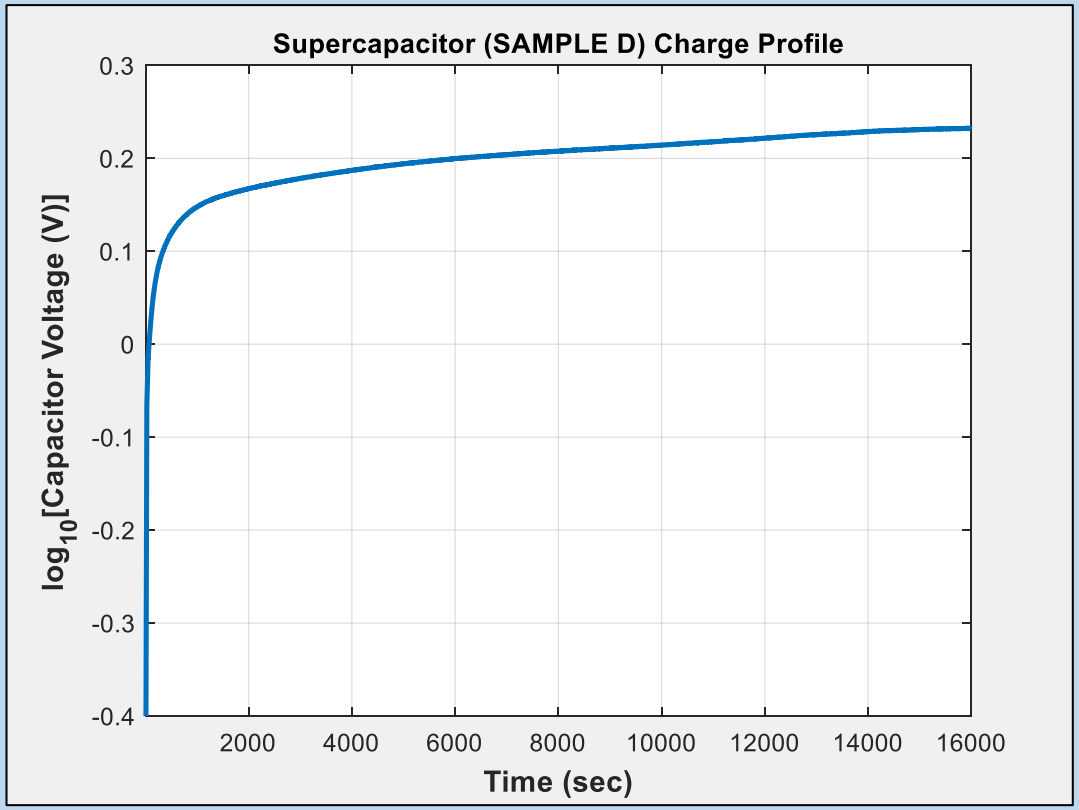

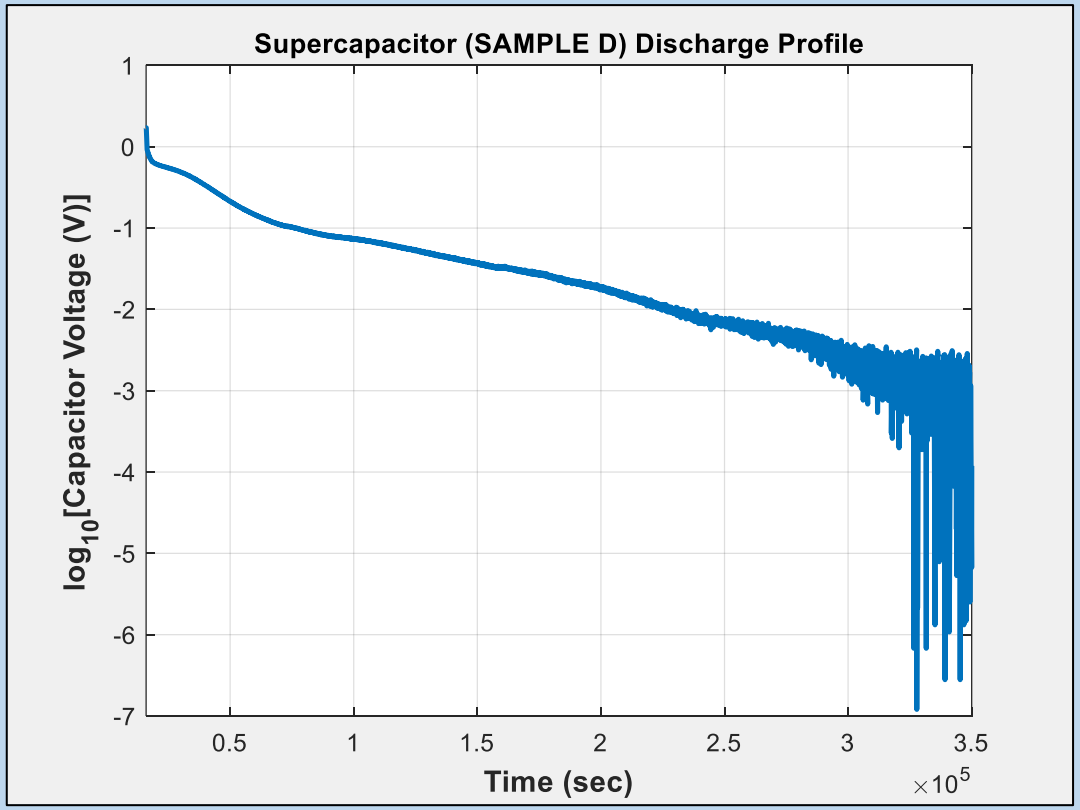

Figure 3. Charge (a) and discharge (b) profiles of Sample D supercapacitor. Charging voltage of 5.2 volts. Charging is through a 1 kΩ resistance and discharging is through a 10 kΩ resistance.

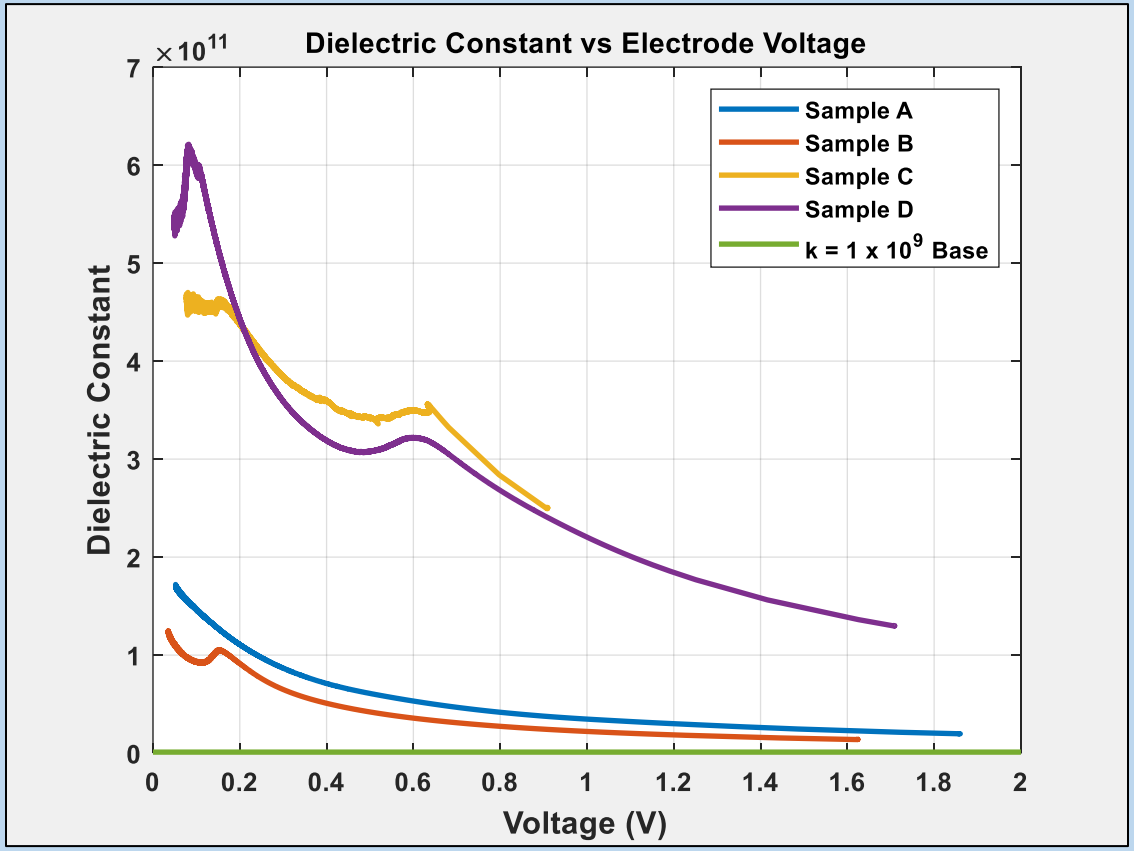

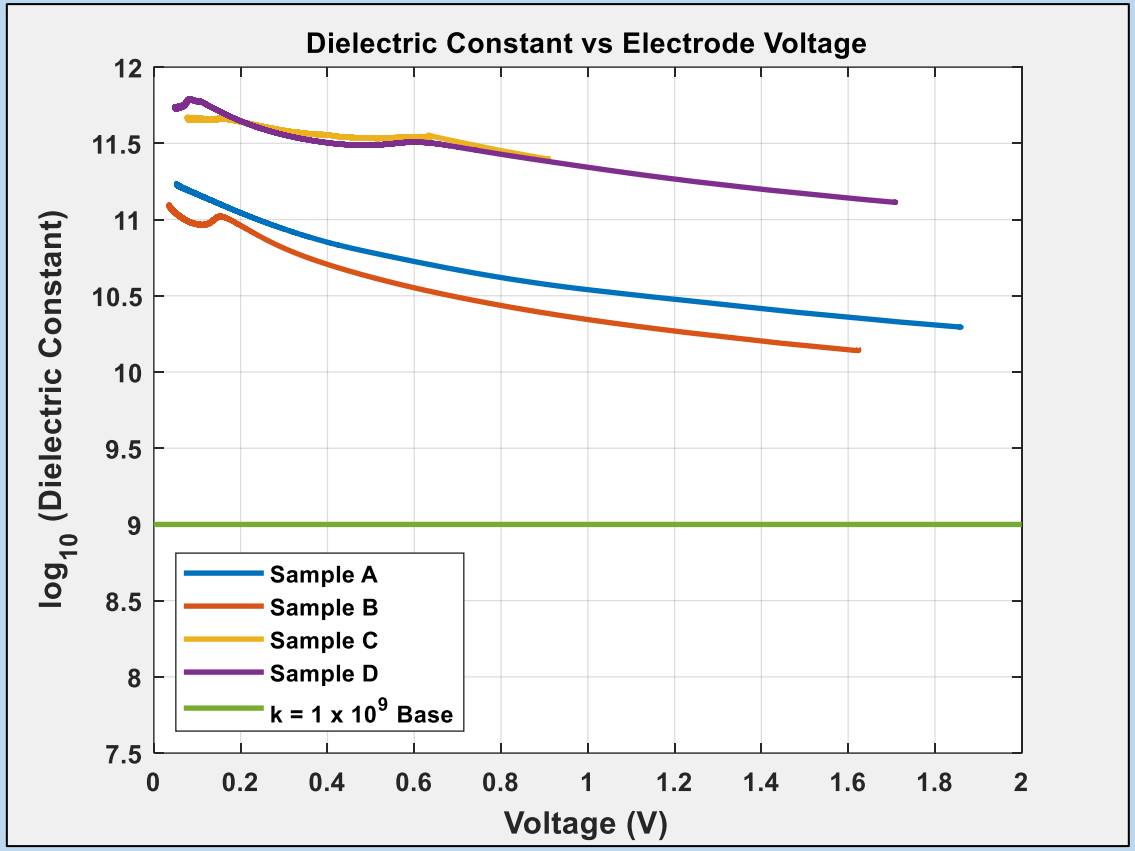

Figure 4. Resultant measured dielectric constants of the four tested super-capacitors. (a) linear scale, (b) log scale.

The already colossal super-dielectric constants measured can be further improved. Firstly, electrolytes using higher ionic charge ions, such as $MgCl_2$ as an example, can be used to increase the ion density and thus dipole moment formation in the super-dielectric, and thus increase the potential charge capacity on the electrodes. Additionally, the pores and cavities of the super-dielectric matrix posses a large variance in size, volume, and orientation due to the powder, electrolyte manufacturing process. The pores and cavities of the super-dielectric matrix can be precisely manufactured with precise optimal geometries and orientations using micro-chip, nano-technology, and MEMs manufacturing methods – masking, lithography, deposition, etching, liftoff, and so forth as is well understood to anyone in the art. *(see figure 6 and accompanying text in the ultra-magnet technology deck)*

Dielectric constant values in excess of 10^{12} can likely be attained with improvements to the manufacturing process and materials used. Throughout the current invention description, a dielectric constant value, k, of 1×10^9 has been used as the baseline to determine the strength of the magnetic fields produced and/or the thrust/lift a magnetic propulsion system would produce. In the analyses within, a rotation rate on the electrodes of 100,000 RPM has been used as the baseline rotation rate. With a k value of 10^{12}, the same magnetic field strengths and same propulsion forces as described may be achieved with an electrode rotation rate of 100 RPM (1.67 Hz), a modestly slow rotation rate. Likewise, the 100,000 RPM rotation rate may be maintained with all other parameters kept the same, except to increase the k value to 10^{12}. In this example the magnetic fields and propulsion forces would increase a thousandfold. As described herein, the limits of the magnetic fields that can be produced and the propulsion forces that can be achieved are primarily limited by the strength of the materials used to construct the devices. As an example of another tradeoff, the thickness of the super-dielectric may be increased to get the same performance as a thinner super-dielectric layer with a lower k value, if a thicker dielectric layer thickness were desired. There are many engineering tradeoffs and a wide parameter space to choose from to tailor the desired performance of the magnetic and propulsion devices described herein. The higher the k value, the more choices and tradeoffs are available in the design parameter space.

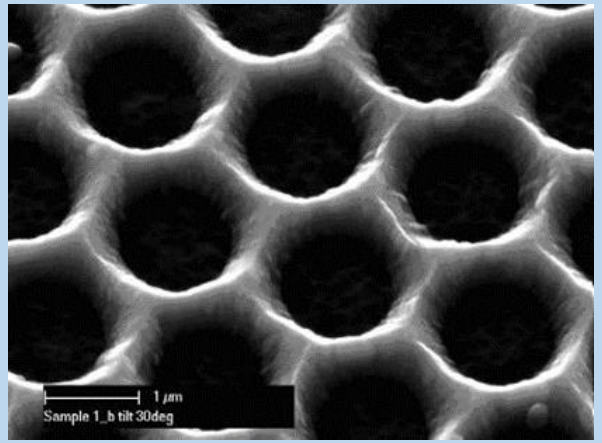

(see figure 6 and accompanying text in the ultra-magnet technology deck)

References

1. Halliday, Resnick & Walker, Fundamentals of Physics, 4th Ed, Extended, Wiley 1993

Propulsive Performance

Specific Impulse, I_{sp}, is a relative measure commonly used by rocket and jet engine manufacturers to compare propulsion system performances. Fundamentally, Specific Impulse measures how effectively a propulsion system can convert fuel to thrust. The larger the specific impulse the more effective the propulsion system is converting a given mass of fuel into thrust. Specific Impulse is defined as

$$F_{thrust} = g\dot{m}I_{sp} \qquad (1)$$

where F_{thrust} is the thrust produced by the propulsion system, g is the gravitational acceleration at the Earth's surface, and $\dot{m}$ is the mass of fuel used per unit time.

In the current case, the mass of fuel consumed by the propulsion system can be calculated by

$$\dot{m} = \frac{P_L}{\eta_C E_F} \qquad (2)$$

where P_L is the power losses in the propulsion system, E_F is the energy per unit mass of the fuel, and η_C is the cycle efficiency of the motor that turns the discs.

Conventionally, the thrust is partially or wholly produced by expulsion of mass from the propulsion system. Since the present invention does not expel exhaust as part of its thrust mechanism, the calculation herein can be thought of as an Effective Specific Impulse.

Propulsive Performance

A number of different types of fuel can be used to power the current invention; for instance, a nuclear-powered craft, be it fission or fusion, would produce much larger numbers than those shown below. However, to keep it simple and to help provide direct comparisons the example power source will be assumed to be the simple combustion of hydrogen and oxygen, a common rocket fuel source. This combustion powers a mechanical motor that rotates the discs. Each kilogram of the hydrogen-oxygen fuel contains 13.4 megajoules of energy. It is assumed the thermal to mechanical conversion efficiency of the motor is 30 percent; a typical value of efficiency for a combustion engine. For the exemplary example, the 10-cm MUM as shown in Fig 78B will be used. The default MUM produces a thrust of 124 lbs (551.6 N) as discussed earlier. The design values used for the MUM are disc diameters = 10 cm, k = 1 x 10^9, V = 2 Volts, electrode spacing = 0.1 mm, dielectric thickness = 1 micron, and RPM = 100,000, number of discs = 100. The power consumption of the propulsion system primarily comes from the rotational friction that each disc experiences inside the MUM; rotational bearing friction was also taken into account though is typically small compared to disc friction. As described herein, the power consumption, and thus the needed fuel consumption, is primarily driven by the friction of the discs inside the DSC devices. For the given example, the Specific Impulse vs Friction per Disc for the 10 cm MUM is shown in Figure 1. For reference, the Specific Impulse value for the space shuttle solid rocket booster is 250. As can be seen, the propulsion performance of the 10 cm MUM is many orders of magnitude better than the solid rocket booster of the space shuttle. Figure 1A also illustrates the importance of mitigating the disc friction of a DSC propulsion system. The frictional power loss is directly proportional to the rotational velocity of the disc. As will be shown later, it may be possible to produce much higher k values than 1 x 10^9. For instance, if a k value of k = 1 x 10^{12} can be achieved, the same thrust can be achieved with a rotation rate of only 100 RPM versus 100,000 RPM. Figure 1B shows the Specific Impulse values vs Friction per Disc for k = 1 x 10^9, k = 1 x 10^{12}, as well as for the space shuttle solid rocket booster for reference; log scale. As a point of reference, for a k = 1 x 10^9 and a per disc friction of 100 N, the 10 cm MUMs propulsion system has roughly one thousand times the performance of the space shuttle solid rocket booster, for a k = 1 x 10^{12} and a per disc friction of 100 N, the 10 cm MUMs propulsion system has roughly one million times the performance of the solid rocket booster. While combustion of hydrogen and oxygen was used in this example, other forms of power can be used to power the propulsion system be it nuclear, electric, combustion, or fuel cells. This list being in no way exhaustive. Each fuel source having its own energy per unit mass value will yield its own Effective Specific Impulse value.

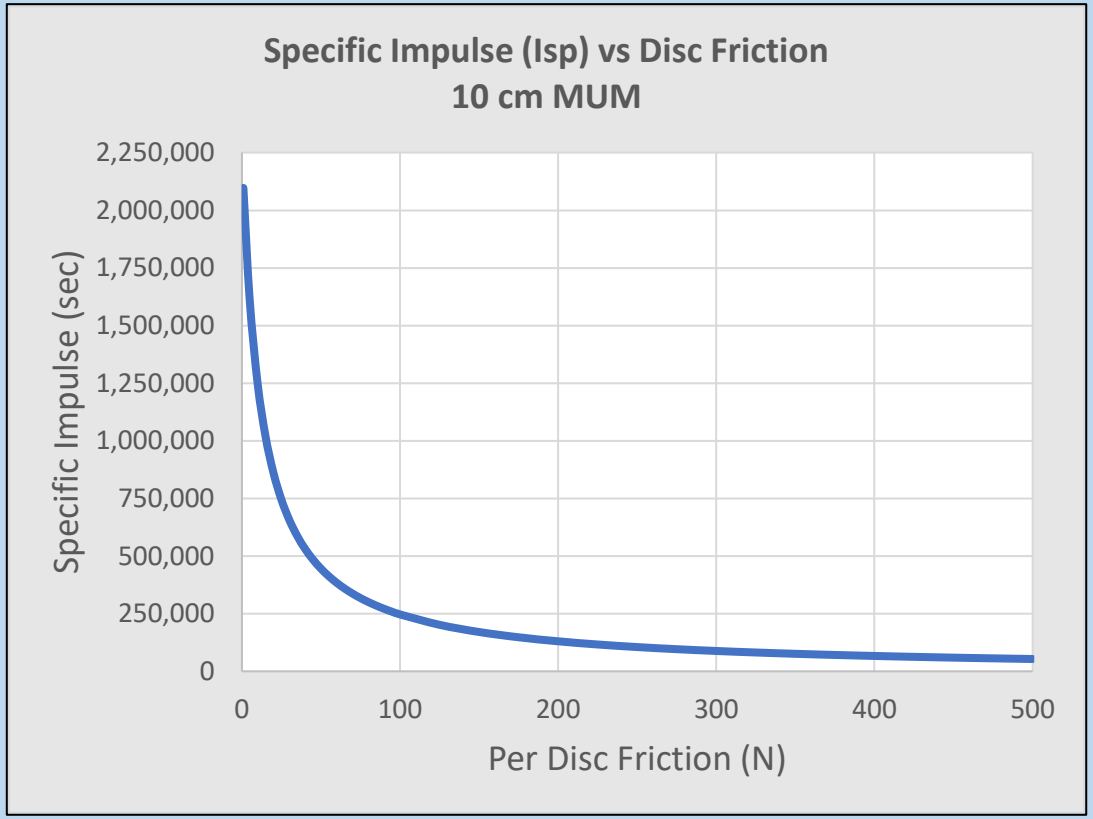

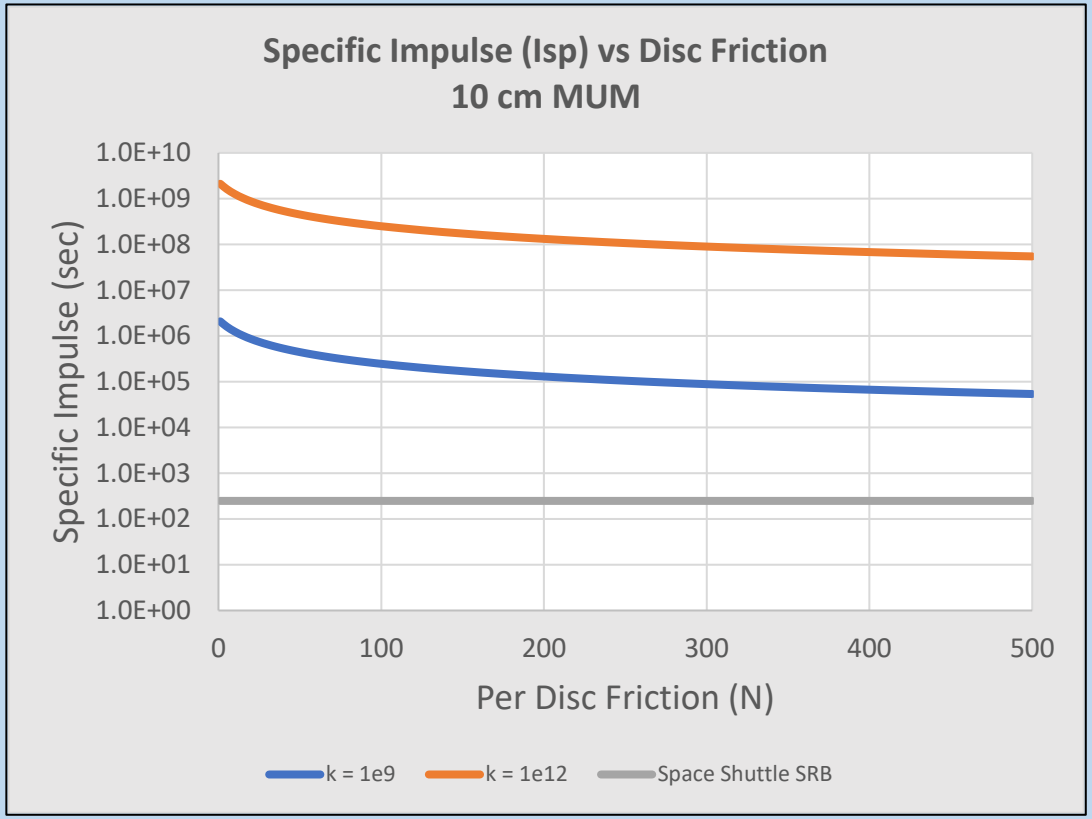

Figure 1. Specific Impulse versus the friction per disc inside a 10 cm MUM; (A) for a k value of 1×10^9. (B) for $k = 1 \times 10^9$ and $k = 1 \times 10^{12}$ as well as the Specific Impulse for a space shuttle solid rocket booster for reference; log scale.

Terminal Velocity

- Using a configuration like that in Figure 37(b) and assuming a craft weight of ten metric tons and a cross sectional area of 2 meter^2 , presenting a spherical windward surface, the achievable velocity of the craft at sea level can be estimated to be a little over Mach 12.
- This number can likely be improved on by making the craft more aerodynamic, material choices, and overall engineering design.